Stabbing Resistance of Soft Ballistic Body Armour Impregnated with Shear Thickening Fluid

A thesis submitted to the University of Manchester for the degree of
Doctor of Philosophy
in the Faculty of Science and Engineering

2016

Yue Xu

School of Materials

Table of Contents

LIST OF FIGURES

LIST OF TABLES

ABSTRACT

Shear thickening fluid (STF) is a non-Newtonian fluid whose viscosity increases under shear loading [5]. The use of STF with high tenacity fabrics to enhance the performance against impact loading has received substantial attention [1-3], due to the negligible contributions to the thickness and stiffness of the fabric [4].

This research investigates the feasibility of ballistic armour panels impregnated with STF aiming for higher stabbing protection. STFs were made from SiO_2 and polyethylene glycol (PEG), and efforts were made to control their critical shear rate and increase of STF viscosity. STF-Twaron® fabric specimens were fabricated to ensure full impregnation and STF continuity in the STF/fabric panels. To evaluate the stabbing resistant performance, as well as ballistic performance, 6 fabric panels were designed with STF from 12nm and 650nm silica particles with 3 different particle concentrations. Non-impregnated fabric panels with the same areal density and same number of layers as the impregnated one were also created. Stabbing impact test and ballistic test were carried out using these engineered panels.

This work confirmed that rheological properties of STFs can be tuned by tailoring the production parameters. Larger SiO_2 nanoparticle size led to lower critical shear rates and more obvious thickening effect. Higher particle concentration related to lower critical shear rates and greater jump in viscosity. The research revealed the existence of a minimum level of particle concentration for shear thickening behaviour to appear, and that higher molecular weight of PEG resulted in lower critical shear rate and more dramatic viscosity jump.

The experimental results showed that for the 12-layer Twaron® fabric panels, the STF impregnated panel absorbed at least 58% of the impact energy, compared to the 20%

absorption of the impact energy by the untreated panel. On the basis of the same areal density, the STF impregnated 12-layer panels provides 100% more enhanced energy absorption than the 24-layer untreated Twaron® fabric panel. The employment of STF in the panels also significantly reduced the back-face deformation caused by the knife impact. These findings indicate the feasibility of achieving more protective stabbing panels with lower weight and less bulkiness when STF impregnated panels are used against stabbing impact.

Furthermore, STF impregnated Twaron® targets exhibit superior ballistic resistance compared with untreated Twaron® targets. This research explored the possibilities for new designs of smart textiles that could combine shear thickening behaviour with ballistic fabrics to achieve lighter soft ballistic body armour with higher stabbing protection.

DECLARATION

No portion of the work referred to in the thesis has been submitted in support of an application for another degree or qualification of this or any other university or other institute of learning.

COPYRIGHT STATEMENT

ACKNOWLEDGEMENT

I would like to express my gratitude to the following people:

My supervisor, Dr Xiaogang Chen, for his guidance, keen support, valuable suggestions, encouragement, understanding and motivation.

My co-supervisor, Dr Hugh Gong, for his guidance and valuable suggestions during the project.

Mr Phil Cohen and Mr David Kenyon for their assistance in producing the shear thickening fluid, and the late Ms Alison Harvey for their technical support in testing the mechanical properties of the fabrics.

Mr Stuart Morse and Dr Jonathan Duff for their help and training in quasi-static tensile & compression tester and in high strain rate testing equipment.

Mr Teruo Hashimoto and Dr Weihong Gao for the high resolution of Scanning Electron Microscope imaging.

Our research team members, including Mr Haoxian Zeng, Mr Zishun Yuan, Mr Yan Wang, Dr Shengnan Min, Ms Nan Wang, Mr Hang Zhou, Ms Jowan Majeed Whaley, Mr Jiawen Qiu, Mr Kaichen Wang, Mr Wang Xu and Ms Lei Zeng for their support, discussions and friendship.

I am grateful to Teijin Aramid for providing Twaron® fibres used in this research.

I appreciate greatly the financial support provided by the Zhongyuan University of Technology, China for tuition fees and the Chinese Scholarship Committee for providing the maintenance scholarship.

Special thanks go to my parents for their endless love, encouragement and huge supports during the study.

PUBLICATIONS

1. Xu, Y., Chen, X., Wang, Y. and Yuan, Z. (2017), *Stabbing resistance of body armour panels impregnated with shear thickening fluid*, Composite Structures 163 465–473, http://dx.doi.org/10.1016/j.compstruct.2016.12.056

2. Xu, Y., Chen X., Wang Y., *Parametrical control of rheological properties of shear thickening fluid made from SiO_2 and polyethylene glycol*, Journal of Rheology, under review.

3. Xu, Y., Chen, X., Wang, Y. (2016). *Stabbing resistance of 3D multi-layered woven ballistic panels impregnated with shear thickening fluid*. Paper presented at 7th World Conference in 3D Fabrics and Their Applications, Roubaix, France.

4. Xu, Y., Chen, X. (2015), *Stabbing resistance woven ballistic body armour impregnated with shear thickening fluid*, LISTEN conference held by MOD & DSTL, , a poster presentation.

Chapter 1

Introduction

1.1 Background

Body armour for the military has traditionally been designed to provide protection against fragmentation and ballistic threats. High performance fibres such as Aramid (Kevlar®/Twaron®), ultra-high-molecular-weight polyethylene (Dyneema®), Glass fibres, have been used to make soft ballistic body armours [6] for the realization of lightweight, flexibility and comfort. These high strength, high modulus, high tenacity fibres have resulted in significant improvements in the performance of body armours against ballistic threats [7]. However, not sufficient attention was paid to the engineering of ballistic body armour with the anti-stabbing capability which is obviously a serious concern for the body armour users. Anti-terrorist actions and regional conflicts necessitate the further development of protective and flexible armour systems with additional stab-resistant capabilities. Stab threats encountered by the body armour users include direct attacks from knives and sharpened instruments such as spikes, as well as physical contact with debris, broken glass, razor wire and so on. The demand for improved stab protection has also been motivated by civilian police forces, particularly in Europe, where restrictions on gun ownership have led to an increase in the proportion of assaults which are committed with knives [8].

Body armour designed with anti-ballistic function is not necessarily resistant to penetration of blades and armour specifically designed to withstand blade penetration is prohibitively bulky and heavy [9]. Hence, fabrication of body armour that provides protection against ballistic and stabbing impacts represents a meaningful effort. The major difficulty in improving the stabbing resistance of ballistic body armour is due to the fact that the stabbing resistance mechanisms differ that for ballistic protection, because of the different impact velocity and different sharpness of the impactors [10]. Compared with ballistic impact, the stabbing impact is more likely to cause stress concentration because of the sharp edge of the impactor in a stabbing situation. In contrast, the main mechanism for ballistic protection is based on stress wave distribution. It is a fact that in most cases, the stabbing impact velocity (1 to 20 m/s) is lower than that of ballistic impact (200 to 1,000 m/s) [8].

In order to improve the stab resistance of ballistic fabrics, thermal-sprayed hard ceramic coatings were applied to aramid fabrics [11]. The resulted material demonstrated increased energy absorption during the quasi-static stabbing test, but also added to fabric weight significantly the same time. Aramid fabrics with high yarn count were also developed to provide stabbing (puncture) resistance. However, these high yarn count fabrics were expensive to manufacture and typically resulted in decreases in the ballistic protection efficiency of the fabrics [12]. One of the approaches to enhance the stabbing resistance is to roughen the surface of fibres or yarns by sanding or corona treatment to achieve higher coefficient of friction. However, such roughening is believed to have limited utility due to the resultant degradation in the fibre [13].

Shear thickening fluid (STF) has attracted attention for impact protection due to its unique properties subject to impact [14]. STF is a non-Newtonian fluid and shear thickening behaviour is triggered by a sudden increase of shear rate to the STF, which causes colloidal dispersions to concentrated exhibiting an abrupt increase in viscosity. This transforms a liquid dispersion into a solid-like material state [15-17]. Novel

liquid body armour based on STFs has shown promising prospects towards improved protection with flexibility [18]. When subjected to a predetermined shear rate, STF would undergo a dramatic and substantial increase in viscosity due to the formation of hydro-clusters. These hydro-clusters cause higher energy dissipation due to giving a higher viscosity [19].

Barnes [15] and Brown [20] reported that the shear thickening behaviour of an STF is influenced by the particle size and size distribution, particle shape, polydispersity of the particles, particle concentration, and interactions among particles, as well as the properties of the dispersion medium. He also worked on the determination of the critical shear rate and the degree of severity of shear thickening phenomenon. Hoffmann [21] worked to confirm the influence of medium viscosity on the onset of shear thickening. Xu [22] studied the influences of particle concentrations and the results showed that the shear thickening behaviour was significantly enhanced when increasing the concentration, and the mechanism of enhancement was quantitatively explained with the formation of large particles clusters. The particle size dependence of the reversible shear thickening transition in dense colloidal suspensions was explored by Maranzano and Wagner [23]. As a particular case, Lee *et al.* [24] investigated on the influence of silica particle sizes of 100, 300 and 500 nm at fixed volume fraction of 65%, and found that an increase in particle size would decrease the critical shear rate of the STF.

Much work has been done to investigate impact properties of fabrics impregnated with STFs. A few research groups have reported that STF enhanced fabrics were able to take advantages of STF properties for the enhancement of ballistic performance and stabbing resistance [1-3]. Work on the ballistic and stabbing performance of body armour showed that improved impact resistance of STF-impregnated fabrics could be attributed to the shear thickening behaviour [25, 26]. The deformation and energy absorption modes of STF impregnated and untreated Kevlar® woven fabrics upon impact has been analysed by Majumdar *et al.* [27], and they reported that in the neat

Kevlar® fabrics, only the primary yarns, directly engaged by the impactor, participated the load sharing and energy absorption, leading to low energy absorption. In the case of STF impregnated fabrics, the STF was transformed into a solid-like material upon impact and the transformed STF acts as a bridging matrix that converted the network of yarns in the fabric into a single structure. In this case, the entire fabric rather than only the primary yarns participated in load bearing and energy absorption. The failure of the STF impregnated structure is by rupture of fibres and yarns rather than their slippage. Some other studies showed that the enhancement of impact resistance was due to higher inter-yarn friction in the fabric brought by STF with constraining the pull-out of yarns [14, 25, 28, 29].

It is clear that STF is able to enhance the impact performance of the fabric panels against high and low velocity impact. However, further fundamental understanding still needs to be established through systemic investigation on how the rheological properties of STF work and affect the woven fabric panels impregnated with STFs. In addition, the STF impregnation would definitely add weight to the panel. Consequently, this work aims to investigate the feasibility of lightweight armour panels impregnated with STF for improving the stabbing resistance while retaining the high ballistic performance. Moreover, this research presents an investigation on the use of shear thickening fluid (STF) and how STF can be efficiently utilised to improve the stabbing resistance of soft ballistic body armour. STFs were produced from polyethylene glycol and spherical colloidal silica nanoparticles. Rheological properties of different compositions of STFs producing with different silica nanoparticle sizes, different nanoparticle weight fractions (concentrations) and different dispersing medium were chosen to explore the influence on the STF rheological properties. On the basis of the knowledge of how to control the rheological properties of STFs, different types of STFs with different synthetization parameters were used to impregnate the Twaron® woven ballistic fabrics. STF impregnated woven fabric panels were created and tested for dynamic and quasi-static stabbing resistance performance comparing with untreated Twaron® woven fabrics

under the same areal density basis and same fabric layers basis. Additionally, in order to study the STF impregnation effect on the ballistic performance of Twaron® woven fabrics, bullet shooting tests were conducted on STFs impregnated Twaron® fabrics and untreated Twaron® fabrics. The influence of STF impregnation into Twaron® fabrics was systematically discussed and the energy dissipation mechanisms were analysed. High speed tensile tests and yarn pull-out tests were carried out to support the theoretical assumptions of STF impregnation mechanisms.

1.2 Statement of the Problem

Soft ballistic body armour offers certain protection against knives or spikes, but if expected to attain the NIJ standard requirements, specialised stabbing resistant body armour would be required. In this regard, body armour which can provide ballistic protection as well as offers stabbing resistance is a vital topic within this field.

The major difficulty in improving the stabbing resistance of ballistic body armour is that the stabbing resistance mechanisms differ from that of ballistic resistance. The stabbing force exerted from knife to stabbing resistant material is based on the principle of shear strength of the fibre, cutting or fracture of armour materials and inter-yarn friction, and the range of energy distribution in a stabbing event is relatively narrow. In this regard, pointed knife and spike are hard to defend. However, for the ballistic body armour, the energy distribution is depended on deformation of the bullet, fibre fracture and propagation of impact wave, in order to disperse or consume the energy of the bullet at high velocity. Bullets are generally blunt projectiles and are often deformed considerably upon impact. Knives differ in their extreme sharpness and small contact area. It has been proven that the effects of the force and functioning time are different between stabbing and ballistic impacts [8].

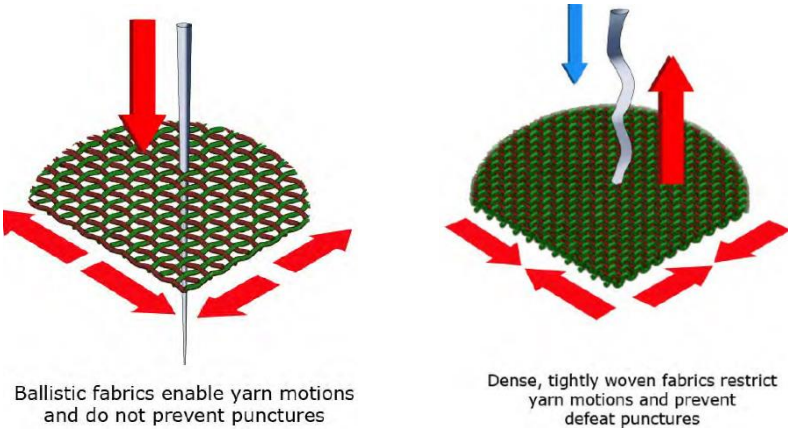

Figure 1.1 Different mechanisms make the different fabric areal density between ballistic body armour and stabbing resistant body armour

Because of the mechanisms difference, textiles designed for ballistic protection require sufficient yarn mobility within the fabric to avoid premature failures but will not perform well for stab protection. Textile designed for stab resistance requires dense fabrics to prevent yarns from being pushed aside from the tip of sharp-pointed objects such as knives, needles, awls, and ice picks. Dense fabrics that prevent punctures can lead to premature or punch-through failures in ballistic impacts [30]. Design parameters for optimising both ballistic defence and stab defence often work against each other, as shown in Figure 1.1.

The effect of sharpness on penetrative ability may also help to explain why textile ballistic armour is not resistant to knives. Textile armour is designed primarily to defeat soft and blunt projectiles such as those illustrated in Figure 1.2 (a). It can be seen that these projectiles are initially blunt and are further blunted and flattened during impact with the armour. Due to the blunt shape and deformable nature of handgun bullets, the energy could be assumed to be dissipated over an area equal to the projectile calibre. Although the knife has a lower energy and a lower velocity this is concentrated at the tip of the blade. The cutting edges of a blade easily part or cut textile fibres such that the impact energy could be assumed to act over only the contact area of the tip or cutting edges, and the knives and spikes were presented in Figure 1.2 (b).

(a) (b)

Figure 1.2 (a) Handgun projectiles used in the HOSDB body armour tests [31], from left to right 9mm, 0.357" magnum and 0.44" magnum. Similar projectiles after impact with textile armour are shown to the rear. (b) HOSDB stab test knife used in all tests on stab proof vests [32], from left to right, SP spike, HOSDB p1/a knife, HOSDB p1/b knife, SIG spike and NIJ spike.

1.3 Aims and Objectives

The aim of this research is to engineer and develop a soft body armour system for ballistic protection with improved stab resistant performance. STF will be made and impregnated into the fabric, in order to create the new soft body armour with sufficient resistance to both bullet and stab impact. The research is subdivided into two parts:

The first part is to prepare STF specimens and parametrical control of rheological properties of shear thickening fluid made from SiO_2 and polyethylene glycol. The study in this part is on parametrical control of STF critical shear rate and shear thickening viscosity by optimising the STF parameters including the size of silica nanoparticles, silica nanoparticle weight fraction (concentration), and the dispersing medium. In order to explore the influence of the STF production parameters on the rheological properties, the preparation plan for making STF specimens are as follows:

Category 1: STFs are generated by dispersing 12nm silica, 15nm silica, 200nm silica and 400nm silica into PEG200 with a silica particles volume fraction of 25% (PEG200 is used as the dispersion medium because of its low viscosity for easier

production of STFs).

Category 2: STFs are produced by dispersing 12nm silica into PEG200 at different silica particle volume fraction of 10%, 15%, 20%, 25%, 30% and 33%, respectively.

Category 3: STFs are synthesised by dispersing 12nm silica into three different molecular weight of PEG: PEG200, PEG400 and PEG600 with the particle volume fraction being 20%.

After all the STF samples are made, they will be taken to carry out the rheological tests using a stress-controlled rheometer under the temperature of 24ºC, following which discussions on the mechanisms of shear thickening will take place.

The second part is to manufacture STF-Twaron® composites by impregnating STFs into the high performance Twaron® woven fabrics and to evaluate the stabbing resistant performance and ballistic performance of the STF-Twaron® composites. The corresponding STF impregnation effects on the impact performance are systematically discussed and the energy absorption mechanism was analysed. For the purpose of evaluation of stabbing resistant behaviour and ballistic performance, the objectives in this part of the work are listed below:

1) To manufacture the composite, the STFs are impregnated into Twaron® plain woven fabrics according to the fabrication procedures. The weight ratio of STF adds on to the Twaron® fabrics is controlled to make sure each STF-Twaron® composite samples were fabricated consistently.

2) To carry out stabbing impact tests, the response and failure mode of STF impregnated Twaron® fabric is investigated compared with untreated Twaron® fabric samples. The factors influencing the stab resistant performance of STF impregnated Twaron® fabrics are also discussed.

3) To conduct ballistic tests, the response and failure mode of STF impregnated fabric subjected to ballistic impact is investigated. The influencing factors of the ballistic performance of STF impregnated Twaron® fabrics are studied.

4) To investigate the STF impregnated Twaron® fabrics energy dissipation mechanisms, high speed tensile tests and yarn pull-out tests were carried out to support the mechanism analysis.

1.4 Thesis layouts

The objective of this Chapter (1) has been to motive and set the scope of the work, putting it in a wider context.

Chapter 2 presents an overview of the backgrounds on fabric response upon stabbing impact and ballistic impact. It also investigates the factors influencing fabric stabbing resistant performance and ballistic performance of the body armour. The Chapter also discusses in Non-Newtonian fluid and their rheological properties, emphatically introduces shear thickening fluid and the factors influencing their rheological properties. Additionally, various techniques employed by other researchers in improving the stabbing resistance of ballistic body armour are investigated and STF applications on human protection applications. Finally, the concept of liquid body armour is introduced based on STFs are reviewed and discussed.

Chapter 3 provides the preparation processes of STF samples and fundamental investigations on rheological properties of STFs. This Chapter presents a systemic study on the control of STF critical shear rate and STF shear thickening viscosity by optimising the size of silica nanoparticles, silica nanoparticle weight fraction (concentration) and the dispersing medium. Rheology tests were carried out to determine the shear thickening behaviour of STF samples, and the mechanism of shear thickening phenomenon was explained with the particle cluster formation theory and Péclet number theory.

Chapter 4 shows the experimental study of STF effects on stabbing resistant performance of STF impregnated Twaron® fabrics. Dynamic and quasi-static stabbing impact tests were performed to correlate the shear thickening behaviour of STFs with the impact resistant performance. The role of STF impregnation on stabbing impact resistant performance is clarified and discussed. By comparing the stabbing resistant performance of untreated Twaron® fabrics and STF-Twaron® fabrics on the basis of the same number of fabric layers and same areal densities, the results from this part of the research investigated the possibility of lighter ballistic fabric panel materials for higher stabbing protection.

Chapter 5 provides the methodologies employed to analyse the energy dissipation mechanisms of STF impregnated Twaron® fabrics. Yarn pull-out tests under the quasi-static condition and fabric tensile tests under both high strain rate and quasi-static mode are conducted to support the proposed mechanisms of energy dissipation of STF impregnation effects. Modulus and inter-yarn friction of STF impregnated Twaron® fabric are theoretical studied and the influence on specimen energy absorption are discussed.

Chapter 6 describes the experimental investigation of STF effects on ballistic performance of STF impregnated Twaron® fabrics. Both perforation and non-perforation ballistic tests are carried out on fabric specimens to study the ballistic performance. The ballistic energy absorption mechanisms of the fabric specimens are discussed and analysed. The fabric specimen response upon the bullet impact and the failure mode of the fabric specimen subject to bullet impact are systematically studied and discussed.

Chapter 7 is the concluding part of the thesis summarises the achievements from this research, discussing in brief their strengths and weaknesses. Using these conclusions as a starting point, potentially promising paths for further research are investigated and proposed. Recommendations for future work are included in the end.

Chapter 2

Literature Review

2.1 Introduction to literature review

Knife and ballistic impact on fabric target are an important area and has been studied for many years. A quantitative understanding of the energy absorption of fabric target has gradually been built up through both experimental and theoretical efforts. This Chapter aims to provide a comprehensive literature review on this topic and to indicate how this correlates the present work on developing fabric target.

This research aims to investigate the feasibility of lightweight armour panels impregnated with shear thickening fluid (STF). According to that, the concept of Non-Newtonian fluid and rheology are introduced and reviewed in this Chapter. The theories of STF, the creation of STF and the influencing factors on rheological properties of STF are reviewed from the previous papers and books.

The last part of this Chapter will review the work which researchers have been done on STF application on ballistic fabrics and stabbing resistant fabrics, the concept of liquid body armour based on STF impregnation is introduced as one of the major applications of STFs. In the end, approaches to improve the stabbing resistance of ballistic body armour proposed from researchers are reviewed and discussed.

2.2 The Stabbing Threats

Nowadays, gun ownership by the citizen is forbidden in many countries. As a result of that, most of the threats come from attacks associated with knives, spikes, ice picks or any sharp pointed weapons. Murray and Green [33] reported a rising trend of stabbing injury and death over the last 30 years and concern over this increase dates back at least as far as 1966. Approximately 1500 assaults per year involved the use of a weapon of some type although the proportion involving edged weapons which are unknown [34].

Stab threats encountered by soldiers in the field include direct attacks from knives and sharpened instruments, as well as physical contact with debris, broken glass, and razor wire. Anti-terrorist actions and regional conflicts necessitate further development of protective and flexible armour system with improved stab resistant capabilities. The demand for stab protection has also been motivated by civilian police forces, particularly in Europe, where restrictions on gun ownership lead to an increase in the proportion of assaults which are committed with knives [35].

A number of studies have been made to investigate the type and location of stab wounds and particularly fatal wounds. Rouse [36] examined stab wounds according to the site and found that out of a total of 69 single fatal wounds 50 were to the chest, 12 to the head and neck, and 7 to the abdomen and lower limbs. For multiple fatal wounds (81 cases), the wound causing the fatality was to the chest in 61 cases. Murray and Green [33] stated that of 27 single fatal wounds 18 were to the chest. It has been concluded from these studies that fatalities from stabbing are chiefly caused by chest injuries. That being so, protection of the chest will carry the highest priority if the aim is to prevent fatal stabbing attacks. A study of 92 mainly non-fatal injuries by Fligelstone [37] showed that 37 resulted in injury to the abdomen and 29 in injury to the chest. It was stated that the majority of injuries reported in the study were minor and only one fatality had occurred.

2.3 Stabbing attack mechanisms

The human stab attack was divided into two stages for convenient description and analysis [8]. The first of these was the approach phase, ending when the knife tip first touched the target and the second was the impact phase, from the end of the approach phase to the point when the knife was brought to rest by the target.

Stab threats are classified into two categories: puncture and cut. Puncture refers to penetration by instruments with sharp tips but no cutting edge, such as ice picks. These threats are of primary concern to correctional officers since sharply-pointed objects are relatively easy to improvise. Cut refers to contact with knives with a continuous cutting edge. Knife threats are generally more difficult to stop than puncture since the long cutting edge presents a continuous source of damage initiation during the stabbing event.

Knife attack has four components of the load during the impact phase: axial force (along the length of the blade), cutting force (parallel to the breadth of the blade), lateral force (across the blade) and torque (twisting action) [9]. Various knives and layout of the instrumented knife are shown in Figure 2.1. A recent kinematic study of stab attacks, using two-dimensional video analysis, reported mean approach velocity for an overhand style to be 12 m/s, and that for a thrust style to be 6.6 m/s [38]. In that study, the target was freely suspended and the mass of the knife was 192 g. The body segments associated with the knife was modelled as a series of rigid segments: trunk, upper arm, forearm and hand. There are three styles of stabbing: a short thrust forward, a horizontal style sweep around the body and an overhand stab. The velocities of these segments, together with knowledge of the mass distribution from biomechanical tables, allowed the calculation of the individual segment energy and momentum values. Horsfall *et al.* [39] found that knife handle size and shape having only slight effects on the magnitude of impact energy. The use of a finger guard or hilt was shown to increase the mean energy delivered to the target by approximately 5J

compared to a handle having no guard. It was also found that the characteristics of energy delivery were strongly influenced by the position of the grip relative to this guard. Stab or puncture failure is a common type of damage mode when a sharp object stabs fabric. During stab deformation, fabrics are under multi-directional stress.

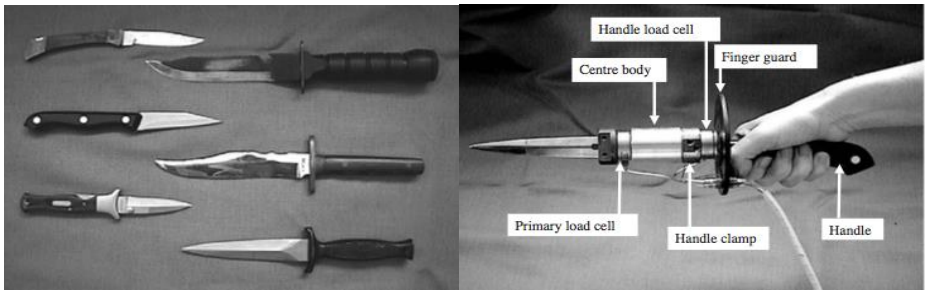

(a) (b)

Figure 2.1 (a) Various knives showing a range of handle shapes and (b) the layout of the instrumented knife

2.4 Stabbing impact on a fabric target

The ability of a knife to penetrate a variety of targets was studied using an instrumented drop tower [8]. It was found that the penetration process consisted of three stages, indentation, followed by perforation then further penetration as the knife slides through the armour while leading to a steadily enlarging hole in the armour. This sequence is superimposed upon a complex interaction of the impacting mass of the knife and the person propelling it with the armour and its wearer. Significant compliance exists between each of these components such that any momentum transfer between the knife and the armour is complicated by the other parts of the system.

2.4.1 Knife resistant systems and energy absorption

In general, the stab resistance can be divided into two categories: knife stab resistance and puncture resistance.

The interaction between a knife and armour is complex with a number of different mechanisms and stages. The energy dissipated against the target was shown [9] to be primarily the combination of the kinetic energy of knife and arm of the attacker. The compliance between the hand and the knife was shown to significantly affect the pattern of energy delivery. Flexibility and the resulting compliance of the armour were shown to have a significant effect on the absorption of this kinetic energy.

Mechanisms of energy absorption in conventional fabric armours are based on fibre fracture, yarn pull-out and fibre plastic deformation. The kinetic energy of the knife can therefore be absorbed by the resistance of perforation of the armour and by providing resistance to further penetration after perforation. And it is apparent that friction plays a major part in the energy absorption process [8].

2.4.2 Fabric failure modes and penetration mechanisms

Both stab and puncture failures are a common type of damage mode caused by a sharp object stabbing into a fabric target. During stab deformation, fabrics are under multi-directional stress.

The fabric failure modes for the knife impactor and the spike impactor are different. The stab resistance includes the knife stab resistance and the puncture resistance. For the fabric failure under the knife drop tower, the cutting of the yarns in the fabric is dominant, while for the fabric failure under the spike drop tower. Therefore, the dominant influencing factors for the cutting and puncture resistance performance of the fabric targets are different.

Due to the paucity of scientific knowledge on the specific case of knife penetration, it is necessary to determine the key effects and mechanisms which occur in the interaction of a knife with an armour.

The penetration of knife blades appears to be relatively complex and involves a number of different mechanisms, the relative magnitude of which depends upon the knife geometry and target material and geometry.

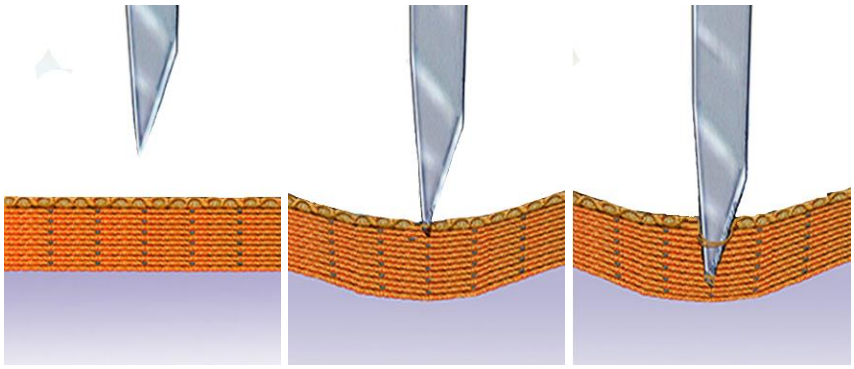

(a) (b) (c)

Figure 2.2 (a) Flexible layer system, (b) indentation, (c) perforation.

Penetration of a blade through a target material occurs in three stages: (i) contact pressure of the tip of the knife withstand a fibre strand, leading to a steady increase in force with knife displacement; (ii) friction of the knife tip against the fabric, leading to a resumption of the increase in force with displacement and (iii) yarn breakage caused by the cutting edge of the knife through the fabric resulting in a steady decrease in force, as shown in Figure 2.2. In multi-ply fabric systems, also it has also been found that the maximum force on the knife occurs during friction against its knife tip (regime ii), i.e. after knife puncture by the tip has occurred [40].

2.5 Factors influencing fabric stabbing resistant performance

2.5.1 Fibre strength

The dominant influencing factors for the cutting and puncture resistance of the fabric targets are different, but the strength of yarn used in the fabric is a critical factor to enhance the stab resistance of the fabric target.

The general features of fibres or yarns used in the target fabrics for energy dissipation are high tenacity and high tensile modulus. Such materials are regarded as impact

resistant materials. The tensile modulus and shear modulus of yarns are the main parameters affecting the stabbing and puncture resistance performance. At the same time, it may be desirable to utilise a fabric having benefits of relatively low bulk and high flexibility. To achieve such properties, polymeric fibres such as aramids and ultra-high molecular weight polyethylene (UHMWPE) make good candidates for the construction of flexible, stab-resistant materials [41].

High performance fibres such as Aramid (e.g. Kevlar® and Twaron®), UHMWPE (e.g. Dyneema® and Spectra®) are the most common materials used to produce soft body armour due to their low-density, high strength, and high energy absorption [42]. The mechanical properties of these commercialised high performance fibres are shown in Table 2.1.

Table 2.1 Typical properties of high performance fibres

Fibre type	Commercial name	Density (g/cm^3)	Elastic modulus (GPa)	Tensile strength (GPa)	Strain to failure (%)
Glass	S-Glass	2.48	90	4.4	5.7
Aramid	Technora	1.39	70	3.0	4.4
	Twaron	1.45	121	3.1	2.0
	Kevlar 29	1.44	70	2.96	4.2
	Kevlar 129	1.44	96	3.39	3.5
	Kevlar 49	1.44	113	2.96	2.6
	Kevlar KM2	1.44	70	3.3	4.0
HMWPE	Spectra 900	0.97	73	2.4	2.8
	Spectra 1000	0.97	103	2.83	2.8
	Spectra 2000	0.97	124	3.34	3.0
	Dyneema	0.97	87	2.6	3.5
PBO	Zylon HM	1.56	270	5.8	2.5

Aramid has aromatic rings between the amide groups that contribute to the high tensile strength and thermal resistance of the fibres. According to the differently orientated chemical linkages, there are meta-aramid (e.g. Nomex®) and para-aramid (e.g. Kevlar® and Twaron®), which have been shown below in Figure 2.3. Because of the structural differences, para-aramid fibres demonstrate higher mechanical properties than the meta-aramid fibres.

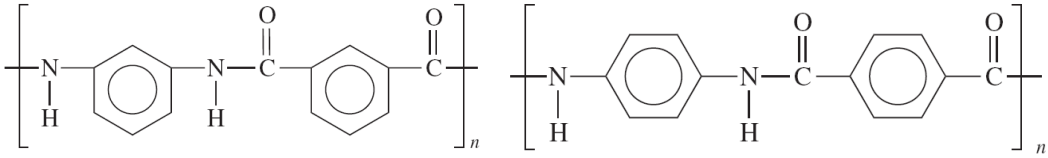

(a) Meta-aramid (b) Para-aramid

Figure 2.3 Chemical structural formulas of the two varieties of aramid

Aramid fibres have unique properties that set them apart from other fibres. Aramid fibre tensile strength and modulus are significantly higher than those of earlier organic fibres, and fibre elongation is lower. They also exhibit inherent resistance to organic solvents, fuels, lubricants and exposure to flame.

The mechanical properties of representative commercialised Meta-aramid and Para-aramid fibres have been shown below in Table 2.2.

Table 2.2 Properties of commercially representative reinforcement fibres [43]

Fibre type	Commercial name	Density (g/cm^3)	Elastic modulus (Gpa)	Tensile strength (Gpa)	Strain to failure (%)
p-Aramid	Kevlar®49	1.44	113	2.96	2.6
	Twaron®	1.45	121	3.1	2.0
m-Aramid	Nomex®	1.38	17	0.65	22

One approach is to weave yarns of these fibres into plain-woven fabrics. These fabrics can provide outstanding ballistic resistance, but in general provide poor stab resistance [44]. Typically, polymer fibres having high tensile strength and high modulus are highly oriented, thereby resulting in very smooth fibre surfaces exhibiting a low coefficient of friction. This lack of energy transfer may correlate to a reduced efficiency in dissipating kinetic energy.

An alternative approach is to incorporate polymer coatings or laminated films into

woven fabrics. The polymer matrix provides additional toughness to the woven fabrics, requiring more energy to cut and separate fibres and yarns. In some cases, abrasive fillers are added to the coatings to further enhance cut resistance. An additional advantage of these materials is that, because they are based on woven high-performance fibres, they can be used to construct body armours resistant to both stab and ballistic attacks [45].

2.5.2 Yarn structure

Apart from yarn strength, yarn structure is also important for stabbing resistant performance. Commercially available, high yarn count aramid fabrics (Kevlar Correctional™, DuPont Company) have been specifically developed to provide stabbing (puncture) resistance. However, these high yarn count fabrics are efficient at stopping spike threats but do not protect against knife threats and they are expensive to manufacture [12]. Additionally, if the warp and weft densities were different, the fabric properties would be different despite the use of the same yarns for the warp and weft directions.

2.5.3 Inter-yarn friction

The yarn pull-out drop tower test attached with knife and spike according to the National Institute of Justice (NIJ) standard for stab testing of protective armours (NIJ 0115.00, 2000) were conducted to evaluate their protection performance [46-47]. The fabric failure modes under the knife and spike drop tower were analysed and the mechanism for the enhancement effect on the knife stab and puncture resistance performance were carefully discussed. Analysis indicated that yarn pull-out can be an important energy absorption mechanism during the stabbing impact of woven Kevlar® fabrics.

Analysis of the indentation process [8] shows that for slimmer indenters, as represented by knives, frictional forces dominate, and indentation depth becomes

dependent upon the coefficient of friction between indenter and sample. Analytical models are demonstrated to provide a reasonable estimate of energy absorption during and after penetration for a wide variety of knives and armour materials. The key armour parameters are shown to be the frictional interaction with the blade and the strength of the target material. The performance of knife blades is shown to increase with increasing sharpness, slimness, and surface finish. No single knife design performs best against all types of armour, and no single armour is best against all knife blades.

Several techniques [48] [18] are known for increasing the inter-yarn friction between the fibres or yarns, such as roughen the surface of the or yarns by sanding or corona treatment, to coat the fabric with a polymer having a high coefficient of friction, coated with a dry powder that exhibits dilatant properties or spinning of high strength fibres in combination with weaker fibres having a higher coefficient of friction. In their work, the fibres demonstrated an improved ability to distribute energy during stabbing threat due to the enhanced inter-fibre friction.

2.5.4 Fabric structure

To improve the stabbing resistant performance of fibres, there one approach is to weave yarns of the fibres into woven fabrics with different structures. Baucom and Zikry [49] compared two-dimensional (2D) and three-dimensional (3D) composite samples. They found that the 3D woven system possessed superior penetration resistance due to the interaction between the surface of the weft and *z*-crimps. Sun [50] tested the puncture behaviours of three kinds of woven fabrics: plain woven, 2/2 twill woven, and 2/1 twill, and found that the yarn strength and yarn pullout behaviour were the key factors influencing the fabric puncture performance. In addition, the fabric construction will also influence the puncture strength because of the different interlacing points.

2.5.5 Panel construction

The approaches adopted in previous paragraphs have specifically excluded the investigation of target flexibility and the interaction of the target with its support. Historical data suggests that armour was almost always backed with heavily padded layers ostensibly to absorb impact energy and reduce trauma. Recent work by Watson *et al.* [51] has shown that the presence of padding layers in front or behind the armour can significantly increase its penetration resistance. It is considered that such layers aid in the movement of the armour in the same direction as the impact such that the initial contact stresses are reduced and the interaction distance is increased.

It has been shown [13] that the measured penetration resistance of an armour is substantially increased when a softer backing block material is used. In theory, it should be possible to describe an armour which dissipated no energy at all but simply transfers the input momentum onto its support where it is then dissipated in plastic deformation or movement. The significance of this effect can be examined by investigating the effect of target support compliance.

Mayo *et al.* [45] laminated Polyethylene, Surlyn, and co-extruded Polyethylene Surlyn films of various thicknesses into fabrics and compared with neat fabrics at equal weights and layer counts. The thermoplastic-laminated fabrics improve the stab and puncture resistance of the fabrics by means of combining increased cut resistance and reduced windowing. Wang *et al.* [52] coated the resin in the woven fabric, dramatically improving the puncture resistance of the uncoated woven fabric by the uniform distribution of stress during puncture damage.

2.6 Evaluation of stabbing performance

The protection levels for body armour are regional and variable throughout the world. There are two most commonly recognised standards for body armour, which are the US National Institute of Justice (NIJ) and the UK Home Office Scientific

Development Branch (HOSDB). These are the considered "model" standards, and they are used by many other countries around the world.

2.6.1 NIJ Standard

NIJ Standard-0115.00 defines the minimum stab armour needed conditions to protect the body from sharp injuries. At the same time, the standard also describes the testing methods and detailed explanation of tools. The tool is divided into two categories of edged blade and spike. The protection level will be divided into two zones El and E2, and each protection level also includes three different protection levels. The protective levels are shown below:

Table 2.3 The protective levels of the NIJ standard [53]

Protection Level	"E1" Strike Energy (J)	"E2" Overtest Strike Energy (J)
1	24±0.50	36±0.60
2	33±0.60	50±0.60
3	43±0.60	65±0.60

The stab experiments in the NIJ standard include an experimental knife, knife holder and a knife rail device for falling. This knife rail device guides freefall impact on the pre-determined point. Impact knives include of Pl type unilateral edged blade knife and S1 type bilateral edged blade knife. Schematic of armour and knife arrangement is shown in Figure 2.4.

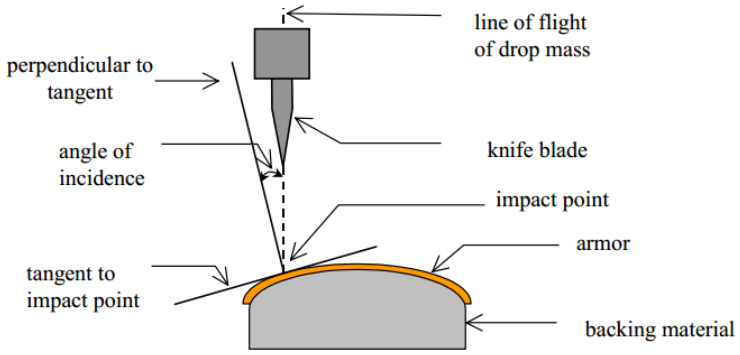

Figure 2.4 Schematic of armour and knife arrangement [53]

2.6.2 HOSDB Standard

The HOSDB are considered the leading organisation in the world in stab and spike testing for body armour [54]. The test rig they developed makes use of a guided rail drop tube assembly, enabling the knife/spike missile to fall under the influence of gravity and strike the armour sample at a pre-determined point of impact. The guide rails, situated inside the tube, prevent the knife/spike missile from rotating about its vertical axis during its descent. These rails also ensure that the test implements strikes at the correct orientation so that any weakness in the armour design can be fully determined. Drawings of the drop tube and knife/spike missile are available from HOSDB.

The knife/spike missile consists of separate steel and alloy knife and spike holders of mass 0.65kg ± 6.5g (including the knife or spike) housed in a nylon missile casing of mass 1.25 kg ± 13g. The casing is designed to ensure minimal friction between the missile and the inner walls of the tube during its falling motion. The missile length is sufficient to ensure that part of the body remains inside the drop tube throughout a test drop impact. The nylon body must be replaced if it becomes damaged. The knife/spike holder is free to slide vertically within the nylon body casing. However, sandwiched between the base of the knife/spike holder and the nylon casing, are two 50mm diameter discs of Plastazote® foam. As the knife/spike holder is forced into the casing under load, the foam is increasingly compressed. The typical test apparatus for knife and spike testing is shown in Figure 2.5.

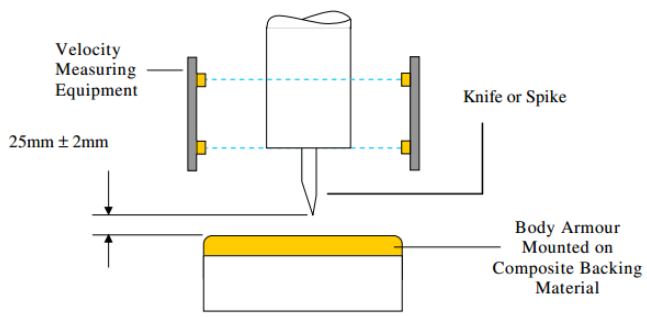

Figure 2.5 Typical Test Apparatus for Knife and Spike Testing [55]

2.6.3 Comparison between NIJ and HOSDB Standards

The NIJ and HOSDB often work together and share testing methods, so a piece of body armour that meets a standard set by the NIJ will also pass the equivalent HOSDB standard. The standards that cover 3 areas of protection for body armour - ballistic, stab and spike. It is important to note that a piece of body armour will only provide protection against the threats that it is designed to stop. For example a bullet proof vest will not provide protection against stab based attacks, equally a stab proof vest will not stop a bullet.

The NIJ is considered the world leader for ballistic testing for body armour, they perform a full range of tests and provide details of the results in their body armour standards. The HOSDB are considered the leading experts in the world in stab and spike testing for body armour, and their standards also feature full details of the tests performed and the protection levels achieved.

The NIJ and HOSBD body armour standards outline exactly what threats each piece of body armour will protect against, and also the strength of the attack it will stop. For example, a bulletproof vest will only provide protection against a certain velocity of the bullet, and that protection depends on the level the vest has been tested to. The same is true for a stab proof vest, it will be tested to a certain level of protection, depending on the strength of the threat it can withstand.

2.7 Research approaches for stabbing resistant textiles

Stab attacks generate high loads [56]. In order to defeat them, armour needs to be of a certain thickness and stiffness [57]. Stab resistant body armour is now a standard item of equipment for police officers in the United Kingdom. The armour is usually required to have a stab resistance as specified by the Police Scientific Development Branch standard (Croft, 2003). The body armour must resist penetration by a specific

blade type, delivered at a specific energy level or range of levels. The body armour is formed from composites which include layers of a fabric base, formed from high tenacity fibres, and a rubber layer bonded to the fabric base. A thermoplastic bonding layer may be used to bond the fabric and rubber layers together. If ballistic resistance required, the body armour also need include a ballistic resistant composite of a network of high tenacity fibres. Brooker [58, 59] presented a user-defined material constitutive model with the finite element program ABAQUS to predict the puncture behaviours of a pipeline under external interference loading by excavator teeth. In addition, a parametric study was performed to derive a design equation giving the puncture load for contact normal to a pipeline. Sun *et al.* [50] reported the quasi-static puncture behaviours of three woven fabrics with different structural parameters by using experimental and FEA approaches. The microstructure level FE model of woven fabric revealed three damage stages during puncture process.

In the references reported so far, few researches have been carried out on the stab behaviour of the woven fabric. The numerical simulation is valuable for providing detailed information on the stab damage and the influence of fabric property parameters on the stab strength [52].

2.8 Ballistic impact on a fabric target

When a projectile strikes a target, the response is believed to be a combination of global and local effects [60]. Global response indicates the material behaviour away from the impact point and local response refers to the material behaviour directly contacting the projectile, as shown in Figure 2.6. Impact velocity is, if not the only factor, one of the most important factors to determine target response. Cantwell and Morton suggested that, on a composite target, at high impact velocity, local damage plays a major part in energy absorption, While at low impact velocity, global plate deflection becomes more important [61, 62]. The velocity classification indicated the

range of high velocity and low velocity, as is shown in Figure 2.7 [60]. This phenomenon is also observed in textile materials. Carr [63] found that Textile yarns also tend to have a global failure model (transmitted stress wave) at low impact velocity and a shear or plug failure mode at high impact velocity.

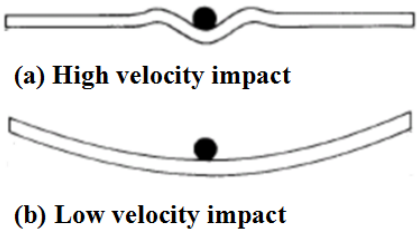

Figure 2.6 Response of a fabric target subjected to transverse impact

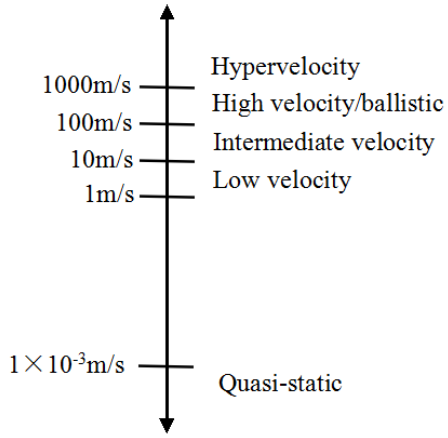

Figure 2.7 Standard classification of impact velocity [60]

2.8.1 Global response

At low impact velocity, as there is enough time for projectile kinetic energy to be transferred to the fabric target, larger areas get involved in energy absorption than at high impact velocity cases. The existence of yarn crossovers significantly influences the propagation of longitudinal waves. It has been observed that reflection of longitudinal waves takes place on at yarn crossovers and the strain distribution in the woven fabric is therefore influenced by the crossover density [64]. The longitudinal wave speed in plain woven fabric is suggested to be slower than that in a single yarn by a factor of $\sqrt{2}$. Roylance [65] also pointed out that wave reflection is associated with fibre modulus and coefficient of friction.

2.8.2 Local response

At high impact velocity, as the projectile engaging time with the fabric target becomes short, the influence of global response on energy absorption diminishes. Fabric local reaction or failure mode has a major effect on ballistic performance. One of the major fabric failure modes is yarn or fibre rupture. This occurs when the yarn or fibre strain exceeds their failure strain. Different fibre rupture is characterised by different broken ends. For para-aramid fibres, it has been observed that fibre failed by fibrillation. Shear failure was noticeable on the UHMWPE fibre broken ends [66].

2.9 The response of fabric target to ballistic impact

Cunniff [67] states that the energy absorption characteristics of fabric systems under ballistic impact are influenced by a number of factors including fibre properties, weave style, the number of fabric layers, areal density, projectile parameters, and impact parameter.

The propagation of the longitudinal and the transverse wave

When a fabric sample is impacted, two wave fronts are generated, namely a transverse wave and a longitudinal wave. Energy is dissipated through the propagation of the two types of wave. The longitudinal wave travels outward along the fibre axis at the sound velocity of the material from the point of impact. This wave also causes the yarn to be stretched and have in-plane movement. The longitudinal wave travels at a velocity

$$c = \sqrt{\frac{E}{\rho}} \qquad (2.1)$$

where c is the longitudinal wave speed in m/s, E is the fibre modulus in Pa, and ρ is the yarn bulk density in g/m^3.

Regarding the equation, the velocity of propagation in the para-aramids is directly

proportional to the square root of the modulus and inversely proportional to the square root of the fibre density which is about 800m/s. This relates directly to the volume of matter that can participate in the wave propagation and energy dissipation.

At the same time, the projectile tends to push the yarn forward and therefore deflect the yarn vertically, which consequently results in an out-of-plane motion of the material. Gu studied the velocity of the transverse wave [68], and determined the velocity with respect to the laboratory u_{lab} as below.

$$u_{lab} = c(\sqrt{\varepsilon(1+\varepsilon)} - \varepsilon) \qquad (2.2)$$

where ε is the strain in yarn.

The two types of wave are depicted in Figure 2.8.

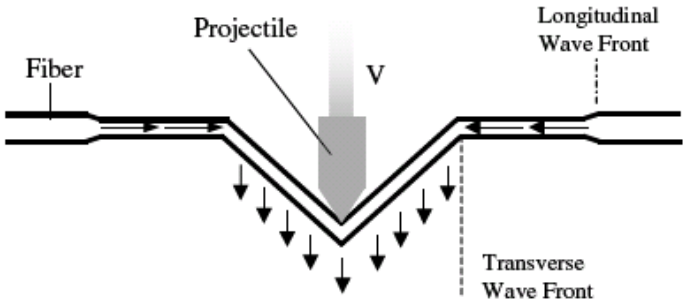

Figure 2.8 Projectile impact into a ballistic fibre [64]

Transverse and longitudinal wave propagations have common physics, although the former more directly affects the local deformation and penetration of the matter being impacted at the ballistic strain rate.

2.10 Factors Influencing Fabric Ballistic Performance

Literatures regarding the influencing factors on fabric ballistic performance have been mentioned in a number of works [69-71]. The energy absorption behaviour of ballistic

fabric is an interplay of many mechanisms. It is difficult to isolate and discuss any one of them. For example, if fabric ballistic performance is solely dependent on fibre tensile strength, nylon would be a better material than Kevlar [72]. The fact is that Kevlar proves to be the most popular high-performance fibre in making soft body armour. This section will give a detailed description of those factors.

Cunniff [67] identified fibre properties, fabric structure, the number of fabric layers, areal density, projectile parameters, and impact parameters as the major factors in the energy absorption of high tenacity fabrics. A critical review by Cheeseman and Bogetti [7] added that in addition to the factors above, the interactions between fabric layers, the boundary conditions, friction between yarns and friction between the yarns and the projectile are also important factors in impact energy absorption. Recently, novel solutions to enhance the ballistic performance of fabrics have been proposed. The most common characteristic of those methods is to modify the fabrics to enhance the efficiency of the interaction of the yarns to defeat the projectile.

2.10.1 Fibre properties

As a mechanism for energy dissipation, the energy absorbed due to yarn/fibre rupture is based on fibre properties. Roylance and Wang [73] established that approximately half of the total energy absorption is stored in the form of strain energy. By comparing the ballistic resistance of dry Spectra fabrics with their corresponding laminates, Lee *et al* [74] correlated the number of broken yarns to the energy absorbed. He also found that fibre straining is the primary mechanism of energy absorption. In the fabric target, the accumulation of strain energy is determined by the area getting strained. The strained area is directly associated with the velocity of sound in the material [75], which is also considered to be the velocity of the longitudinal wave. According to equation 2.1, this velocity is a function of material modulus and density. By using a numerical model, Roylance and Wang [73] established that higher modulus fibre

gives higher wave velocity, which leads to a rapid energy absorption rate. As the modulus is decreased, the wave velocity is decreased and the strain is more concentrated in the vicinity of the impact zone, as shown in Figure 2.9 This is reinforced by Field and Sun's experimental work [76]. They used a high speed photographic approach to observing the behaviour of fibres and woven fabrics upon transverse impact. They found that fabric with high modulus can spread load onto other fibres and layers more quickly, which is beneficial in ballistic applications.

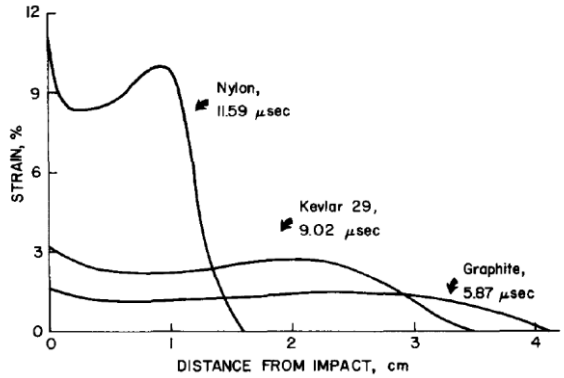

Figure 2.9 Strain profile along orthogonal yarns passing through the impact point

Nevertheless, Roylance [77] analysed the strain energy-fibre modulus relationship and reported that a fibre of high modulus was usually obtained at the sacrifice of elongation at break. He suggested that high modulus (graphite) leads to a high rate of energy absorption, but the panel would fail at an early stage and therefore not be able to extract energy as effectively as the low modulus fabrics, such as Kevlar or Nylon. This feature greatly decreases the total energy absorbed by the fabric panel, which is shown in Figure 2.10 [73].

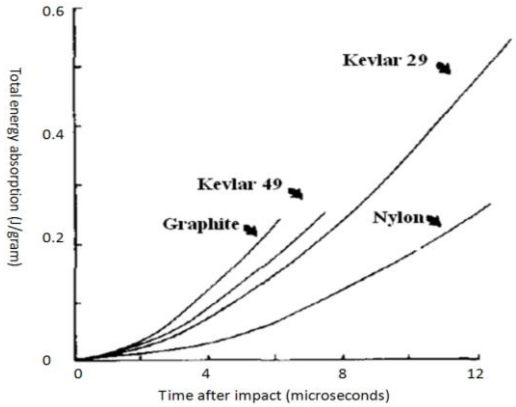

Figure 2.10 Comparison of total energy absorption for different fabric panels [73]

As a result, it is difficult to take into account just one or two factors when selecting high performance fibres for ballistic applications. Through research work, Cunniff [78] has determined that fibre ballistic property is a function of a number of parameters, including material density and the velocity of sound in a fibre. The fibre property is to be denoted by U^* (having units of m^3/s^3):

$$U^* = \frac{\sigma\varepsilon}{2\rho}\sqrt{\frac{E}{\rho}} \qquad (2.3)$$

where σ is the fibre ultimate tensile strength in N/m^2, ε is rupture strain.

2.10.2 Yarn structure

The effect of yarn structures on ballistic protection mainly depends on the utilisation efficiency of individual fibres. Cunniff [79] found that the efficiency is lost in going from a fibre to a yarn, from a yarn to a fabric and from a single fabric to a multi-layer fabric. This is because each individual fibre shares different loads when it comes into contact with a bullet, and therefore fibres tend to break successively instead of together. In order to achieve even load sharing, finer fibres are used in ballistic applications due to the higher fibre to fibre cohesion. In addition, yarn used in ballistic fabric usually has a low twist or even no twist. Too high a yarn twist angle will lead to yarn slippage and the projectiles are more likely to penetrate the fabric through the yarn spacing. Rao and Farris [80] found that the optimum twist angle which is able to maximise the yarn strength while giving the minimum yarn slippage is around 7°. Other yarn features such as the fibre array have an influence on yarn mechanical properties as well.

2.10.3 Fabric structure

The most commonly used fabric structure in the soft body armour area is woven fabric. Woven fabrics stop projectiles by forming a network of fibre or yarns. This

network enables the fibre or yarns to be stretched, transmitting projectile kinetic energy to the fabric. Among various weave patterns, the plain fabric is the most common pattern due to its high interlacing yarn density and dimensional stability [81]. Cunniff [79] also pointed out that loosely woven fabric or fabric with an unbalanced pattern result in inferior performance. 3-D fabrics have also been studied for their applicability in ballistic protection. Angle interlock fabrics were investigated by Yang [82] for use in female body armour and the orthogonal fabric was modelled and tested by Shi *et al* [83].

Weave density of the fabric, which is known as "cover factor", is a function of the number of warp picks and weft ends in a unit of length of fabric and indicates the percentage of area covered by the fabric. High cover factor will increase the available dissipation of strain energy capability by getting more fibres and yarns engaged with a projectile. Shockey [84] studied Zylon fabrics with various weave densities and observed that the increase in energy absorption is almost in proportion to the increase in weave density. It has been suggested that the cover factor should be in the range of 0.6 to 0.95 [85] for ballistic applications. When cover factors are greater than 0.9, yarn properties degrade in the process of weaving and when the cover factor fall below 0.65, the fabric will become too loose. The 'wedge through' effect is more likely to occur on loosely woven fabrics, which is depicted in Figure 2.11.

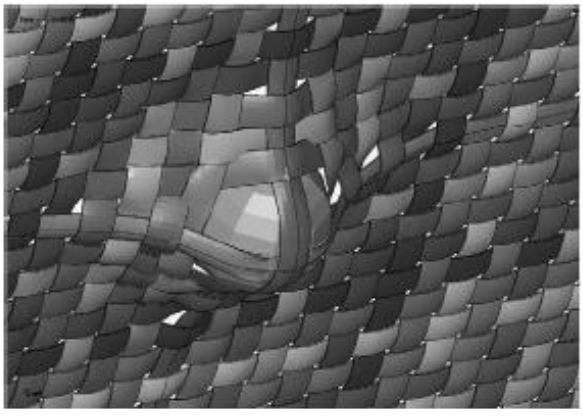

Figure 2.11 "wedge through" effect [69]

2.10.4 Panel systems

There is no shortage of work regarding the ballistic performance of multiplied textiles. Shockey *et al.* [86] observed that the energy absorption is always in proportion to the number of plies. Lim *et al.* [87] investigated the reinforcement effect of backing layers on the ballistic performance with different projectiles. The comparison showed that the spaced armour system gives better performance than the layered system except for flat-nosed projectiles. They also concluded that the benefit of reinforcement is largely highly dependent on the impact velocity and projectile nose shape. This is supported by Porwal and Phoenix' s theoretical work. Porwal and Phoenix [88] developed an analytical model to study the response of materials in a double-plied armour system. They observed that the V_{50} degrades progressively as the spacing of the layers increase when compared to the system without spacing (the definition of V_{50} will be presented in section 2.11.3.

Cunniff [79] also suggested that the subsequent plies of fabric may constrain the transverse deflection the front plies, which is considered to affect the performance of a panel. As a result, he believed that placing low modulus materials on the impact face and high modulus on the subsequent plies may avoid this phenomenon and improve the performance of the ballistic panel. In addition, Nader and Dagher [89] used non-aggressive barbed needles to place fibre through the thickness in a panel, preventing the projectile from spreading the individual yarns and the adjacent layers from delamination. Chitrangad [85] found that the weft yarns are stretched to break before the warp yarns in a ballistic event. By using a fabric with the weft yarns having a higher elongation to break than the weft yarns may enable the warp and weft yarns to break at the same time, which improves the performance of a fabric or panel.

2.10.5 Friction

Another energy absorption mechanism is friction. This includes energy dissipated by friction between warp and weft yarns, projectile and fabric target and between

adjacent fabric layers. Although they are considered to contribute very little to overall energy absorption, frictional effects greatly influence the strain and kinetic energy absorbed by fabric [90]. The absorption of the kinetic energy of the projectile is related to the wave propagation, transversely and longitudinally, and the penetration stress/strain profile which largely depends on the frictional energy dissipation [6].

Frictional mechanisms include frictional dissipation due to yarn slippage，the interaction of the projectile and fabric or the interaction between adjacent layers. It is believed that the magnitude of frictional energy is influenced by many factors, such as the yarn-yarn coefficient of friction and boundary conditions [91]. Duan *et al.* [90] investigated the role friction played in a ballistic event through finite element analysis. They found that although energy dissipated by friction accounts for a small amount of the total energy, projectile-fabric friction resists yarn slippage and enables more yarns to engage with the projectile, which greatly increases the kinetic energy and strain energy associated with the fabric target. The fact that impact load could be distributed along the periphery of the projectile fabric contact zone also delays yarn failure. Yarn-yarn friction, however, restricts yarn movement and leads yarns to fail at an early stage.

Another fabric failure mode is yarn pull-out. When the impact velocity is low or yarn-yarn friction is low or the fabric target is loosely gripped, principal yarns will be pulled out rather than damaged. Bazhenov [92] found that yarn pullout is related to the energy absorption of a ballistic fabric. Starrat [93] used a series of photographic and velocity measurement technologies and concluded that yarn pullout contributes a significant amount of energy absorption in non-penetration cases. Kirkwood and his colleagues [94, 95] present a semi-empirical model to quantify the energy dissipated yarn in pull-out. They believed that the two main mechanisms associated are yarn de-crimping and yarn translation. And the pull-out force is highly dependent on yarn-yarn friction.

2.10.6 Boundary conditions

In penetration tests, as the fabric or panel samples need to be gripped by a clamp, the boundary condition plays an important role in fabric energy absorption. Cunniff [79] used a chisel-nosed fragment simulator to test a single-ply Kevlar woven fabric on an aluminium plate with different apertures. He found that the ballistic performance is strongly dependent on the aperture size at impact velocity near the ballistic limit of the fabric. It was believed that a small holder aperture constrains both transverse and longitudinal deflection. As the impact velocity increases, the effect of aperture decreases. Slippage of the fabric between sample holders was observed, but Cunniff paid less attention to the relationship between the fabric performance and the clamping pressure. Lee *et al.* [74] investigated the energy absorption capability of compliant Spectra laminate over a range of clamping pressures in a quasi-static drop-weight test. They found that the energy absorption at a clamping force of 2 kN was about 4.5 times higher than that at a force of 254 kN. When the clamping force exceeds 254 kN, the energy absorption is found to be independent of the clamping force, indicating that no slippage took place during impact. Chitrangad [96] noticed that tensioned fabrics give better ballistic performance than un-tensioned fabrics.

Zeng *et al.* [97] and his colleagues carried out ballistic tests on fabrics with three types of boundary conditions: four-edge-clamped, two-edge-clamped and four-edge-clamped with yarns running 45° to the edges and the built up computational simulation to study the effects of yarn orientations and clamping directions on energy absorption. The results suggested that for a high velocity regime, such as at an impact velocity of 450m/s, the amount of energy absorbed by the fabric on three different boundary conditions is almost equal, which is shown in Figure 2.12.

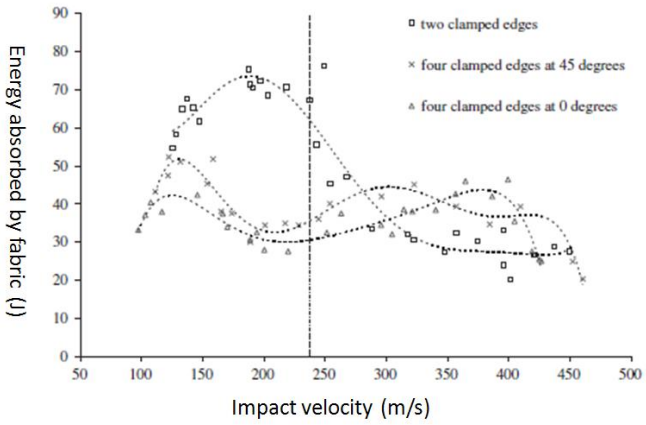

Figure 2.12 Energy absorption of fabric targets with different boundary conditions [97]

Under a low impact velocity regime (lower than 250 m/s), fabrics clamped along only two edges give superior energy absorption characteristics to those of the other two conditions for the low velocity regime. It is quite interesting to note that clamping the four edges at 45° improve the ballistic resistance slightly. The prime reason for this phenomenon is that the rotation of the fabric contributes to an increase of strain energy in the whole fabric. When compared to fabric with a clamped angle of 0°, the length of the primary yarns increases and yarns originally remote from the impact point become shorter. As a result, longer principal yarns are able to distribute more projectile kinetic energy and shorter secondary yarns are more easily stretched, and therefore more of the fabric gets involved in the deformation zone.

The looseness of the yarn ends at the boundaries is key elements in terms of the wave propagation, both longitudinally and transversely. A simplified physical explanation relates to the reflection of the wave at the boundaries, which if they are too tight or compact, tend to promote a series of multiple reverberations back to the impact region, amplifying the local stress and causing stress concentration, further helping the projectile penetration [6].

2.11 Evaluation of ballistic performance

When an individual wearing body armour is hit by a bullet, penetration through the vital organs is most often fatal. A non-penetrating injury, in which the deformation of armour results in blunt trauma, can cause severe internal damage [112]. Thus, ballistic materials with the capability to both prevent a bullet from penetrating and reduce blunt trauma by absorbing impact energy are demanded.

As the investigation of ballistic impact progresses, the evaluation methods used for assessing the ballistic performance of body armour have been established as well. According to the requirements of ballistic soft body armour, there are three test methods frequently used. They are perforation test, non-perforation test and ballistic limit test. These three methods are applied to evaluate the different aspects of ballistic performance. The perforation test is mainly to assess energy absorption. The non-perforation test is to assess the blunt trauma caused by the deformation of the soft body armour during actual application. Ballistic limit test aims to evaluate the limit of ballistic performance, in other words, the pass or fail performance.

2.11.1 Perforation test

The perforation test is described by that a projectile or a bullet fully getting through a testing target during the impact process. In the perforation test, the impact velocity and the residual velocity can be measured. Thus, variation in projectile energy loss can be calculated from these two velocities [98-102], as shown in Equation 2.4. In order to compare the projectile energy losses of panels with different weights, an indicator of total energy loss divided by the areal density of the fabric panel is also used.

$$\Delta E = \frac{1}{2} m(v_s^2 - v_r^2) \qquad (2.4)$$

where ΔE is projectile energy loss; m is the mass of a projectile; v_s is impact velocity, and v_r is residual velocity.

Without any other external force action and without considering energy loss by heat, intermolecular friction, air resistance, acoustic energy and so on, the projectile energy loss can be assumed to be fully absorbed by the fabric based on the law of energy conservation. The energy dissipation in the fabric takes place mainly in three ways [103-109]: (i) kinetic energy due to the movement of the fabric caused by longitudinal wave and transverse wave; (ii) strain energy due to the deformation of yarns stressed; and (iii) frictional dissipation energy because of inter-yarn friction. The energy transfer between the projectile and fabric can be simply described in the following equation：

$$E_p = E_f = E_{KE} + E_{SE} + E_{FDE} \qquad (2.5)$$

where, E_p means projectile energy loss; E_f means energy absorption of a fabric; E_{KE} means kinetic energy (KE); E_{SE} indicates strain energy (SE); E_{FDE} represents frictional dissipation energy (FDE).

2.11.2 Non-perforation test

The non-perforation test is used to understand the ballistic resistance of soft body armour in real situations. Normally, in the test, a fabric panel is positioned on the surface of a backing material, which is made of oil-based clay and used for simulating human skin. After impacting, a hole would be left on the surface of the backing material due to the transverse deflection of the panel. The hole is an indication of blunt trauma brought to a wearer, which is also harmful to the wearer. Although the fabric deflection is a manner to dissipate the projectile energy, it is still anticipated that the fabric would transversely deflect as little as possible at the end of impacting.

The blunt trauma of a fabric panel is usually evaluated by the depth of the hole, depressed on the backing material. The depth of the hole is measured from the plane defined by the front edge of the backing material fixture [110] as shown in Figure

2.13. The measurements have been comprehensively described in the US National Institute of Justice (NIJ) standard [110] and the Home Office Scientific Development Branch standard (HOSDB) [111], both of which are widely used as trauma test models.

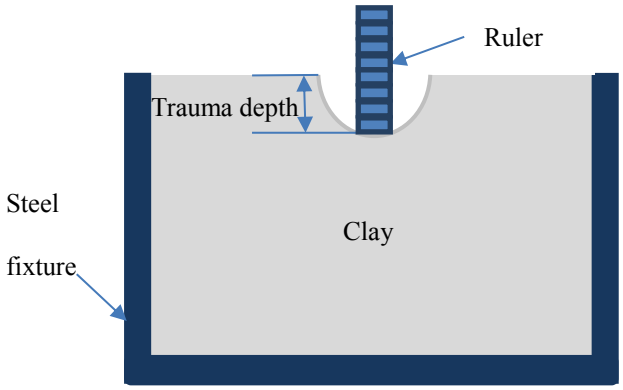

Figure 2.13 Methods of measuring back-face deformation

According to National Institute of Justice (NIJ) Standard 0101.04, ballistic armour is classified into seven levels. Type I, IIA, II and IIIA offer increasing levels of protection against handgun threats. Types III and IV are designed for protection against high powered rifle rounds, which are intended for application only in tactical situations [110]. The maximum deflection of a soft armour vest can undergo without perforation is 44 mm for all levels of ballistic threats. The apparatus for the test is shown in Figure 2.14.

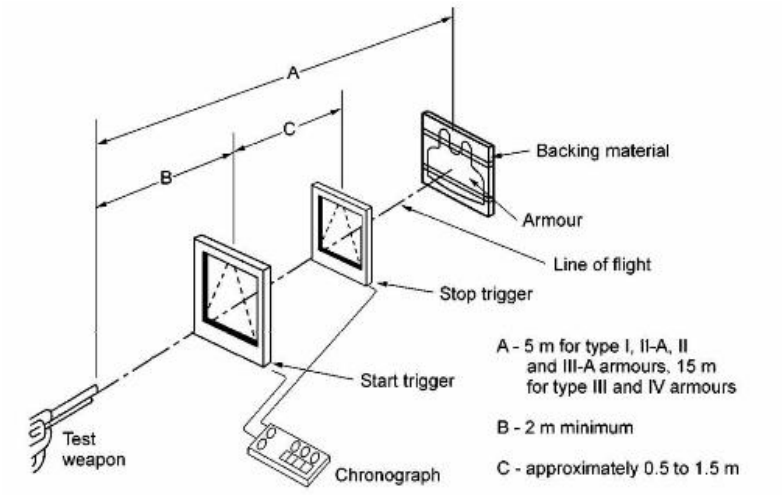

Figure 2.14 Test range configuration [110]

HOSDB standard presents a method used for evaluating the ballistic performance of body armour system for the British Police, which is required to protect the human body sufficiently against both projectile perforation and blunt trauma. The number of the ballistic performance level is five, including HG1/A, HG1, HG2, SG1 and RF1. The maximum indentation depth permitted from any test shot is 25 mm measured from the top edges of a steel tray containing the backing material except that the maximum indentation depth for HG1/A is 44 mm.

The depth of the hole is a simple indicator for the blunt trauma of a fabric panel [112-118]. Other indicators are also developed to denote it. Karahan [119] tried to regenerate the volume of the hole by Spline curve fitting technique. It may be suitable to a regular hole formed on the backing material. However, when it encounters irregular shape, it would fail. In most cases, the geometry of the hole left on the backing material is irregular. The energy absorbed by the backing material is associated with the volume of the hole formed on the backing material. Due to the difficulty in measurement of the volume, the energy absorbed by the fabric in the non-perforation test is still difficult to obtain.

2.11.3 Ballistic limit test

To evaluate the fail or pass property of body armour in a ballistic impact event, the ballistic limit test is applied. Ballistic limit designates a velocity at which a projectile completely perforates specific armour when hitting at a specified angle of obliquity. This velocity is named as ballistic limit velocity. It is the incident impact velocity for a specific projectile and target combination, which would lead to complete perforation of the target with the projectile tip reaching the back face of the target with zero residual velocity [120, 121]. Villanueva and Cantwell [122] derived an equation for estimating the ballistic limit of laminates, expressed in Equation 2.6.

$$V_b = \frac{\pi\tau\sqrt{\rho_t\sigma_e}D^2T}{4m}\left(1+\sqrt{1+\frac{8m}{\pi\tau^2\rho_tT}}\right) \qquad (2.6)$$

where V_b is ballistic limit, τ is a projectile constant determined experimentally, ρ_t is the density of the laminate, $\sigma_e$is the static linear elastic compression limit, D is the diameter of the projectile, T is the thickness of the laminate, m is the mass of the projectile.

Due to the cost of ballistic impact tests, the impossibility of controlling impact velocity exactly and the difficulty in distinguishing complete perforation from partial perforation under apparently identical conditions, statistical approaches are necessary, based upon limited firings [123]. Hence, V_{50} is commonly used instead of V_b. V_{50} is defined as the average of an equal number of highest partial perforation velocities and lowest complete perforation velocities for a specific projectile and target system, which occurs within a specified velocity range. In other words, V_{50} defines incident impact velocity at which there is 50% probability of perforation and 50% probability of non-perforation [120, 121]. The normal up-and-down firing procedure is applied. A 0.51 mm thick 2024 T3 sheet of aluminium is positioned 152 ± 12.7 mm behind and parallel to the target to witness complete penetrations. Normally, A minimum of two partial and two complete perforation velocities are used to compute V_{50}. Four, six, and ten-round ballistic limits are frequently used. The maximum allowable velocity span depends on the armour material and test conditions and spans of 18, 27, 30 and 38 m/s are commonly used [123]. In addition, Nilakantan *et al.* [124] attempted to approximate the complete perforation velocity and no complete perforation velocity. They derived two ballistic limit velocity, V_1 and V_{99}, for evaluating the ballistic limit performance of almost non-perforation impact and almost perforation performance respectively with consideration of the probabilistic nature. The method for calculating V_1 and V_{99} are shown in Equation 2.7 and Equation 2.8 respectively.

$$V_1 = \delta - 2.3263\gamma \qquad (2.7)$$

$$V_{99} = \delta + 2.3263\gamma \qquad (2.8)$$

Normally, V_{50} ballistic velocity limit is accepted as the performance parameter.

2.12 Research approaches for ballistic textiles

It is understood that impacting the fabric in the transverse direction with a high-velocity projectile is a dynamic, complicated and instantaneous physical process. It is far different from the quasi-static mechanical action. Currently, three methodologies are frequently adopted in the analysis of this complex physical phenomenon: empirical, analytical and numerical. These three approaches can be applied individually in research or combined to provide more understandings about the damage and failure mechanism of the fabric subjected to ballistic impact.

2.12.1 Empirical approach

Empirical methodology usually acquires the first-hand data based on a certain experimental design and the device provided. Through analyses of data, the response characters of a fabric can be examined and the constitutive relations can be established. The analysis process may consist of curve fitting, nonlinear regression analysis of experimental data, and the use of statistical distributions [125]. It is powerful and useful when a few numbers of variables are to correlate to [126-131]. Majumdar *et al*. [27, 132] and Park *et al*. [133, 134] used it to investigate the ballistic performance of treated fabrics. However, the disadvantage is also obvious for that it is a time consuming and material costly process. Additionally, the accuracy of the obtained results to a large degree depends on the correctness and completeness of collected data.

2.12.2 Analytical approach

The analytical methodology is mainly from a physical perspective and relies on general mechanic laws to set up governing equations using various parameters involved in the ballistic impact process. In the analysis, the whole process is divided into *n* steps by a small increment of time. At the first increment, the equations are usually derived based on energy conservation, impulse theory and Newton's second law. Analogously, step by step, until the ultimate time, all the equations at every time

increment are derived. Up till now, numerous researchers devoted themselves to making a contribution to this field and applied this method to provide insight into the mechanism of damage and failure of a fabric in the impact event [135-148]. The results predicted by this method are usually validated by comparing with experimental results. Compared with the empirical method, the analytical method consumes fewer materials and relies on less labour. However, it needs a complete understanding of ballistic impact process. Additionally, in order to simplify the process, some of the parameters tend to be neglected. Inter-yarn friction is one of those factors. The truth is that the inter-yarn friction plays a significant role in energy absorption during the impact [103, 104].

2.12.3 Numerical approach

Over the previous decades, continuing efforts are made to reduce the extent of experimental test programs. Investigation of ballistic impact is developing towards the direction of simulating. Owing to the advent of the computer, the study of ballistic impact with computer-based analyses and simulations is possible. The numerical investigation is an investigation approach on the basis of the Finite Element (FE) theory and commercial computer software, such as ABAQUS, ANSYS and LS-DYNA, to establish projectile-fabric simulation model for elucidating the mechanism behind a fabric subjected to impact. FE theory is better suited to analyse dynamic mechanic problems and a bullet striking a piece of fabric is rightly a dynamic mechanics problem. The conception of FE theory is that the integrity is divided into limited and small units, which is called mesh, and the displacement, strain and stress of individual mesh are computed step by step when loaded. Eventually, varieties of stress and strain experienced by a yarn can be acquired. It is an efficient and effective approach because the complex and instantaneous process would be converted into a controllable and visual process through the simulation. Consequently, a large number of researchers started to investigate ballistic behaviours of fabrics using FE simulation.

2.13 Introduction to Shear Thickening Fluid

2.13.1 Understanding the rheology of structured fluids [149]

2.13.1.1 Types of fluids: simple and structured fluids

Fluid materials, by definition, are systems which flow when subjected to stress. How they respond to an input stress is the heart of rheological testing and is a complex issue. There are many types of fluids: pure substances, mixtures, dispersions and solutions, falling into the categories of either simple or structured fluid. Each has its own unique behaviour when subjected to stress. In general, when a material has a uniform phase, such as a solution or pure substance, it is referred to as a simple fluid. Materials which contain more than one phase, such as solid particles dispersed in a liquid, gas particles in foam or an emulsion of immiscible liquids are considered structured fluids since their rheological behaviour is in general dominated by the interactions of the constituents.

Many of the materials we use are structured fluids. Most foods, cosmetics, pharmaceuticals and paints contain particles or droplets of an immiscible fluid suspended in a carrier liquid. A number of soft semisolid materials also fall under the category of structured fluids since they have a multiphase structure and exhibit complex flow behaviour. Some examples would be cheeses, lipstick, caulk, and bread dough.

Many factors affect the stability of structured fluids. The viscosity of the liquid phase in dispersions usually plays an important role on the flow properties of the material. Dispersions have wide variations in performance depending on particle size, shape, concentration, and any attraction with the continuous phase in which they are suspended. When there is a repulsive electrostatic or steric force between particles they tend not to settle rapidly, instead of forming a network structure which will stabilise the suspension if undisturbed. Shearing or even Brownian motion can destroy this delicate structure and break down the viscosity of the fluid.

Structured fluids do not obey a simple linear relationship between applied stress and flow (Newtonian fluid behaviour) for suspensions of latex particles with increasing volume fraction in water. Nearly all these materials have a viscosity that drops at higher rates of shear stress. This is the phenomenon of shear thinning which becomes progressively larger as the volume concentration of solid particles increases. At high concentration of solid content, the low shear rate viscosity region disappears completely, the material is yielding. Some materials show after the shear thinning region with increasing rate or stress, an increase of the viscosity, usually due to structure rearrangements as a result of the applied shear. This is referred to as flow induced shear thickening.

2.13.1.2 Characteristic flow parameters and functions of structured fluids

(1) Bingham Flow

Materials which exhibit Newtonian flow beyond the yield bear the name Bingham Fluids. This kind of fluids must attain a critical level of stress in order to initiate flow, which the reason why you need to shake or tap a bottle to make the ketchup flow.

(2) Plastic Flow

Most materials do not exhibit Newtonian flow after the yield, but have a viscosity that decreases (shear thinning) until a plateau is reached. Lipsticks, drilling muds and toothpaste are good examples of shear thinning non-Newtonian materials.

(3) Pseudoplasticity

Some materials do not have a yield stress, nevertheless they behave nonlinearly. These are considered pseudoplastic. They flow instantaneously upon application of stress but also display shear thinning behaviour. Polymer solutions exhibit pseudoplastic flow as does bread dough and many paints and cosmetics.

(4) Dilatancy

Dilatancy, also known as shear thickening, is an unusual phenomenon whereby materials actually increase their viscosity upon stirring or shearing. In some cases, these are dense suspensions of solid particles in a fluid medium, which develop greater spacing between particles during agitation. This behaviour is infamous in quicksand, moist beach sand and certain pharmaceuticals such as a suspension of penicillin. The properties of these suspensions depend on Hamaker theory and Van der Waals forces and can be stabilised electrostatically or sterically. Shear thickening behaviour occurs when a colloidal suspension transitions from a stable state to a state of flocculation. Shear thickening often results from material instability and structure rearrangements or phase separation.

(5) Thixotropy

For many fluid materials, the viscosity is mostly independent of time and is only a function of the shear rate and temperature. For concentrated dispersions, their viscosity does not reach a steady value for some time upon application of stress, or shear rate. This steady state is dependent on the stabilisation of internal network structures, which can be broken down by shearing and require time to rebuild. A steady state plateau in viscosity is reached if equilibrium has been established between structure breakdown and rebuilding. Upon ceasing the shear rate which caused the breakdown, the material reforms its internal network and the viscosity recovers. The term used to describe this phenomenon is Thixotropy.

(6) Rheopexy

Whereas a thixotropic fluid's viscosity decreases over time under an imposed constant shear rate, a rheopectic fluid's viscosity increases under an imposed shearing action. A rheopectic fluid such as a dense suspension of latex particles or plastisols will gel when agitated. If allowed to rest, a rheopectic fluid will return to its original lower viscosity. The viscosity-shear rate curve forms a hysteresis loop and the hysteresis can be repeated indefinitely. This is a way to distinguish between true and apparent

rheopectic behaviour - fluids that change physically or chemically (gelling, solvent evaporation) while a shear is imposed also experience a viscosity increase. These changes, however, will not be reversible and therefore do not represent true rheopexy.

(7) Time Dependency- Creep and Creep Recovery

The stress and strain rate dependent behaviour of a material may be only part of the picture. In many cases, time dependency has to be considered also. Materials are also time dependent. Hookean and Newtonian materials respond immediately upon an input stress or strain rate. When a stress is imposed on a so-called 'viscoelastic' material, it does not immediately respond with constant flow, even though the stress may be sufficiently above the critical stress or yield point. Upon removal of the stress, these types of materials recover to their original state, but slowly, and usually incompletely. This behaviour is referred to as creep. Creep studies can also be used to determine the yield stress of materials. A series of creep and recovery (application of a constant stress followed by a period of zero stress) can be performed in incrementally higher and higher stress levels. Below the yield stress, the material behaves as a solid, with complete recovery. When the material fails to recover completely, it has reached its yield stress.

2.13.2 Theory of STF

2.13.2.1 Background

To gain a better understanding of STFs, it is necessary to know some fundamental concepts of fluid mechanics and the rheological behaviour of these fluids. It is known that rheological fluids behave in such a manner that the shearing stress acting on them is not linearly associated with the rate of shearing strain. When subjected to shear stresses, most fluids follow Newton's law with the constant viscosity. A fluid that obeys this linear relation is called Newtonian, which means that its viscosity is independent of a shear rate for the shear rates applied. Glycerine, water and mineral

oils are typical examples of Newtonian liquids. Newtonian behaviour is also characterised by constant viscosity with respect to the time shearing and an immediate relaxation of the shear stress after cessation flow. Furthermore, the viscosities measured in different flow kinematics are always proportional to one another. However, a number of fluids can condense under compression and, consequently, they have an unusual (non-Newtonian) behaviour under shear stresses. These substances are known as STF, their viscosity can increase or decrease under variable shear stress magnitude, which is referred to a shear thickening and shear thinning respectively. Figure 2.15 (a) and (b) show the general shape of the curves representing the variation of viscosity as a function of shear rate and the corresponding graphs of shear stress as a function of shear rate.

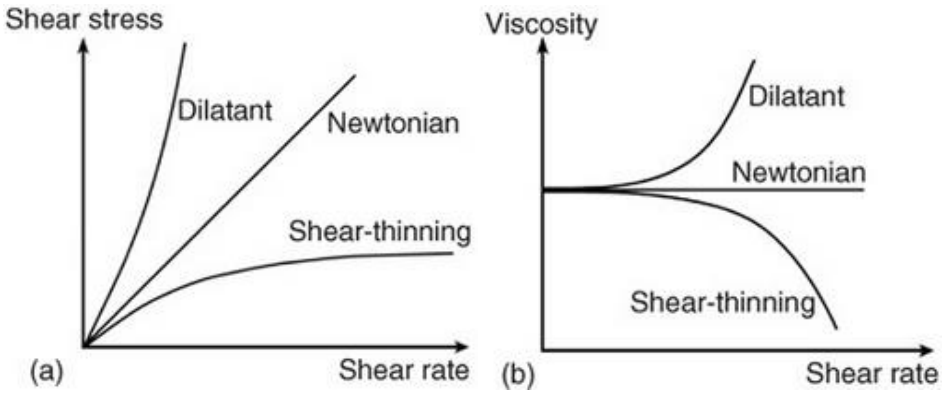

Figure 2.15 Typical flow curves for Newtonian, shear thinning and shear thickening (dilatant) fluids: (a) shear stress as a function of shear rate; (b) viscosity as a function of shear rate.

A simple experiment shows how STF work: Put a stick in a wet paste of corn starch. Stir slowly, and the viscous liquid flows around the stick, and the path left in the paste slowly fills in; move the stick quickly through the paste and it suddenly becomes solid, the wet gloss of its surface disappears, and the paste cracks and breaks like a hard material; The force applied by the stick to the paste transforms it from liquid to solid state; Upon release of stress, it becomes liquid again. Shear thickening in dense colloidal suspensions often occurs as an abrupt increase in viscosity on increase shear

rate beyond a critical shear rate [150-152]. In other words, under the high-speed shear rate, the viscosity of STF increases dramatically and acts like a solid. However, after removal of impact stress, STF reverses its status to liquid-like as soon as shear removes. This phenomenon has been observed in concentrated colloidal suspensions.

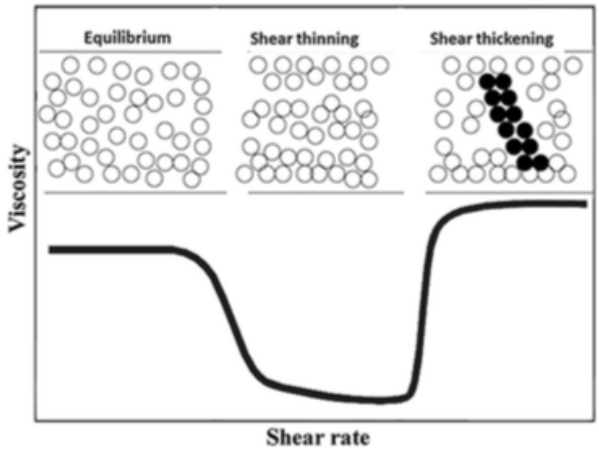

Figure 2.16 Schematic representation of shear-thinning and shear-thickening behaviours of particle suspensions

Figure 2.16 shows the particles in an STF during shear-thinning and shear-thickening with increasing shear rate. It can be observed from the figure that in equilibrium, the silica particles were dispersed well in mediums. As the shear rate increases, the particles start to flow forming layers of particles, which has resulted from the disordered state of the particles under the applied stress. Upon further increase in shear rate, the particles turned to aggregate due to the formation of hydro-clusters. This shear-thickening is completely reversible; after the removal of impact stress, the suspensions turned back to be an easy flowing state and flow like any other liquid [153-156]. Researchers, working in the domain of rheology, have proposed several theories to explain the mechanism of shear thickening [157]. Among the proposed, ‘order-disorder theory’ and ‘hydrodynamic clustering’ are the two widely accepted theories.

2.10.2.2 Order-Disorder Theory

Metzner *et al.* [158] suggested that particle suspensions experiencing high shear rates form layered particles structures which slide over one another. Later Hoffman [21] experimentally verified the same with highly concentrated suspensions of monodisperse particles under shear. Hoffman [5] analysed the forces which develop in colloidal suspensions under shear to model the flow instability which is responsible for discontinuous and dilatant viscosity behaviour in concentrated polymeric resins. It was proposed that the flow instability is caused by the action of forces like van der Walls-London, electric double layer and shear stresses on a group of particles. He further proposed that the particles within the moving layers experience hydro-dynamically induced forces which are responsible for pulling them out of their layer thus disrupting the ordered flow. When shear stress crosses a critical value, the particles are pulled out of their ordered layers, jam into one another and cause the rise in viscosity.

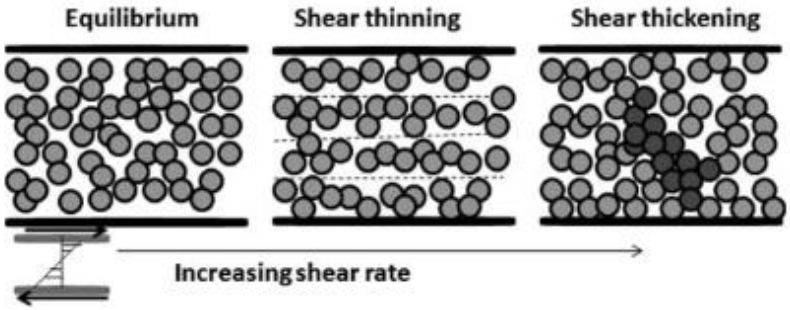

Figure 2.17 Schematic representation of particles in an STF during shear thinning and shear thickening w.r.t. increasing shear rate [151].

Hoffman [159] also demonstrated with light scattering that during shear thickening the hexagonally packed layers disrupt into a disordered state. This phenomenon was called order-to-disorder transition (ODT). This transition appeared with a drastic increase in the viscosity at the critical shear rate. Bazhenov *et al.* [160] reported that the particles show the dilatant behaviour due to the disturbance in the balance between inter-particle and hydrodynamic forces. Assuming that shear thickening is a consequence of ODT, Boersma *et al.* [161] proposed that the critical shear rate for

thickening can be determined from a balance between the electrostatic and shear forces acting on a pair of particles. According to Woodlock [162], shear thickening is not exhibited by molecular fluids of a single component but it is a consequence of medium dependent effective colloidal potentials. With molecular dynamics calculations, he showed that a simple molecular model for a viscous fluid predicts a subtle shear thickening response under very limited modelling conditions. Most of the simulation work showed that an order-disorder transition state involved atomic fluids. Later Durlofsky *et al.* [163] developed a method to simulate concentrated colloidal dispersions where both interparticle forces and hydrodynamic interactions were taken into account.

2.13.2.3 Hydrodynamic Clustering Theory

The other theory for shear thickening, the hydrodynamic clustering theory suggests that shear thickening results from strong lubrication forces generated by the formation of clusters of particles. Colloidal dispersions in strong viscous flows can exhibit a unique transition that is characterised by a self-organization into stress-bearing clusters, often denoted by the term ‘‘hydro-clusters.’’ This self-organized microstructure is thought to be a consequence of the dominance of hydrodynamic lubrication forces, whereby the flow generates transient packed clusters of particles separated from one another only by a thin solvent layer. Percolation of these hydro-clusters leads to ‘‘jamming,’’ or the discontinuous, often erratic increase in shear viscosity at a critical shear stress. Evidence for the hydrodynamic basis of this phenomenon is provided by rheo-optical experiments [19, 164], flow ultra-small-angle neutron scattering (flow-USANS) [165] and stress-jump rheological measurements [166]. Simulation predictions by Bossis [167] and co-workers using the method of Stokesian dynamics, and later by Boersma and co-workers [168] and Farr and co-workers [169, 170] provide computational evidence of the mechanism, whereas the statistical mechanical theory of Brady [167, 171, 172] provides an

understanding of the microstructure resulting from the singular nature of lubrication hydrodynamics. It should be noted that there are only limited measurements of the actual stress induced microstructure [164], such that comparison of theory and experiment are limited at present to macroscopic rheological response.

Further, Bossis *et al.* [167] supported this theory and observed that shear thickening occurs as a result of the transient hydrodynamic cluster formation instead of an order-to-disorder transition. These clusters are formed when shear forces operate on particles and force them into compact groups. The simulations show that hard-sphere suspensions thicken without any shear ordering. Bergstrom [161] also supported the same theory. Boersma *et al.* [173] found with their simulation work that above the critical shear rate, hydrodynamic forces induce cluster formation and these clusters are responsible for high viscosities. van der Walls-London forces are found to sharpen the shear thickening transitions by inducing stronger cluster formation. Under high shear rates, the distance between the particles reduces to such an extent that they are separated only by a very thin layer of liquid. This generates large hydrodynamic lubrication forces which are responsible for the formation of clusters out of particles. In the absence of these hydrodynamic forces, the particles would arrange themselves into strings along the flow direction, thus actually cause shear thinning. Thus, this hydro-cluster mechanism is distinct from the ODT hypothesis.

Although these two microscopic mechanisms have been used to explain shear thickening phenomenon, the ‘‘hydro-cluster’’ mechanism is a more accurate and generalised model.

2.13.2.3.1 Hydrodynamic lubrication forces

The ‘‘hydro-cluster’’ mechanism is based on particle interactions in a liquid medium. Based on this, the shear thickening behaviour in concentrated colloidal suspensions is caused by hydrodynamic lubrication forces between particles. The concept of

hydrodynamic clustering has been introduced to explain thickening, but its precise meaning has not been explored.

The flow behaviour of colloidal (often also termed Brownian) dispersions is controlled by the balance between hydrodynamic and thermodynamic interactions as well as Brownian particle motion. Thermodynamic interactions mainly include electrostatic and steric repulsion and van der Waals attraction. Hydrodynamic interactions between particles are multi-interactions comprise attractive interactions on the microstructure of suspensions [174].

The lubrication force opposes the relative motion of the particles [175]. The particles simulated here have crude models for short-range polymer coats with both a conservative repulsive force and a lubrication interaction modified from that of hard spheres. The coats define a particle contact which is crucial to the physics [176]. Lubrication interaction can be strongly enhanced by polymer coats on the particles. Thickening occurs once the bulk stress is sufficient to compress the coats against their conservative (spring) forces to a point at which the relaxation time of the coats is longer than the inverse shear rate. This is confirmed by the simulations [177]. A jamming at a critical shear stress can also occur for models with coat interactions if the springs have a maximal force [169].

The strong hydrodynamic lubrication interactions will act to resist particle separation in the extensional quadrant of the flow. It is important to recognise that the lubrication forces also act to hinder particles from separating once they are in close proximity [178]. It has been long established by molecular and Brownian dynamic [179] simulations that no shear thickening is observed in the absence of the hydrodynamic lubrication forces. The greater shear forces are necessary to bring particles into close enough proximity for the lubrication hydrodynamics to dominate the particle behaviour. The analysis demonstrates that shear thickening is governed by hydrodynamic interactions [180].

2.13.2.3.2 Péclet number theory

There is a strong need to accurately identify the process of aggregation of small particles in order to understand the cluster configuration within the colloidal suspensions. In a hard-sphere suspension, particles interact through hydrodynamic and Brownian forces. The balance between these two forces will determine the structure and properties of concentrated colloidal suspensions.

The dynamics of colloidal dispersions is inherently a many body, multiphase fluid mechanics problem. But first consider the case of a single particle. Fluid drag on the particle leads to the Stokes-Einstein-Sutherland fluctuation–dissipation relationship:

$$D_0 = \frac{kT}{6\pi\mu a} \tag{2.9}$$

The particle diffusivity (diffusion coefficient) D_0, $m^2\ s^{-1}$, scales with the thermal energy kT divided by the suspending medium's viscosity μ and the particle's hydrodynamic radius a. k is the Boltzmann's constant, $1.38 \times 10^{-23}\ JK^{-1}$, and T is the temperature. That diffusivity sets the characteristic time scale for the particles' Brownian motion; it takes the particle a^2/D_0 seconds to diffuse a distance equal to its radius. The time scale defines high and low shear rates γ. A dimensionless number known as the Péclet number, Pe, relates the shear rate of a flow to the particle's diffusion rate; alternatively, the Péclet number can be defined in terms of the applied shear stress τ:

$$Pe = \frac{\dot{\gamma}\, a^2}{D_0} = \frac{\tau a^2}{kT} \tag{2.10}$$

The Péclet number (Pe), which is the ratio of hydrodynamic shear to Brownian forces (given by Equation 2.10), measures the relative importance of perikinetic and orthokinetic aggregations. It is known that perikinetic aggregation is due to Brownian motion and is relevant with nanoparticles. This aggregation occurs when, as a result

of their random motion, particles collide, and stick together. Once clusters are formed, the average length between aggregates and the Brownian time increases. By increasing the shear rates, clusters tend to break up and at higher shear rates the distance between the particles reduces. The tension present in the curved streamlines surrounding two particles produces a net force on the particles that pushes them together. This leads to orthokinetic aggregation, in which hydrodynamic interactions become predominant (Figure 2.18). It was suggested that the more significant shear thickening effect can be achieved by the better aggregation effect of dispersed particles [181].

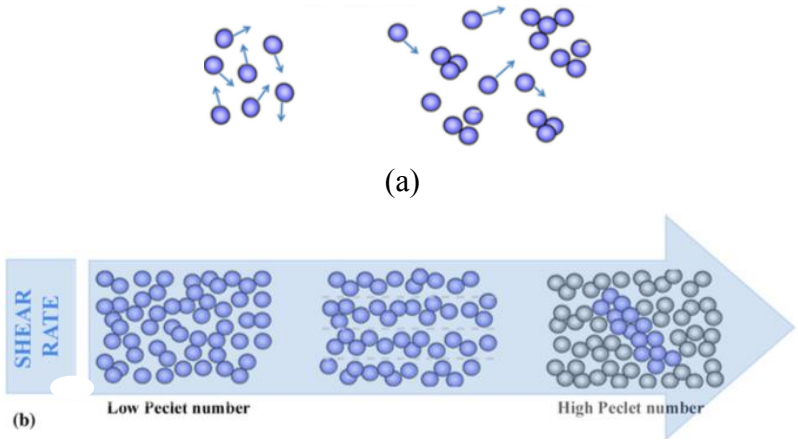

(a)

(b)

Figure 2.18 (a) Perikinetic aggregation due to Brownian motion (low Péclet number), and (b) orthokinetic aggregation when hydrodynamic interactions become predominant (high Péclet number)

The number is useful because dispersion rheology is often measured by applied shear rates or shear stresses. Low Pe is close enough to equilibrium that Brownian motion can largely restore the equilibrium microstructure on the time scale of slow shear flow. At sufficiently high shear rates or stresses, though, deformation of the colloidal microstructure by the flow occurs faster than Brownian motion can restore it. Shear thinning is already evident around Pe ≈ 1. And higher shear rates or stresses (higher Pe) trigger the onset of shear thickening [1, 2, 151]. Despite the fact that shear thinning behaviour is considered as more common than shear thickening behaviour, it was suggested that shear thickening may occur in all dense suspensions under proper

conditions [182]. However, one of the key challenges is why all dense suspensions do not exhibit shear thickening behaviour. One of the more puzzling challenges is that why the suspensions consisting of soft particles, which can deform easily to shear past each other, do not shear thicken, whereas densely packed suspensions of hard particles exhibited shear thickening behaviour.

Recent studies demonstrated that the behaviour of nanoparticles differs substantially for hard spheres because of strong Coulomb movement, charge-dipole, dipole-dipole, and van der Waals interactions. In particular, the state of the nanoparticles in such systems is determined by the interaction between the nanoparticles and between the nanoparticle and liquid medium. It is important to realise the fundamentals of these interactions under shear that need further investigation. While much experimental and simulation work has been done on shear thickening in steady state shear flow, rather limited amount of work has been done to investigate the viscoelastic properties of an STF. This is because when high stress levels cause a highly nonlinear response, the study of shear thickening phenomenon becomes difficult. Laun *et al.* [183] and Lee *et al.* [17] correlated the nonlinear viscoelastic properties to the steady shear response for an STF. Chow *et al.* [184] investigated the dependence of shear thickening on gap size. They found that while all suspensions which were ordered at rest, showed shear thinning; shear thickening occurred at volume fractions greater than a critical value. They also reported that shear thickening is sensitive to shear history. Barnes [15] concluded in a review that all dispersions exhibit shear thickening. However, in only a few does it occur at shear rate values measurable in commercial rheometers.

2.13.3 Creation of STF [151]

Shear thickening fluid is a concentrated colloidal suspension consisting of colloidal particles disperses in a liquid medium. The solid particles used may be synthetic or naturally occurring mineral, including SiO_2 or other oxides, calcium carbonate, or

polymers, such as polystyrene (PS) or polymethylmethacrylate (PMMA). The particles need to be hard, can be stabilised in solution or dispersed by charge, Brownian motion, adsorbed surfactants, and adsorbed or grafted polymers, polyelectrolytes, polyampholytes, or oligomers. Also, the particles can be monodisperse, bidisperse, or polydisperse in size and shape. Preferably the particles should have a size less than the diameter of the fibre, which is 100 microns or nanometres, so that the particles can be impregnated and embedded in the weave of the material. Particle shapes include spherical particles, elliptical particles, or disk-like or clay particles.

The liquid medium can be aqueous in nature (i.e. water with or without added salts, such as sodium chloride, and buffers to control pH) for electrostatically stabilized or polymer stabilized particles, or organic (such as ethylene glycol, polyethylene glycol, ethanol), or silicon based (such as silicon oils, phenyl trimethicone). The dispersing medium should also be environmentally stable so that they remain integral to the fabric and suspended particles during service.

Thus, STF is commonly a composite material containing solid nanoparticles embedded in a liquid polymer with a persistence of mobility, i.e., it is a highly concentrated suspension in a polymer dispersion medium (concentrated colloidal suspension).

2.13.4 Rheological properties of STFs

2.13.4.1 Basics of rheology

Rheology is the study of the flow of matter, primarily in a liquid state, but also as ‘soft solids’ or solids under conditions in which they respond with the plastic flow rather than deforming elastically in response to an applied force [185]. The rheological behaviour of materials can be regarded as being between two extremes:

Newtonian viscous fluids, typically liquids consisting of small molecules, and Hookean elastic solids, for example, rubber. However, most real materials exhibit mechanical behaviour with both viscous and elastic characteristics. Such materials are termed viscoelastic.

Isaac Newton first introduced the notion of viscosity as a constant of proportionality between the force per unit area (shear stress) required to produce a steady simple shear flow and the resulting velocity gradient in the direction perpendicular to the flow direction (shear rate):

$$\eta = \frac{\sigma}{\dot{\gamma}} \qquad (2.11)$$

where η is the viscosity, $\sigma = F/A$ is the shear stress, is the ratio of force/area on a surface when the force is aligned parallel to the area, and the $\dot{\gamma}$ is the shear rate. Here A is the surface area of the sheared fluid volume on which the shear force F is acting.

$$\dot{\gamma} = \frac{v}{h} \qquad (2.12)$$

where h is the height of the volume element over which the fluid layer velocity v varies from its minimum to its maximum value.

Viscosity, also called dynamic viscosity or absolute viscosity, is a measure of a fluid's resistance to deformation under shear stress. For example, crude oil has a higher resistance to shear than water does. The property of viscosity is important to engineering practice because it leads to significant energy loss when moving fluids contact a solid boundary.

2.13.4.2 Basics of rheological properties

The rheological properties of colloidal dispersions are determined by the interplay of thermo-dynamical and fluid mechanical interactions. In dispersion at rest, the particle distribution is determined by Brownian motion and direct potential interactions between the particles; the distribution functions are fully determined by the thermo-dynamics. In a sheared suspension, the flow field disturbs the equilibrium particle distribution and then both thermo-dynamical and fluid mechanical variables determine the structure [186].

2.13.4.3 Experimental methods of rheology [174]

Rheometers can be categorised according to the flow type in which material properties are investigated: simple shear and extensional flow. Shear rheometers can be divided into rotational rheometers, in which the shear is generated between fixed and moving solid surfaces, and pressure is driven like capillary rheometer, in which the shear is generated by a pressure difference along the channel through which the material flows. Extensional rheometers are far less developed than shear rheometers because of the difficulties in generating homogeneous extensional flows, especially for liquids with low viscosity.

- Rotational Rheometry

Rotational instruments are used to characterise materials in steady or oscillatory shear flow. Basically, there are two different modes of flow: controlled shear rate and controlled shear stress. Three types of measuring systems are commonly used in modern rotational rheometry, namely, concentric cylinder, parallel plate and cone-and-plate. Typical shear rates that can be measured with rotational rheometers are in the range 10^{-3} to 10^{3} s^{-1}.

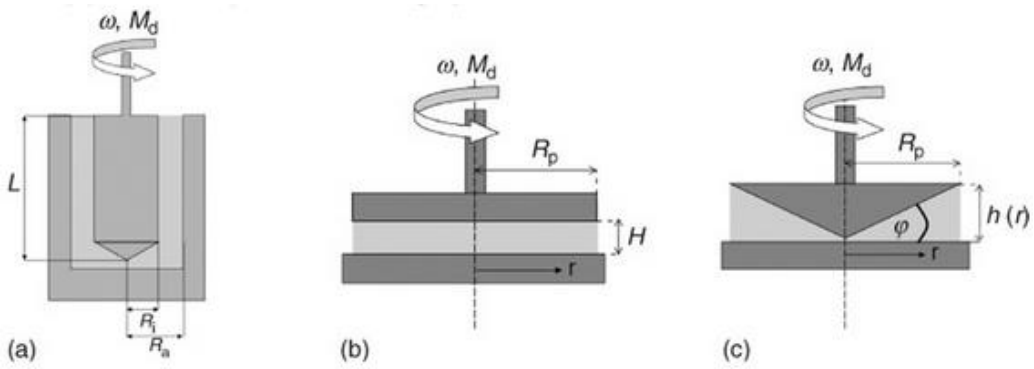

Figure 2.19 Schematic representation of (a) concentric cylinder, (b) parallel-plate and (c) cone-and-plate measuring system.

As shown in Figure 2.19 (a), a cylinder measuring system consists of an outer cylinder (cup) and an inner cylinder (bob). There are two modes of operation depending on whether the cup or the bob is rotating. The gap between the two concentric cylinders should be small enough so that the sample confined in the gap experiences a constant shear rate.

When the bob is rotating at an angular velocity ω the shear rate is given by:

$$\dot{\gamma} = 2\omega \frac{R_a^2}{R_a^2 - R_i^2} \tag{2.13}$$

where R_i and R_a are the radii of the bob and the cup, respectively. If the torque measured on the bob is M_d, the shear stress σ in the sample is given by:

$$\sigma = \frac{M_d}{2\pi R_i^2 L} \tag{2.14}$$

where L is the effective immersed length of the bob.

Having the shear rate $\dot{\gamma}$ and shear stress σ, the sample viscosity η can be calculated according to Equation (2.11).

The concentric cylinder measuring system is especially suitable for low viscous liquids, since it can be designed to offer a large shear area and at high shear rates the sample is not expelled from the gap. Other advantages of this geometry are that sample evaporation is of minor relevance since the surface area is small compared to the sample volume, the temperature can be easily controlled due to the large contact area, and even if suspensions exhibit sedimentation and particle concentration varies along the vertical direction the measured viscosity is a good approximation of the value.

- Parallel-plate Rheometry

The parallel plate geometry is shown in Figure 2.19 (b). The sample, confined within the gap of height H between the two parallel plates, is sheared by the rotation of one of the plates at angular velocity ω. Thereby, the circumferential velocity v depends on the distance from the plate at rest h and the distance r from the rotational axis:

$$v(r,h) = r\omega\frac{h}{H} \tag{2.15}$$

thus:

$$\dot{\gamma}(r) = \frac{v}{h} = \frac{r\omega}{H} \tag{2.16}$$

The shear rate $\dot{\gamma}$ at constant ω is not constant within the gap. Typically, the calculations and analysis of rheological results in parallel-plate measuring systems are the rim of the plate ($r = R_p$). The shear rate can be varied over a wide range by changing the gap height H and the angular velocity ω.

The shear stress σ is a function of the shear rate $\dot{\gamma}$, which is not constant within the gap. Thus, to relate the shear stress to the total torque an expression for the σ ($\dot{\gamma}$) dependence is necessary. For Newtonian liquids the shear stress depends linearly on the shear rate and can be expressed as follows:

$$\sigma(R) = \frac{2M_d}{\pi R_p^2} \qquad (2.17)$$

This expression is called the apparent shear stress. For non-Newtonian fluids, Giesekus and Langer [187] developed a simple approximate single point method to correct the shear rate data, based on the idea that the true and apparent shear stress must be equal at some position near the wall. It was found that this occurs at the position where r/R_p=0.76 and this holds for a wide range of liquids.

The parallel-plate measuring system allows for measurements of suspensions with large particles by using large gap heights. On the other hand, by operating at small gaps the viscosity can be obtained at relatively high shear rates. Small gaps also allow for a reduction of errors due to edge effects and secondary flows. Note that for sedimenting suspensions the viscosity is systematically underestimated since the upper rotating plate moves on a fluid layer with reduced particle loading.

- Cone-and-plate Rheometry

A cone-and-plate geometry is shown schematically in Figure 2.19 (c). The sample is contained between a rotating flat cone and a stationary plate. Note that the apex of the cone is cut off to avoid friction between the rotating cone and the lower plate. The gap angle φ is usually between 0.3° and 6° and cone radius R_p is between 10 and 30mm. The gap h increases linearly with the distance r from the rotation axis:

$$h(r) = r tan\varphi \qquad (2.18)$$

The circumferential velocity v also increases with increasing distance r.

$$v(r) = r\omega \qquad (2.19)$$

Hence the shear rate is constant within the gap and does not depend on the radius r.

$$\dot{\gamma} = \frac{dv(r)}{dh(r)} = \frac{\omega}{tan\varphi} \approx \frac{\omega}{\varphi} \qquad (2.20)$$

The shear stress is related to the torque M_d on the cone:

$$\sigma(R) = \frac{3M_d}{2\pi R_p^3} \qquad (2.21)$$

A great advantage of the cone-and-plate geometry is that the shear rate remains constant, thus provides homogenous shear conditions in the entire shear gap. The limited maximum particle size of the investigated sample, difficulties with avoiding solvent evaporation and temperature gradients in the sample as well as concentration gradients due to sedimentation are typical disadvantages of the cone-and-plate measuring system.

- Capillary Rheometer

Figure 2.20 shows a schematic diagram of a piston driven capillary rheometer. A piston drives the sample to flow at a constant flow rate from a reservoir through a straight capillary tube of length L. Generally, capillaries with circular (radius R) or rectangular (width B and height H) cross-section are used. The measured pressure drop Δp along the capillary and the flow rate Q are used to evaluate the shear stress, shear rate correspondingly, and viscosity of the sample.

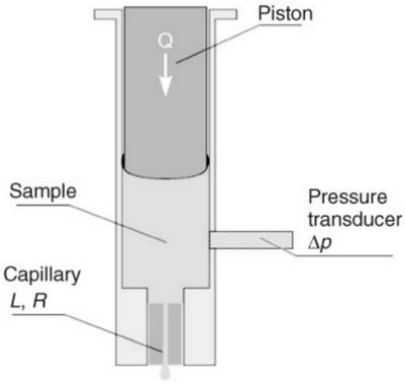

Figure 2.20 Schematic representation of a controlled flow rate capillary rheometer

Pressure driven flows through a capillary have a maximum velocity at the centre and maximum shear rate at the wall of the capillary, that is, the deformation is essentially inhomogeneous. Assuming Newtonian behaviour and fully developed, incompressible, laminar, steady flow, the apparent wall shear stress σ_a in a circular capillary with radius R is related to the pressure drop Δp by:

$$\sigma_a = \frac{\Delta pR}{2L} \qquad (2.22)$$

In addition, the apparent or Newtonian shear rate at the wall can be calculated on the basis of measured flow rate according to:

$$\dot{\gamma} = \frac{4Q}{\pi R^3} \qquad (2.23)$$

Therefore, we can evaluate the viscosity in terms of an apparent viscosity based on Newton's postulate (Equation 2.11).

The major advantage of the capillary rheometer is that the flow properties of fluids can be characterised under high shear conditions (up to $\dot{\gamma} = 10^6$ s^{-1}) and process-relevant temperatures (up to 400°C). Another advantage is that the capillary flow is closed and has no free surface so that edge effects, solvent evaporation, and other problems that trouble rotational rheometry can be avoided.

2.13.4.4 Analysis of PEG/SiO_2 system rheological properties

SiO_2 has relatively high surface energy, so the particle aggregation is very easy to occur and this particle aggregation is irreversible. There are a large number of silanol group (Si-OH) on the particle clusters, but the polar dispersion medium PEG has ether-oxygen group and hydroxyl group. Consequently, the functional group of polar dispersion medium and particle clusters will react to form hydrogen bond, solid SiO_2 and liquid PEG (Polyethylene Glycol) can form a complicated network structure and this dispersion system is comparatively stable. When there is no exogenic action, the hydrogen bond between the liquid dispersion medium and particle clusters stay in a dynamic equilibrium state, the total number of the broken and reformulation of the hydrogen bond will maintain constantly. When the system suffer from slight shear force, the reformulation of hydrogen bond rate tend to be slower than the breakdown of the hydrogen bond, a certain amount of weakening of the constraint (hydrogen bond) to the particle movement will arise fairly, therefore, shear thinning will turn up

to this system [188]. When high velocity shear force emerged, although a large quantity of hydrogen bond will break and the network structure will be damaged, the degree of disorder of the particle movement rises or the formation of the "particle clusters" enormously impede the flow of the liquid and shear thickening appears to this system. After the external force was eliminated, hydrogen bond will be formed again and network structure will be reconstructed as back to the original state. Hence, the breakage and reformulation of the hydrogen bond result in the breakdown and reconstruction of the network structure which leads to STF behave shear thickening and shear thinning in macroscopic view [151].

2.13.4.5 General concept of STF rheological properties

As it was mentioned earlier in this section, STFs exhibit a low viscosity at imposed rates lower than the critical shear rate and show a marked increase in viscosity when beyond a critical shear rate. Many researchers have focused on determining rheological properties of STFs under steady shear and oscillatory shear flow. Steady shear research indicated that the common feature of the materials' rheogram is a sharp increase in viscosity which occurs at a critical shear rate [189]. Critical shear rate, as the main mechanism triggering shear thickening transition, can be determined by experimental and theoretical methods. It has been shown that the viscosity of STFs first slightly decreased with increasing shear rate. However, when the shear rate reaches a critical value, the viscosity increases abruptly which marks the transition to shear thickening behaviour [188]. A review of the literature showed that, apart from achieving critical shear rates, there are other factors affecting on rheological properties of STFs.

2.13.4.6 Factors affecting shear thickening behaviour

The rheological properties of STFs are dependent upon many factors which are mainly divided into three categories: particle (shape, size distribution, solid volume fraction, and interaction with other particles), dispersion medium (viscosity of the

medium solvent), and flow field (types, rate and time of flow deformation). It has been found that all these factors have synchronised effect on the shear thickening behaviour which included the critical shear rate and degrees of severity of shear thickening phenomenon [15].

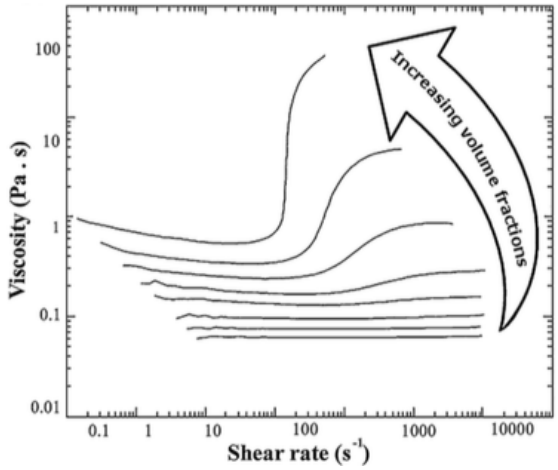

Figure 2.21 Shear-thickening behaviour of STFs for steady shear flow at various volume fractions ranging from 0.05 to 0.4 [191]

Solid-volume fraction, which is the fraction of the total volume of the system occupied by particles, is found to be the most important factor affecting shear thickening [190]. Shear thickening is only observed when the solid volume fraction exceeds a certain minimum level. Barnes [15] reported that above 0.5 solid volume fraction, the behaviour of fluid changes drastically with the change in shear rate. Critical shear rate (the shear rate at which shear thickening begins) decreases as solid volume fraction increases. Figure 2.21 shows the viscosity as a function of the steady shear rate for the STFs at various volume fractions. Both shear thinning and thickening behaviour are observed. Increasing the shear rate, the viscosity underwent a decrease followed by a transition to shear-thickening behaviour at high shear rates. From the figure, it can be seen that at higher shear rates in the shear-thickening region, the high volume fraction dispersion exhibits a greater increase in viscosity.

Boersma *et al.* [168] predicted the critical shear rate for different dispersions and also confirmed its dependence on the solid volume fraction. Figure 2.22 shows the

viscosity as a function of the shear rate for the colloidal silica dispersions in polyethylene glycol (PEG) at volume fractions (φ) of 0.57 and 0.62. It was observed that for a dispersion with a solid volume fraction of 62%, the shear thickening transition occurred at a shear rate of 10 s^{-1} while for another dispersion having a solid volume fraction of 57%, the shear thickening behaviour was exhibited at a shear rate of 300 s^{-1}. Moreover, with increasing the silica particle concentration, the shear-thickening phenomenon happened sharply. Hence, increasing the volume fraction of particles in STF leads to a reduction in the critical shear rate [113].

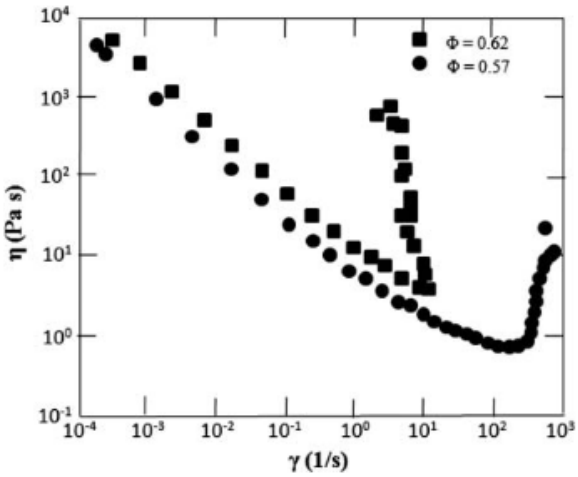

Figure 2.22 Shear thickening behaviour of colloidal silica of average particle size of 450 nm dispersed in ethylene glycol for steady shear flow at volume fractions of 0.57 and 0.62 [113].

In the study on the effect of rheological parameters on shear-thickening behaviour by Wetzel *et al.* [191], it was demonstrated that requirement of the solid volume fraction to reach the critical shear rate decreases as the aspect ratio of the particles increases. They found that the strength of the shear-thickening response increases as solid-volume fraction increases, with discontinuous shear thickening at the highest solid volume fraction. Moreover, as the solid volume fraction increases, the shear rate at which shear-thickening behaviour is first observed decreases. It should be noticed that there must be a limit for solid volume fraction which above it the shear-thickening behaviour cannot be achieved due to the difficulty in obtaining or preparing STFs with high weight fraction. It can be attributed to the tendency of nanoparticles to agglomerate.

Particle shape is another important factor with impact on the flow properties of large particle size suspensions. Figure 2.23 shows the effect of particle shape on shear-thickening of suspension with rods, plates, grains, and spheres for the solid volume fraction of 0.2. It is found that the effect of particle shape on the shear thickening behaviour of suspension with rods is greater than that of plates, grains, and spheres. In the case of rods particle, an increase in viscosity is observed at a shear rate of 200 s^{-1}. Conversely, in the case of spheres, viscosity increases slightly even above a shear rate of 300 s^{-1} [1, 15].

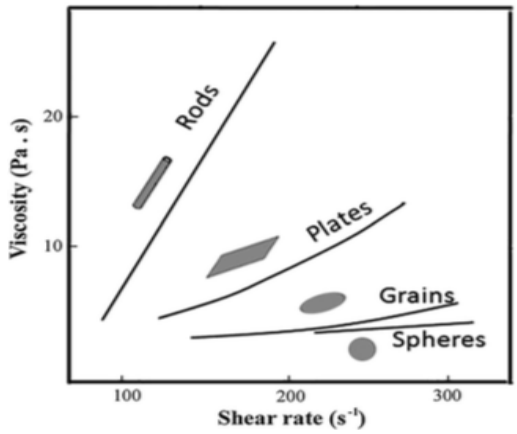

Figure 2.23 Effect of particle shape on shear-thickening behaviour of suspension with rods, plates, grains, and spheres [15]

Another factor which has a direct effect on determining critical shear rate is the particle size. It has been demonstrated that as the particle size increases, the critical shear rate decreases. Maranzano *et al.* [23] studied the effect of particle size on reversible shear-thickening transition in dense colloidal suspensions. It has been shown that with increasing particle size, the flow curves systematically shift to lower shear stresses. In another study, the influence of silica particles suspension containing particle sizes of 100, 300, and 500 nm at fixed volume fraction ($\varphi = 0.65$) was investigated by Lee *et al.* [192]. It is found that increase in particle size significantly decreases the critical shear rate as shown in Figure 2.24.

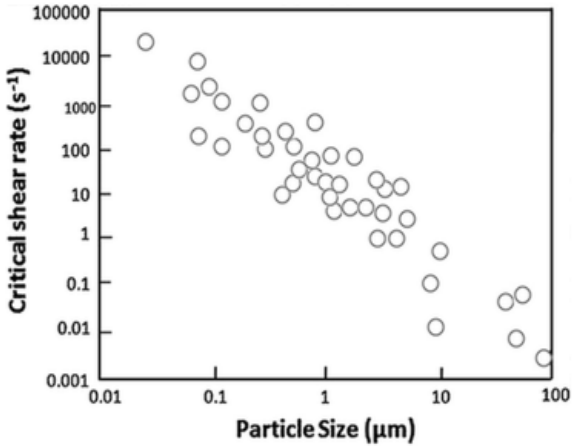

Figure 2.24 Effect of average particle size on critical shear rate for dispersions with volume fraction of φ = 0.50 [182]

Different sort of particles have different acting force between the dispersion medium, the difference of the particle size will result in different specific particle surface area. Smaller the particle size, higher the specific particle surface area, but in other way, it will greatly increase the integrations among the particles surface functional group to form the particle jamming clusters. Consequently, critical shear force and critical shear rate will be lower.

The range of the particle size distribution has a dramatic influence on the rheological properties of STF, if the range of the particle size (diameter) distribution is wide, the small particle will fill the gap between the larger particles, which to be equivalent to the effect of the decrease of the particles concentration and weaken the thickening effect. It was reported that a wide particle-size distribution leads to an increase in critical shear rate. It is noteworthy that removing very small particles from a suspension cause the shear-thickening to occur at lower shear rates [182]. If comparing two different suspensions with the same volume fraction, but one with monodisperse and the other polydisperse particles, the monodisperse suspension will show a stronger shear thickening effect at a lower critical stress [15]. So narrower the range of the particle size distribution, better the thickening effect will be. And a larger degree of polydispersity decreases the severity of the rise in viscosity.

Shear-thickening phenomenon is also affected by the particle-particle interaction. Shear-thickening behaviour has been reported for systems of particles that are either neutral (or what is commonly referred as Brownian or hard spheres) or repel one another (electrostatically charged particles) by virtue of electrostatic, entropic, or steric interaction. It was found that deflocculated suspensions have low viscosity at low shear rates, but exhibit shear-thickening at high shear rate. Flocculated suspensions, however, show high viscosity at low shear rate and are shear-thinning at higher shear rates [182] [206]. The effect of chemically induced flocculation is shown schematically in Figure 2.25.

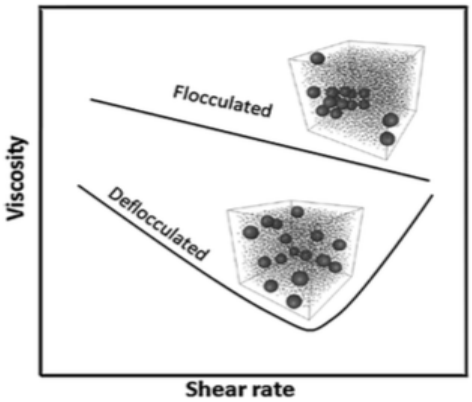

Figure 2.25 Schematic representation of the effect of chemically induced flocculation on shear-thickening behaviour [182]

Shear thickening phenomenon is also affected by the type of particles used. It was found that hardness of particles plays a major role in the behaviour of shear thickening. Silica nanoparticles show better shear thickening behaviour due to its hardness over other particles such as PMMA nanoparticles [193].

A number of researchers have found that the critical shear rate and viscosity of the STF were affected by temperature. With the increase in the temperature of STF, the hydrodynamic force inducing the dilatancy phenomenon increases due to the increased thermal Brownian motion of silica particles in the liquid medium. Figure 2.26 shows the effect of temperature on shear-thickening of suspension. The system temperature will affect the intensity of the particles motion, within a certain range, higher the temperature more intensively the particle movement and higher the critical

shear rate will be. It is found that the viscosity of STF and applied shear rate at critical transition point are on the Arrhenius-type relation, which means the shear-thickening behaviour enhances as temperature decreases [194].

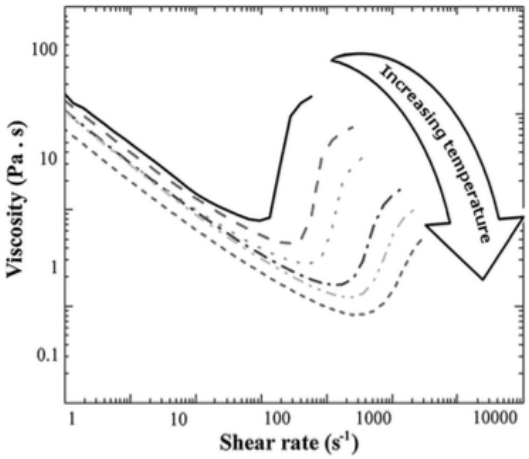

Figure 2.26 Effect of temperature on shear-thickening behaviour of STFs (the temperature was raised from 5 to 55°C) [194]

Apart from the factors mentioned above, the dispersion medium affects the rheological properties of STF need to synthesise the multi-factors such as medium viscosity, space steric hindrance, inter-molecular forces and so on. Within a certain extent, dispersion medium occupies greater volume fraction, critical shear force or critical shear rate will be more difficult to achieve. Xu [22] studied the influences of molecular chain lengths of polyethylene glycol (PEG4000, PEG6000 and PEG10000) and the results showed that the shear thickening effect was significantly enhanced with the increase of the molecular chain length of additives. And the mechanism of enhancement was quantitatively explained with the formation of large particles clusters.

It can be concluded that higher solid volume fraction, higher particle size and higher particle aspect ratio leads to the shear-thickening behaviour appeared at lower shear rates. Therefore, when studying the STF rheological behaviour, it is the synergistic effect of various factors to have the impact rather than single factor does.

2.13.5 STF applications

Research work in the theoretical field of STF was published in as early as the 1970s [21, 159, 190]. The initial work was more about the basic shear thickening phenomenon, its mechanism, the hydrodynamic interactions, simulations etc. Shear thickening fluids and their ability to transition from a low viscosity to a solid-like state have sparked much interest in the field of personal protection and energy absorption. Additionally, the impregnation of STF into high strength fabrics induces little or no increase in the thickness or stiffness of the fabrics [113, 195].

The shear thickening phenomenon can damage processing equipment and induce dramatic changes in suspension microstructure, such as particle aggregation, which results in poor fluid and coating qualities. The highly nonlinear behaviour can provide a self-limiting maximum rate of flow that can be exploited in the design of damping and control devices.

While the rheological response of shear thickening fluids to imposed stress and the associated energy absorption capability make them very good candidates for composite materials for human protection applications. In fact, they can absorb energy through the mechanism of viscous dissipation and during their thickening transition. Additionally, they can remain at low viscosity and therefore they can be flexible during normal operation and thicken when needed. These fluids are particularly interesting because they do not require an external activation mechanism, as magneto-rheological or electrorheological fluids do, rather they 'self-activate' under stress.

Fisher *et al.* [196] and Helber *et al.* [197] investigated the application of STFs in mounting systems for industrial machinery. STFs and STF devices have been developed for application in medical equipment to limit movement of a person’s joint such as shoulder, knee, elbow, ankle, hip, etc., so as to prevent the patient from

subjecting the joint to sudden rapid acceleration [198]. Such devices can help to limit the attendant damage that could result from such rapid acceleration. STF was also used for surgical and medical garments to inhibit penetration of garments. Joanna *et al.* [199] reported that the puncture resistance was increased when the STF was incorporated into surgical garments such as surgical gowns, surgical gloves, surgical masks and other wound-care products, where the STF was used as a layer on at least one of the inner and outer surface of the garment.

The ballistic response of suspensions of solid particles (cornstarch, silicon carbide, and silicon dioxide) in a liquid (ethylene glycol) was experimentally investigated by Oren E. Petel *et al.* [200]. Capsules containing the suspensions were impacted with chisel-nosed fragment simulating projectiles as velocities between 200 and 700m/s. The residual projectile velocity upon exit from the capsule is measured via direct videography. Only shear thickening suspensions with particles having sufficient strength (SiO_2 and SiC) show significant deviation from the hydrodynamic-dominated response, resulting in significant velocity decrements in the projectile attributable to the shear strength of the suspensions.

Amanda *et al.* [201] investigated the transient response of an STF using the split Hopkinson pressure bar technique, which indicates that an STF is able to transition to the shear thickened state faster at higher compression rates.

Concurrently, soft body armour research has continued worldwide, mostly in military industry, with emphasis on the development of lightweight, flexible, and comfortable armours with improved ballistic impact resistance [202]. Kevlar woven fabrics are often used for soft body armour applications. In soft body armours, approximately 20–50 layers of Kevlar fabric are used to stop a bullet fired by a shotgun or revolver. This makes the body armour heavy, inflexible and uncomfortable to the wearer [203]. Liquid body armour, as a new technology to save human's lives, aims to produce a new thin, flexible, lightweight, and inexpensive material making the soldiers safer and

allowing them to remain mobile and not hindering them from moving, running, and aiming their weapons has been developed.

The liquid armour (STFs) was co-developed over the past few years by a joint research team formed University of Delaware and the U.S. Army Research Laboratory [151]. The heart of the liquid armour is an STF composed of hard particles suspended in a liquid. The liquid, polyethylene glycol, is non-toxic and can withstand a wide range of temperature. Hard, colloidal nanoparticles are the other components of STF. This combination of fluidic and hard composites results in a material with unusual properties. Together, they produce an STF that stiffens instantly into a shield when hit hard by an object. It reverts to its liquid state just as fast when the energy from the projectile dissipates. According to Wetzel [204], the STF treatment changes the way in which yarns and fibres interact with each other and with the stabbing or ballistic threat during impact. In puncture applications, for example, the STF treatment prevents pointed weapons from penetrating between yarns in the fabric. The novelty of the STF treatment is that it provides these additional protective benefits without compromising the inherent thinness or flexibility of a woven fabric.

2.14 Researches on ballistic fabric impregnated with STF

The majority of publications devoted to the STF studies are concerned with its use in the body armour applications [113, 205-209]. Extensive analysis of ballistic and rheological properties of several STF systems have shown that improved ballistic performance in STF-treated Kevlar fabrics is attributed to shear-thickening [204]. This property has created special interest towards improving the impact resistance performance of textile structures by application of STFs to fabrics. Most of the literature reports that the significant improvement in impact resistance behaviour of textile fabrics was observed by application of STFs. For instance, Lee *et al.* [113] have investigated the ballistic performance of Kevlar fabrics impregnated with STFs

and found that the ballistic properties of Kevlar fabrics can be improved by the addition of colloidal STFs. They found that the ballistic performance in terms of absorbed energy is more than double. In other words, four layers of STF/Kevlar composite absorbed as much energy as ten layers of neat Kevlar.

2.14.1 Rheological properties of STF associated with ballistic performance

The effect of rheological parameters (such as fluid viscosity, particle loadings, size, and shape) of STF on the ballistic properties of impregnated Kevlar composites are observed in [191]. The most efficient properties can be reached in the case of the use of 200–500 nm spherical particles embedded in polyethylene glycol (PEG-400) or ethylene glycol (EG) of 50–60% volume concentration. Lee *et al.* studied the effect of the silica particle size of STF on the ballistic performance of STF-Kevlar fabrics. The fabric impregnated with an average particle diameter of 100nm showed better ballistic performance than those of the STF-impregnated fabrics containing larger particles and untreated fabrics in terms of impact energy absorption and resistance to blunt trauma, while the earlier failure of their primary yarns in the impacted zone was also observed.

In one such work, only silica particles were used for the treatment of Kevlar fabric. Tan *et al.* [59] used water as the medium or carrier fluid instead of ethylene glycol for STF formation. They investigated the ballistic performance of aramid fabric impregnated with a silica colloidal water suspension (SWS) of different particle concentrations in water. The best improvement in ballistic limits and specific ballistic energy was obtained with double ply fabric systems at 40 wt% SWS concentration. It is also noted that at higher SWS concentration and four and six ply fabric systems, the performance deteriorated. As there was no carrier fluid involved, the improvement in ballistic resistance was attributed to increased projectile-fabric friction and inter-yarn friction caused by silica particles. Apparently, without the carrier fluid the particles

tend to dust off making it a non-durable treatment, and hence it has not been a preferred method of application. Although it brings in focus the role of shear thickening as friction in improving ballistic performance of fabrics. Lee *et al.* [113, 209] impregnated the Kevlar fabric with ethylene glycol alone to see the effect of lubricant and found that the energy dissipation was even lower than the neat Kevlar fabric due to decreasing friction. While fabric impregnated with STF shows a significant increase in the energy dissipation and it increases with the volume of STF (Figure 2.27). Thus, this experiment clearly establishes the role of friction in improving the impact performance of the textile materials.

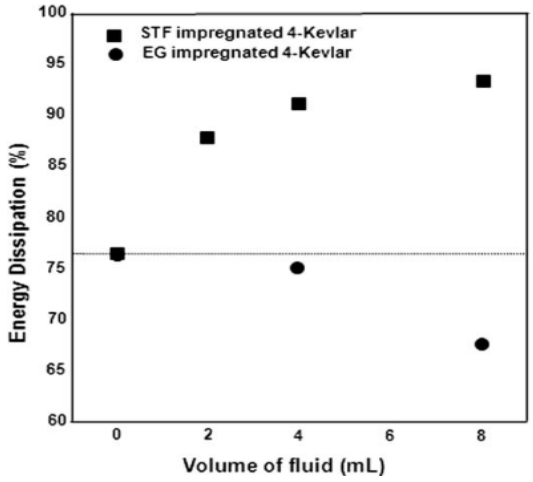

Figure 2.27 Effect of fluid volume on impact energy dissipation of STF and Ethylene glycol impregnated Kevlar fabrics

Majumdar *et al.* [210] employed Box-Benkhen design of experiment (DOE) to analyse the effect of three process parameters (silica concentration, padding pressure, and solvent ratio) on STF application to Kevlar fabrics. They developed response surface equations to relate the STF add-on% and impact energy absorption of Kevlar fabrics with the process parameters. Furthermore, they analysed the significance of the factors in the models in order to understand the level of influence of each parameter. They observed that silica concentration and solvent ratio both influence the STF content on Kevlar fabrics. On the other hand, effects of silica concentration and padding pressure on impact energy absorption were found to be significant. In other words, the impact energy absorption increases with the increase in silica concentration and padding pressure. This was also proved by the work of Srivastava *et al.* [211].

Majumdar *et al.* [210] also reported that the silica concentration has a significant effect in both STF add-on% and impact energy absorption in a similar manner. They noticed that, although the padding pressure influences the impact energy absorption significantly, it has no significant effect on the STF add-on%. It can be inferred that higher silica concentration, higher padding pressure and lower solvent ratio encouraged the higher impact energy absorption by the STF/Kevlar fabric composites.

2.14.2 Increased inter-yarn friction caused by STF associated with ballistic performance

It seems that the improvement in the ballistic protection behaviour of the fabrics treated with STF may partly be due to increase in friction in fabric elements at various levels. The increased friction may prevent inter-yarn mobility at higher strain rates and may lead to increased yarn pull-out energy [212].

Lee *et al.* [113] proposed that the improvement in performance of STF/fabric composites may be due to an increase in the yarn pull-out force. They impregnated the Kevlar fabric with STF and observed the significant increase in the energy dissipation as well as it increases with the volume of STF. However, it is important to point out that the increase in yarn to yarn friction is not the main mechanism responsible for improved ballistic resistance. As an example, Srivastava *et al.* [1] observed that although the increased yarn to yarn friction leads to improvement in yarn pull-out energy, it fails to enhance the ballistic performance.

2.14.3 STF properties associated with ballistic performance

Researches [2] demonstrate that STF enhanced fabrics have taken advantages of the STF properties to fully realise the enhancement of ballistic performance.

Wetzel *et al.* [5] explained that the STF provides coupling and load transfer effects

on a filament-filament, yarn-yarn, or ply-ply level. These interactions modify the fabric's response and may allow the Kevlar yarns to be loaded more efficiently than in absence of STF. A slightly different explanation was that the STF absorbs energy itself, due to viscous dissipation in the fluid. This viscous dissipation would occur as the fluid was sheared, either directly by the projectile or by the relative motion of fabric elements. An alternate interpretation was that the improvements in energy absorption were simply due to increased frictional effects brought about by the increased surface coverage of nanoparticles on the yarn and filament surfaces. However, as has been stated earlier, this may only be partly responsible for the observed effect.

Kalman *et al.* [193] investigated a shear-thickening fluid made from PMMA particles that are softer than both the previous colloidal particles and the Kevlar filaments. Quasi-static spike testing and single layer V_{50} ballistic testing of these STF-fabrics was performed. Interestingly, this composite shows improved performance compared to neat Kevlar under quasi-static spike testing, but exhibits significantly less improvement under low velocity ballistic testing. Microscopy shows little evidence of fibre pitting or significant filament damage, but indicates that the spherical PMMA particles are deformed significantly during loading. The results demonstrate the role of particle hardness in STF-fabric performance.

2.14.4 Properties of STF impregnated fabrics associated with ballistic performance

Apparently, there does not seem to be a clear understanding of the mechanism of enhanced impact resistance of textile structures on the application of STF and research needs to be done to unearth the mechanisms at work during impact loading of STF treated textile structures. Apart from these studies for ballistic performance, it was found in a recent study by Chin *et al*. [213] that untreated ballistic textiles offer

good breathability; in contrast, plastic-coated fabrics such as Argus and Spectra Shield have very low breathability. These materials could cause discomfort if worn in warm climates, unless special carrier design is implemented to manage moisture and heat. The STF treatment slightly decreases fabric breathability, but the fabrics still remain highly breathable. They have found that the use of STF treatments has only a marginally detrimental effect on breathability. So, the fabrics are comfortable yet improve the impact resistance performance.

The development of soft body armours which can provide equivalent ballistic protection with significantly less thickness, more flexibility and proper comfort is necessary to make the user safe as well as not hindering them from moving. Lee *et al.* [113] showed that STF impregnated Kevlar fabrics had superior ballistic protection as compared with neat fabrics without affecting the fabric flexibility and thickness. This was also proved by the work of Hassan *et al.* [203] and Sun *et al.* [214].

2.14.5 STF-fabric panel system associated with ballistic performance

The objective of Park *et al.* [29] research was to characterise the ballistic performance of p-aramid fabrics impregnated with STF focusing on the laminating sequence of the layers. They found that when the STF impregnated fabrics were laminated behind the neat Kevlar layers (N/S-panel), the backface signature decreased compared to the panel of all neat fabrics (N-panel) and the hybrid panel with neat Kevlar layers placed on the backside of the panel (S/N-panel). The enhanced ballistic performance of the N/S-panel was assumed to be due to the synchronized (or coupled) elongation of the facing yarns in the frontal layers and those in the following rear layers during the impact, and this was supported by the method of accumulating successive line segments to present the energy dissipation route of each panel during the impact. The laminating sequence was found to be important to improve the ballistic performance of hybrid panels containing STF, which affected not only the BFS (Backface

Signature) value but also the perforation ratio (or ballistic limit) and bullet expansion. In the patent of Wagner *et al.* [18], they compared the ballistic performance of STF impregnated into Kevlar® fabrics and STF encapsulated in a polyethylene film, stacked on the top of Kevlar® fabrics. Table 2.4 compared the ballistic performance of target E, which consists of 8 ml STF impregnated into 4 layers of Kevlar®, with target F, which contains 8 ml STF encased in polyethylene film, stacked on the top of 4 layers of Kevlar® fabrics. Both target E and F possess the same type and quantity of STF and Kevlar®. However, target E has the STF impregnated into the fabric, while target F stacks the two materials independently. The results show that the impregnated target performs better than the stacked target. This result demonstrates that impregnation of the STF into the Kevlar® fabric is critical to fully realise the enhancement of ballistic performance.

Table 2.4 Comparison of the ballistic performance of STF-impregnated Kevlar® with STF stacked on top of neat Kevlar®

Comparison the ballistic performance of STF-impregnated Kevlar® with STF stacked on top of neat Kevlar®				
Sample Target	Description	Sample Weight (g)	Impact Velocity (m/s)	Penetration Depth (cm)
E	8ml STF impregnated into 4 layers of Kevlar®	13.9	253	0.673
F	8ml STF encapsulated, stacked on top of 4 layers neat Kevlar®	13.9	247	1.72

2.15 Researches on stabbing resistant fabric impregnated with STF

Although extensive work has been done on the application of STF on textiles for

improvement of ballistic impact resistance, a few studies related to stab, puncture and needle resistance have also been investigated. Recently, the stab protection of the STF-based body armour has attracted increasing attention due to their practical applications. STF impregnated body armour will be offered good protection against knives and other handmade sharp weapons.

2.15.1 Researches on STF properties associated with stabbing resistant performance

In some recent studies, Decker *et al*. [12, 205, 208] studied the stab resistance properties of fabrics impregnated with STFs. The STFs used were based on colloidal silica particles dispersed in PEG at a volume fraction of approximately 0.52. NIJ standard 0115.0 for stab resistance of body armour was used for measuring the stab resistance. Testing for stab resistance is commonly known as drop tower test [153]. The apparatus consists of either knife or spike that drops freely under its own weight to strike the armour panel at a specified energy [66]. In addition to the drop tower tests; quasi-static stab tests were also performed. Figure 2.28 shows the results of knife drop tower test of untreated Kevlar and STF treated Kevlar fabrics which demonstrate that penetration depth into the backing material increases with the increase in impact energy. The study of the damage mechanism was done with the help of photographs and SEM images of damaged fabrics. It was found that the extent of fabric damage was less in the STF treated Kevlar fabric. The 12-layer STF treated Kevlar fabric provided better protection than the 15-layer untreated Kevlar fabric. The quasi-static knife testing results showed that STF treatment of the Kevlar fabric significantly enhances the cut resistance even at low loading. Similar results were reported by Egres *et al*. [207] Treatment of silica based STFs on the Kevlar fabric was also reported to significantly improve the puncture resistance with hypodermic needles [205]. Kang *et al*. [215] also reported the similar behaviour with the application of STF on Kevlar fabrics.

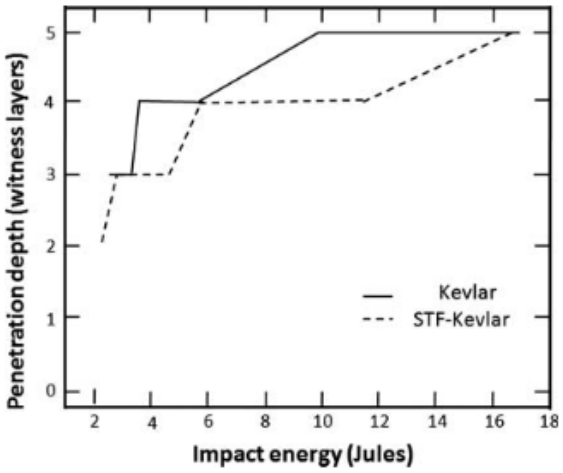

Figure 2.28 Knife drop tower results for neat Kevlar and silica-STF treated Kevlar fabric [195]

Decker *et al*. [195] and Mahfuz *et al*. [25] investigated the stab resistance of STF treated Kevlar and nylon fabric with different fabrication methods and found that the STF-treated fabric exhibited significant improvements over the neat fabrics.

2.15.2 Researches on rheological properties of STF associated with stabbing resistant performance

In Xinglong Gong's research [216], the effect of the particles' types on stab resistance of the body armour has been investigated. In general, the stab resistance can be divided into two categories: knife stab resistance and puncture resistance, which refer to the penetration resistance by knives with sharp edges and by instruments with sharp tips (such as spikes), respectively. In order to investigate the effect of the particle's types on the stab resistance performance, the targets with different kinds of STFs which comprised different types of particles and the dispersing medium Ethylene Glycol, were employed to compare the distinction of stab resistance performance through the drop tower testing. For the STF-fabric targets, the hard SiO_2 particles target exhibits the best knife stab resistance performance, and the soft PMMA particles target has the worst knife stab resistance performance. The results show that the interaction of the particles and the filaments is important for the knife stab

resistance of the fabrics. Harder particles tend to result in a greater strengthening in intension of the filaments than softer particles.

Kalman *et al*. [193] compared the penetration resistance of Kevlar fabric treated with only silica powder (dispersed particles), polymethylmethacrylate alone (carrier fluid), and STF. It was found that both dry particle and STF treatments resulted in improvements in fabric properties relative to neat or polyethylene glycol (PEG) treated fabrics. On comparison of treatments with different particle hardness, the SiO_2 materials performed better in all tests than comparable PMMA materials.

In Gong's work [216], the influence of the STFs' components on the knife stab and puncture resistance performance of the STF enhanced fabric was studied. The intrinsic properties of the STFs were tunable by varying the dispersing particles from the spherical Silica (SiO_2), to polystyrene-ethylacrylate (PSt-EA) and polymethylmethacrylate (PMMA), and the dispersing medium from ethylene glycol (EG) to polyethylene glycol 200 (PEG200) and polyethylene glycol 600 (PEG600). The hardness of the particles was the dominant factor for the knife stab resistance, while the inter-yarn friction played as the critical role for improving the puncture resistance. In comparison to neat fabric, the knife stab and puncture resistance of the shear thickening fluid fabrics exhibited significant enhancement, which can be proven by the results of yarn pull-out testing and optical microscope images investigation.

2.16 Preparation of STF-fabric composites

In the past few years, many researchers [1, 3] have used various techniques to prepare the STF/fabric composite with enhanced impact resistance properties. The recently developed approaches that have been used for the preparation of STF/fabric composite targets are based on impregnating process. For impregnation of the fabrics with STFs, first, the dispersion of nanoparticles in a suitable compatible medium with required composition must be prepared with the help of high speed homogenizer or

ultrasonicator. Since such dispersions are highly viscous, it is difficult to treat textile fabrics uniformly with it and ensure its proper penetration into the fabric. So, they are diluted using alcohols, such as methanol and ethanol, to facilitate impregnation of the STF into the fabric by decreasing the surface tension of the dispersion. These diluted STFs uniformly impregnate the fabrics by padding, followed by the removal of alcohol from the fabrics in a convection oven. It should be noted that the alcohol has no effect on the final STF/ fabric composite.

2.17 Efforts to improve stabbing resistance of ballistic body armour

The flexible armour that has been developed usually gives resistance against ballistics only or sharp cutting impacts only. Protection against both threat systems incorporating the desired lightweight and flexible characteristic is under continual investigation.

Several techniques had been applied such as roughening the surface of fibres or yarns by sanding or corona treatment, or coating fabric with polymer or dry powder that exhibits dilatant properties [48] to achieve a higher coefficient of friction. Higher inter-yarn friction is believed to increase energy transfer properties of ballistic body armour. The polymer matrix provides additional toughness to the woven fabrics, requiring more energy to cut and separate fibres and yarns [217]. However, such roughening is believed to have limited utility due to the resultant degradation in the fibre [13] and the dry powders coated on the fabrics are easy to be removed off. These techniques have been shown to provide outstanding stab resistance but decreased ballistic resistance.

Aramid fabrics with high yarn count were also developed to provide stabbing (puncture) resistance. However, these high yarn count fabrics were expensive to manufacture and typically resulted in decreases in the ballistic protection efficiency of the fabrics [12].

Rainer Gadow *et al*. [218] coated fabrics made of high-tenacity aramid fibres with refractory cermet and oxide ceramics of high hardness by thermal-spray technologies without damaging the initial fibres to enhance their protective performance. The ceramic coating increases the fibre-to-fibre friction that prevents wave distortion and delamination. Penetrating objects cannot change the fabric structure and push the fibres aside. The hard material coatings blunt sharp metal blades by abrasion so they cannot cut the fabric, and the high friction between the ceramic coating and the metal blade stops further penetration. These materials have demonstrated increased energy absorption during the quasi-static stabbing test, but also added to fabric weight significantly.

2.18 Summary

This Chapter reviewed the studies on stabbing attack mechanisms, ballistic impact mechanisms and shear thickening fluids theory and production. Different approaches to improve stabbing resistance and ballistic performance of soft body armour were examined. Various rheological parameters such as dispersed particle size, particle shape, particle size distribution, particle concentrations, dispersing medium viscosity, the temperature of the system and particle-particle interactions were discussed to form the comprehensive studies on rheological properties control of STFs. Finally, different approaches were specified on impregnation of STF into soft body armour for improved impact performance.

Generally, the ballistic and stab protection properties are treated as two different attributes required for different applications and hence engineered independently, however the above findings show that it is possible to incorporate better stab resistance as well as ballistic protection in the fabrics by treatment with STFs.

Chapter 3

Preparation and Parametrical Control of Rheological Properties of STF

3.1 Introduction

As stated in the literature review, despite the establishment of the basic mechanism of shear thickening materials, control of STF production parameters over shear thickening behaviour remain to be further investigated.

Given the vast amount of literature on STF rheology, few experiments have been conducted on control of critical shear rate with the aim of related to the impact shear rate improving the impact resistance performance. There are also a limited amount of researches of investigating severity shear thickening viscosity of STFs because higher viscosity jump would lead to higher energy dissipation during the impact process. Every impact event has its shear rate which can be related to the critical shear rate of STFs. This is necessary for determining how the critical rate affects the shear thickening behaviour of STF because higher energy absorption in an impact event is due to the transformation state of STF from a liquid state to solid-like. Thus, the aim of this research is to determine the critical shear rate and shear thickening viscosity by employing those parameters which may influence the rheological properties of STFs. In this work, factors affecting shear thickening behaviour have been explored in terms

of such suspension parameters as STF dispersion particle size, particle concentrations (solid weight fraction) and dispersing medium on reversible shear thickening phenomenon by performing rheological measurements. Besides these three factors, the ambient temperature is also studied as an environmental influencing factor. Additionally, a predictive method for determining the onset of shear thickening and increase of shear thickening viscosity are presented.

3.2 Design and preparation of STFs

3.2.1 Materials

STF was composed of the dispersed phase and the dispersion medium, in this research the STF colloidal dispersions are made from spherical silica nanoparticles and PEG (Polyethylene Glycol). In order to explore factors that influence the critical shear rate and shear thickening viscosity of the STFs, different particle sizes, particle weight fractions (concentrations) and dispersing media were taken into consideration.

Four different sizes of silica nanoparticles with the specific density of 36.8kg/m^3 (at 25°C) supplied by Sigma-Aldrich (Germany), were selected for STF preparation. The fine, special amorphous powder material (commonly known as fumed silica) with high purity was obtained by chemical vapour deposition method at a high temperature and content of SiO_2 was not less than 99.8%. All the different particle sizes of silica nanoparticles are monodisperse spherical silica particles. Table 3.1 shows the sizes of the particle sizes and their surface areas.

Table 3.1 Silica nanoparticle sizes and surface areas [219]

Particle Size	Surface Area
12nm(TEM diameter)	325m^2/g±25 m^2/g
15nm(TEM diameter)	300m^2/g±25 m^2/g
200nm(TEM diameter)	200m^2/g±25 m^2/g
400nm(TEM diameter)	110m^2/g±20 m^2/g

Changes in dispersing medium, arising from varying the molecular weight are expected to affect the shear thickening behaviour. Three types of PEG solvent media with different values of average molecular weight were selected. PEG was chosen as a solvent due to its non-toxicity, low volatility and thermal stability. The technical information of the PEGs selected for this research is listed in Table 3.2.

Table 3.2 PEG information [220]

Average molecular weight of PEG	Company	Molecular formula	Flashpoint	Melting point	Density
200	Alfa Aesar, UK	$H(OCH_2CH_2)_nOH$	171°C	-55 to 40°C	1127kg/m^3
400			240°C	4-8°C	1126kg/m^3
600			252°C	17-23°C	1120kg/m^3

Experiments on the influence of silica weight concentration on rheological properties of STF were also devised using PEG200 and 12nm silica. The concentrations used in this study were 10%, 15%, 20%, 25%, 30% and 33% (highest particle concentration can be achieved with 12nm silica and PEG200).

Temperature as a significant environmental factor which may influence the rheological properties of the STFs was taken into consideration as well. Each STF samples was tested at five temperatures: 0°C, 10°C, 20°C, 30°C 40°C and 50°C. The measuring temperature was controlled using the Peltier temperature control device on the equipment. The ambient temperature was stabilised at 20°C.

3.2.2 Designs for STF Production

In order to systematically study the influence on the critical shear rate of STF, three categories of STFs were prepared according to particle size, particle weight fraction, and dispersing medium in this research, and the details of which are listed in Table 3.3.

Table 3.3 Preparation of STF samples

Influencing Factor	Compositions	Particle Weight Fractions
Particle Size	12nm + PEG200	25%
	15nm + PEG200	
	200nm + PEG200	
	400nm + PEG200	
Particle Concentrations	12nm + PEG200	10%
		15%
		20%
		25%
		30%
		33%
Dispersing Medium	12nm + PEG200	20%
	12nm + PEG400	
	12nm + PEG600	

3.2.3 Preparation steps in making STFs

STF was prepared primarily by mechanical stirring and ultrasonic vibration method, and the preparation process is described in the following steps:

(1) A certain amount of PEG liquid was added into a beaker, a high speed homogenizer (Silverson L4R homogenizer emulsifier) was used to stir the dispersion so as to achieve an even distribution of particles in STF production, and the stirrer speed was set to 6000r / min.

(2) The SiO_2 powder was added into the homemade funnel, weighed and gradually added into the PEG, the each amount should be kept as not too much, after stirred and dispersed, and then continually added, until reaching the desired content.

(3) Since it was easy to form agglomeration, in order to ensure uniform dispersion of silica nanoparticle, the dispersion was subjected to ultrasonic vibration, to improve dispersion degree of the STF system during the adding process.

(4) During the agitation, SiO_2/PEG dispersion contained a lot of bubbles, so the STF

dispersion was placed in a vacuum oven at room temperature (25°C)to deal with vacuum treatment to remove thoroughly the residual air bubbles for 24 hours prior to rheological measurements.

Figure 3.1 shows the STF preparation process.

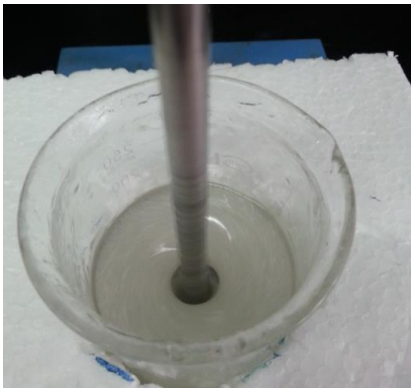

(a) Mechanical stirring

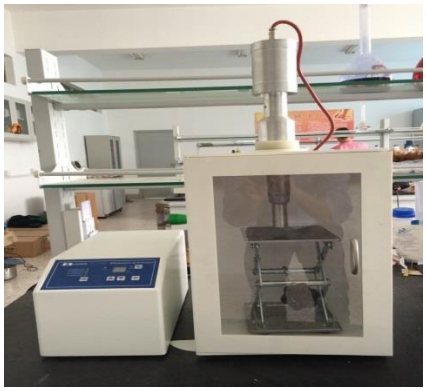

(b) ultrasonic wave vibration

(c) Vacuum treatment to remove bubbles

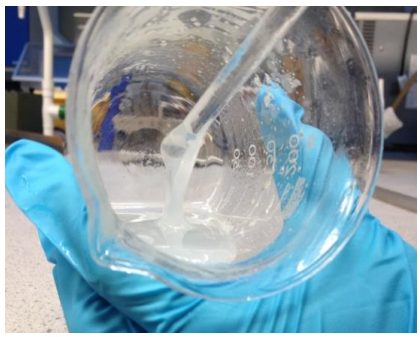

(d) the final product

Figure 3.1 Preparation steps of STF

3.3 Measurement of the rheological Properties of STF

3.3.1 Instrument

The rheological properties of SiO_2/PEG system were measured using TA AR-G2 stress-controlled rheometer with cone-and-plate geometry. The testing principle of this instrument was shown in Figure 3.2. During the testing process, the fluids were located in the inside zone between the upper cone and lower measuring plates. It was reported [184] that the critical stress value marking shear thickening is dependent on

rheometer plate gap interval. In this study, 1mm gap interval between the cone and plate was used for the measurement of all the STF samples, with the cone diameter being 50mm so as to eliminate the effect of the gap size and to neglect the effect of wall slip. The upper measuring cone is connected with air bearing loading by shearing at a constant increasing stress at the shear rate of 0.01 s^{-1} to 1000 s^{-1}. The lower measuring plate was fixed and can control the measuring temperature range from -10°C to 150°C. The relationship between viscosity and shear rate was depicted for different categories of STFs and the tests took place at the ambient temperature.

It should be noted that wall slip could cause loss of material due to centripetal forces in cone and plate rheometers. When the viscosity is dramatically increased, the clusters in the suspension can even be cell spanning and severe wall slip can occur above the critical shear rate. Hereby the viscosity is too large to measure and meaningful experiments cannot be performed anymore.

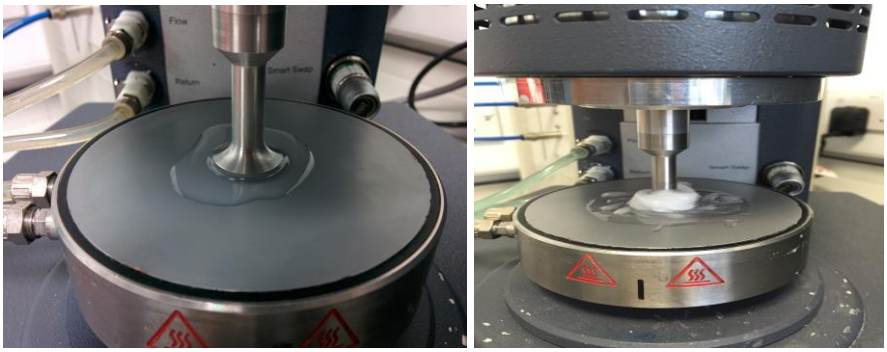

(a) Before the test (b) During the test

Figure 3.2 The TA AR-G2 rheometer

When the upper measuring cone was rotated with angular velocity of ω, the stress τ and shear rate (strain ratio) γ of fluids between the upper and lower measuring plates can be expressed as:

$$\tau = K_{\tau} M \qquad (3.1)$$

$$\dot{\gamma} = K_{\gamma} \omega \qquad (3.2)$$

where， K_{τ} is stress constant, K_{γ} is strain constant； M is twist moment from the

viscosity of liquids to plates. When the diameter of the parallel plate is R, and the height between two plates is H, then the stress constant K_τ and strain constant K_γ can be expressed as:

$$K_\tau = \frac{2G}{\pi(\frac{R}{10})^3} \quad (3.3)$$

$$K_\gamma = \frac{R}{H} \quad (3.4)$$

where G, is gravity acceleration. So the viscosity of fluids η can be expressed as

$$\eta = \frac{\tau}{\dot{\gamma}} = \frac{K_\tau M}{K_\gamma \omega} \quad (3.5)$$

3.3.2 Rheological measurement procedures

In order to improve the consistency of the testing, the trial test was carried out before every official test, as described in the following: firstly, the sample was remained stable for 3 mins under the shear rate of 0.1 s^{-1}, and then sheared 2 mins with a shearing rate of 10 s^{-1}, then, the sample was remained stable for 3 min again, finally shear the sample at the shear rate of 1000 s^{-1} for two minutes. The test temperature is 25°C, and the shearing rate was set to 0.1-1000 s^{-1}.

All the rheological tests follow the general outline below:

- Turn on the computer controller
- Turn on the air supply to the rheometer
- Remove the black bearing lock
- Turn on the power to rheometer
- Select and install the appropriate geometry for the desired tests and testing temperatures

- Take out a small amount of STF samples and place in the middle of the lower plate
- Lower the upper cone to the determined gap geometry
- Trimming the STF samples to the correct filling of the gap
- Run test and STF sample is loaded
- Displaying and analysing results

The rheological properties of SiO_2/PEG system with different compositions were measured to investigate the relationship between the viscosity η and shear rate $\dot{\gamma}$. The viscosity of STF samples was measured as a function of shear rate.

3.4 Test results and discussions on STF rheological properties

The rheological properties of different silica nanoparticle sizes, particle weight fractions (concentrations) and dispersing medium were evaluated. Each of the STF dispersion was tested in same rheological detail and the onset of shear thickening phenomena identified from a double logarithmic plot of the data from rheometer measurements. The critical shear rate $\dot{\gamma}_c$ is defined to be the shear rate where viscosity of STFs will increase abruptly implying the onset of shear thickening which is a vitally important rheological property of STF.

3.4.1 Influence of silica nanoparticle size

The viscosity of the STFs generated with four different nanoparticle sizes is depicted below in Figure 3.3 as a function of the applied shear rate. The rheological data of STF are determined by fitting the double logarithmic plots of viscosity vs. shear rate to a quadratic curve. The particle volume fraction was kept 25% for all STF samples, whose dispersing medium is PEG200.

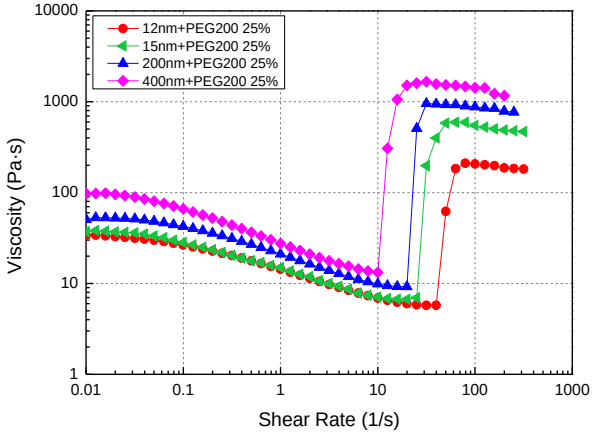

Figure 3.3 Viscosity vs. shear rate for four types of STFs generated with different silica nanoparticle sizes

As can be seen in Figure 3.3, there are three different stages of the system with the increase of shearing rate and the three stages can be described as follows: firstly shear thinning and then shear thickening and finally to a plateau viscosity at high shear rates. At the initial stage, the initial viscosity η_0 (i.e. the viscosity of the first result from the rheological data) of the system maintain at relatively low level, and the viscosity of system decreases gradually with the increase of shear rate, which is called the shear thinning phenomenon. When the critical shear rate $\dot{\gamma}_c$ is reached, the viscosity of system reaches the lowest value and the viscosity named as critical viscosity. Subsequently, the viscosity begins to increase sharply, and reaches to the maximum value. This process is called the shear thickening stage, displaying the transformation from the liquid to the solid state. Finally, the system comes to a viscosity plateau until the wall slip happens. It should be noted that the shear rate which marks the onset of shear thickening is called critical shearing rate, and the maximum viscosity after shear thickening is called the post-thickening viscosity.

A shear thickening behaviour was shown clearly for each of the STF samples at a corresponding shear rate. The viscosity of STF increases abruptly at the critical shear rate, which implying the onset of shear thickening. It is observed that the STF generating with 400nm particle sizes of silica shows the lowest critical shear rate of

$10s^{-1}$ and the STF viscosity finally rises up to 1659 Pa·s, representing the highest viscosity among the four STF samples. On the other hand, the STF with 12nm particle size leads to the highest critical shear rate value of 39.81 s^{-1} and the viscosity reaches to 211 Pa·s. Figure 3.3 demonstrates clearly that the larger is the silica nanoparticle, the lower is the critical shear rate of the STF, and vice versa. It is also apparent from Figure 3.3 that the thickening effect is more obvious at the critical shear rate for STF with larger particles than that with smaller particle sizes. Additionally, the viscosities of the STFs before and after the critical shear rate (i.e. absolute viscosity of STF) increase when the nanoparticle size changes from small to large.

Systematic data are presented for the effect of nanoparticle sizes are shown in Figure 3.4 and 3.5.

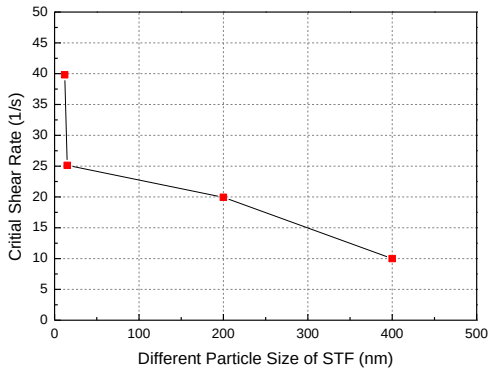

Figure 3.4 Critical shear rates of four types STFs generated with different silica nanoparticle sizes with PEG200 at 25% particle concentration vs. Different nanoparticle sizes

Figure 3.4 illustrates the relationship between the nanoparticle sizes and corresponding STF critical shear rates. In general, the critical shear rate decreases as the silica nanoparticle size becomes larger, as discussed earlier. The curve shows specifically that the decrease in critical shear rate is much more sensitive for STF with small particle sizes. In particular, it is 185 times (calculation results of the gradient) more sensitive between the 12 and 15nm particles than that between 15 and 200nm

particles. In other word, small nanoparticles affect the critical shear rate more obviously than the larger nanoparticles. The critical shear rate of STFs was found to be inversely proportional to the particle size.

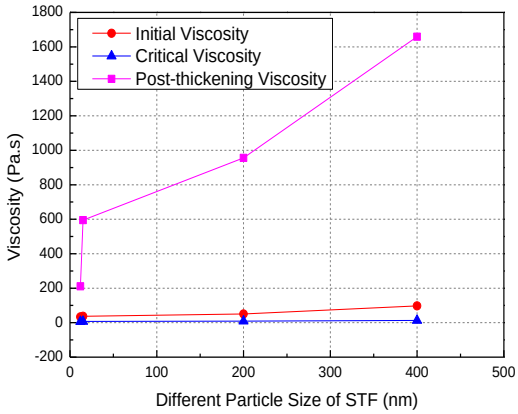

Figure 3.5 Initial viscosities and Maximum viscosities of four types of STFs generated with different silica nanoparticle sizes with PEG200 at 25% particle concentration vs. Different nanoparticle sizes

Figure 3.5 contrasts the viscosity values of the STFs with different silica nanoparticles at different levels of shear rate. For the STFs made from PEG200 with 25% particle volume fraction, whilst the initial viscosity and the critical viscosity hardly change with the increase of nanoparticle size in the STFs, the post-thickening viscosity increases remarkably along with the increase of the nanoparticle size. It is noted that the larger is the nanoparticle size, the bigger is the difference between the critical viscosity and the post-thickening viscosity. For instance, the difference between the critical viscosity and post-thickening viscosity is 205 Pa·s for the STF with 12nm particle, but that for 400nm particle becomes 1646 Pa·s, which is a dramatically increased change on shear thickening viscosity.

In general, the flow curves systematically shift to lower critical shear rates with increasing nanoparticle size. And STFs generating with larger particles lead to more dramatically change on STF's viscosity from critical viscosity to post-thickening viscosity.

3.4.2 Influence of silica nanoparticle weight fraction

Nanoparticle weight fraction (concentration), which is the fraction of the weight of the STF system occupied by the particles, has been studied in this section for its influence on the critical shear rate of STFs. As mentioned earlier, this study is based on STFs based on STFs made from PEG200 and 12nm silica nanoparticles. The weight fraction used for the STFs are 10%, 15%, 20%, 25%, 30% and 33%, whereas 33% is the maximum of the particles weight fraction that can be added into medium to create STF with PEG200 and 12nm particle.

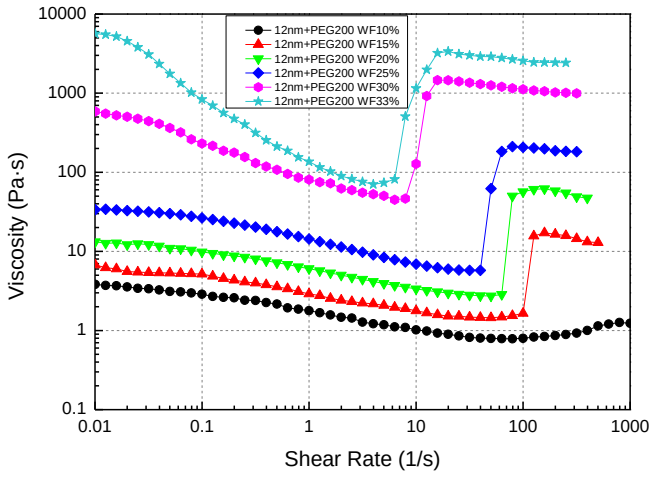

Figure 3.6 STFs' viscosities vs. shear rate for five types of STFs of different nanoparticle concentrations

Figure 3.6 illustrates in logarithmic plots the viscosity change against the change made in shear rate, and it showed that shear thickening happens for STFs with all particle weight fractions except for 10% particle concentration. It indicates that a certain minimum level of particle weight fraction is required to observe the shear thickening behaviour in an STF. Among the weight fraction levels selected for this study, a particle weight fraction higher than 10% would be able to produce obvious shear thickening phenomenon. All the levels of particle concentrations of STF samples exhibited obvious shear thinning phenomenon at low shear rate. After the thinning process, shear thickening behaviour takes place on different critical shear rates and occur in different shear thickening viscosity change amplitude for all STF

samples except the one with 10% particle weight fraction. With increasing the content of silica nanoparticles, the critical shear rate decreases and the increase of viscosity in the shear thickening region increases. Furthermore, the relative viscosity is increased as the silica nanoparticle weight fraction increased.

Systematic data are presented for the influence of nanoparticle concentrations are displayed in Figure 3.7 and 3.8.

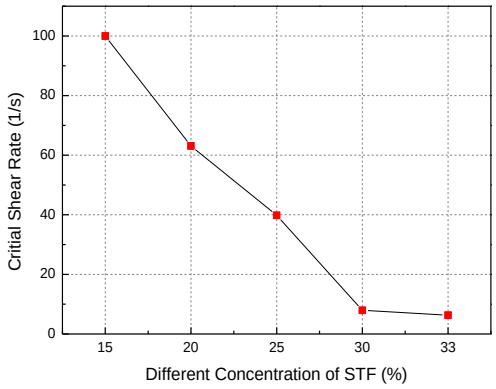

Figure 3.7 Critical shear rate vs. 12nm SiO_2 with PEG200 produced STFs at different nanoparticle weight fraction (concentrations)

Figure 3.7 illustrates the effect of nanoparticle weight fraction on the critical shear rate at which shear thickening is initiated in STF suspensions produced from PEG200 and 12nm silica particles. It is clear from Figure 6 that increasing particle weight fraction leads to lower critical shear rate and the relationship between particle concentration and critical shear rate (CSR) is almost linear for the particle weight fractions from 15% to 30%. It is observed that STF at 33% concentration shows the lowest critical shear rate of $6.31s^{-1}$ and STF at 15% concentrations shows the highest critical shear rate of $100s^{-1}$. It should be aware of that the decrease in critical shear rate becomes less obvious when the particle weight fraction is increased from 30% to the maximum 33%, which is due to the critical shear rate is already quite close to zero. It can be concluded from the curves that shear thickening behaviour is occurring at lower critical shear rates for higher particle concentrations of STFs.

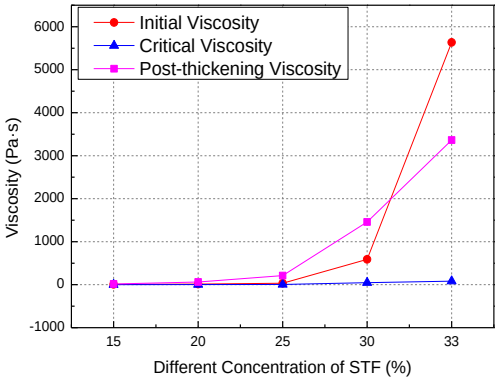

Figure 3.8 Initial viscosity and Maximum viscosity of STFs vs. 12nm SiO_2 with PEG200 produced STFs at different nanoparticle weight fraction (concentrations)

Figure 3.8 summarises STF viscosities on three important statuses of shear thickening phenomena as a function of nanoparticle weight fractions (concentrations) at fixed nanoparticles and fixed dispersing medium. It is spotted that the viscosity of STF at 33% concentration rises from 82 Pa·s up to 3363 Pa·s as a result of the shear thickening. For the STF at 15% particle concentration, the viscosity changes from 2 Pa·s to 17 Pa·s finally. Whilst the critical viscosity is not affected much by the particle weight fraction, the initial viscosity and post-thickening viscosity increase remarkably with the increase of the silica particle weight fraction, most notably at fractions of 30% and 33%. It is worth noting that at the maximum weight fraction 33%, the initial viscosity is even higher than the post-thickening viscosity.

It can be concluded that increasing the particle weight fraction in STF leads to a decrease in the critical shear rate while the aspect ratio of particle increases. And at higher shear rates in the shear thickening region, the higher particle weight fraction STF exhibits a greater increase in viscosity. In general, STFs of higher nanoparticle concentrations have been found to thicken at lower shear rates, and exhibits a greater increase in viscosity.

3.4.3 Influence of dispersing medium

Rheological properties of STFs was investigated based on three different polyethylene glycol (PEG) medium, which have different molecular weight (molecular chain lengths) of 200, 400 and 600. And the nanoparticle used in this experiment is 12nm particle silica and the particle weight fraction in this group of STFs is 20%. The rheological data of these STFs are presented in the form of the double logarithmic plot of viscosity vs. shear rate to a quadratic curve which is shown in Figure 3.9.

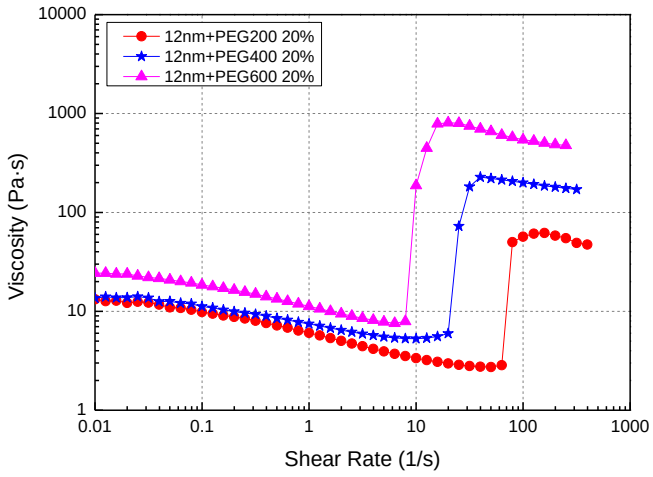

Figure 3.9 Viscosity vs. shear rate for three STFs produced with different molecular weights of PEG

The shear thickening behaviour of the three STFs are demonstrated in Figure 3.9. The same as for the other STF groups, these STFs exhibit shear thinning at lower shear rates before shear thickening is shown at higher shear rates. The STF produced with PEG600 shows the lowest critical shear rate of $7.94s^{-1}$ and the viscosity finally rises up to 808 Pa·s. In general, it apparent that a dispersing medium with a heavier molecular weight is associated with a lower critical shear rate, and vice versa. Equally importantly, the thickening effect is more obvious for STF with a dispersing medium having higher molecular weight than that having lower molecular weight. For instance, the viscosity of the STF with PEG200 increased 21 times after thickening and that with PEG600 showed 102 times.

The critical shear rates of STF colloidal dispersion has been shown in Figure 3.10 as a function of different molecular weights of PEG. The critical shear rate is found to decrease when the molecular weight of the medium increases, as illustrated in Figure 3.10. It is also found that the influence on the critical shear rate is more sensitive to the lighter PEG medium than with the heavier. Based on Figure 3.10, the critical shear rate increase more than 3 times when the PEG molecular weight is reduced from 400 to 200, but the critical shear rate is only doubled when the PEG molecular weight is reduced from 600 to 400. This suggests that PEG with lower molecular weight would cause the critical shear rate to change more effectively.

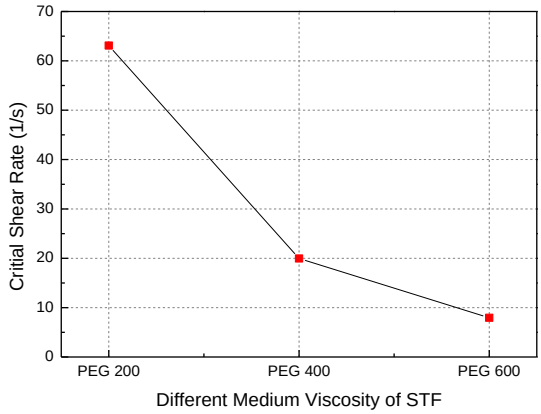

Figure 3.10 Critical shear rate of different medium with 12nm particles at a particle concentration of 20% vs. Different medium viscosity (molecular weight)

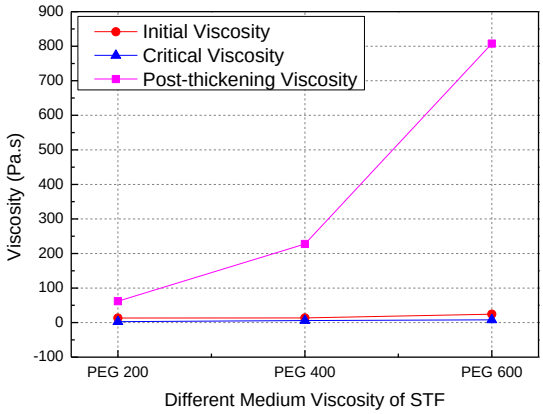

Figure 3.11 Initial viscosity, critical viscosity and post-thickening viscosity of STFs vs. Different medium viscosity with 12 SiO_2 at nanoparticle weight fraction of 20%

The molecular weight of the PEG remarkably influences the thickening effect of the STFs. Figure 3.11 depicts the relationship between different dispersing medium and viscosities of STFs at different stages of rheological tests. As can be seen in Figure 3.11, the post-thickening viscosity of STF with PEG600 reaches 808 Pa·s, representing a 102 times increase in viscosity. On the contrary, the post-thickening viscosity for STF with PEG200 is only 21 times higher than the critical viscosity. Moreover, the absolute STF viscosity increases with increasing medium viscosity. Also, the severity of the shear thickening is amplified for higher molecular weights.

In general, it has been found that changing the medium viscosity expedites shear thickening to lower critical shear rate with increasing molecular weight polyethylene glycol, lower medium viscosity decreases post-thickening viscosity which is achieved after shear thickening phenomenon.

3.4.4 Influence of system temperature

As have been stated in the literature review, system temperature is one of the major influencing factors on STF rheological properties. The nanoparticle size, nanoparticle weight fraction and dispersing medium are dependent on the dispersion production parameters. While the influence of temperature on STF rheological properties are associated with the ambient environment conditions. Due to the rheometer instrument used in this research can adjust the measuring temperatures, STF samples generated from 12nm silica and PEG200 at 25% particle concentration were taken out for investigations on temperature effects. The system temperature dependence on rheological properties of STFs has been studied in this section.

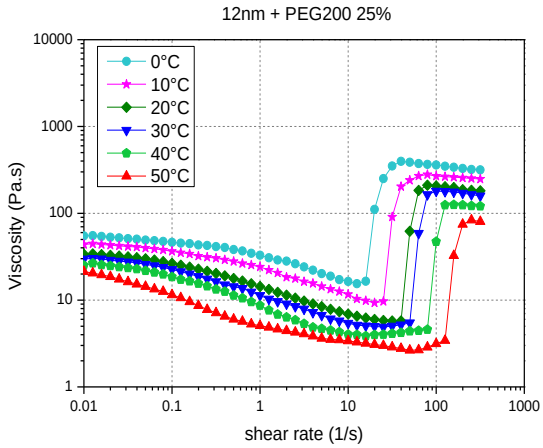

Figure 3.12 Influence of system temperature on STF rheological properties

Figure 3.12 displays logarithmic plots of the STF shear rate vs. STF viscosity through the whole process of the measurement with the temperature ranges from 0°C to 50°C. It can be seen from the diagram, when the temperature was increased from 0°C to 50°C, the viscosity change trend of 12nm SiO_2/PEG200 system is unchanged, and it still can be divided into three stages: shear thinning, thickening and viscosity plateau. However, it can be observed that the critical shear rate and shear thickening viscosity change of the STF samples were varied by changing the temperature. In general, a lower system temperature is associated with a lower critical shear rate and greater shear thickening jump, and vice versa. The logarithmic values are inversely proportional to temperature, which means that the shear thickening behaviour more readily enhances as temperature decreases.

Consequently, it has been demonstrated that the critical shear rate for shear thickening and shear thickening viscosity in the shear thickened state are dependent on the system temperature. And the shear thickening phenomenon still can be observed in the temperature range of 0°C to 50°C. The critical shear rate increases and shear thickening behaviour weakens as the ambient temperature increases. As results of that, the influence of system temperature should be considered in practical application.

3.4.5 Rheological evaluation of pure PEG dispersing medium

The purpose of this measurement is to investigate rheological properties of liquid medium without dispersed particles as a comparison with rheological properties of STFs producing with PEGs. As presented in Figure 3.13, the viscosities of all the three PEGs under different shear rates maintained at a relatively low level, which means they are quite flowable as a liquid medium. For different molecular weight PEG media, the viscosities are relatively constant under the shear stresses. There are no shear thickening or shear thinning phenomenon observed for all three PEGs. Moreover, the relative viscosity of pure PEGs increases with the increase of their molecular weight.

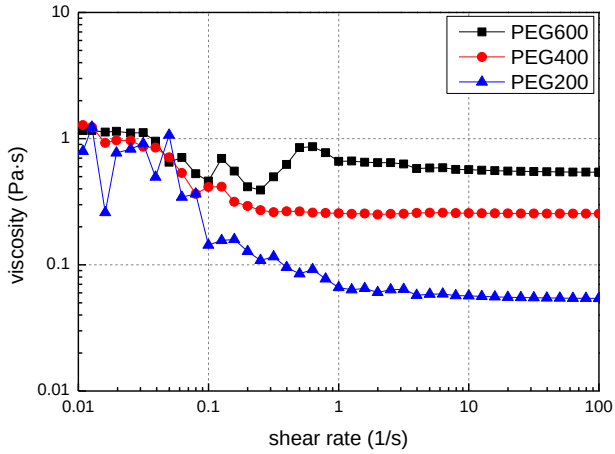

Figure 3.13 Rheological properties of PEG with three different molecular weights

From Figure 3.13, it has displayed the absolute difference in rheological properties of pure PEG media from rheological properties of STFs producing with PEG media.

3.5 Analysis and discussions of shear thickening behaviour mechanisms

All of the rheological testing results presented in this research indicate that shear thickening transition occur and the magnitude of the viscosity increase can be controlled by changing the particle size, particle concentrations and dispersing

medium viscosity. All the results suggest that if all other parameters of the STFs production are held constant, the critical shear rate is independent of each production parameter.

This research confirms that lower critical shear rate and amplified severity shear thickening viscosity of STFs can be achieved by using larger particle size, higher particle weight fraction and higher PEG molecular weight of dispersing medium. In the case of achieving higher critical shear rate, smaller particle size, lower particle weight fraction, and PEG with lighter molecular weight will need to be used, with the sacrifice of reduced thickening of the STF. The background theory and mechanisms of shear thickening phenomenon are associated with the influencing factors were discussed and analysed as follows.

3.5.1 Theoretical background of shear thickening behaviour mechanisms

Many researchers have deeply investigated the connection between the macroscopic rheological properties and the microstructure of STF dispersion, and there are two explanations for the shear thickening mechanism in STF systems: order-disorder theory and hydro-cluster theory. As have been stated in the literature review, currently the ‘particle hydro-cluster’ mechanism is well accepted and convince for an explanation of shear thickening phenomenon [167].

3.5.1.1 Hydro-cluster theory

Shear thickening behaviour in colloidal suspensions relies on the formation of agglomerates of particles, known as hydro-clusters. This name originated from the fact that clusters are formed by hydrodynamic forces. At rest or low strain rates, particles in suspensions tend to move away from each other due to repulsive interparticle electrostatic or Brownian forces, which stabilise the suspension and maintain a low viscosity [190]. With an increase of the flow rates, hydrodynamic

forces increase and tend to move the particles closer. When the hydrodynamic lubrication forces become higher than the repulsive forces, the particles aggregate into clusters [167]. These aggregates hindered the flow and explain the strong increase of viscosity observed at a critical shear rate. However, this hydro-cluster is unstable, and the hydro-cluster will decompose when the shearing rate decreased. The dispersing system will restore the original balance state, and viscosity goes back down. Therefore, the thickening phenomenon is reversible.

3.6.1.2 Péclet number theory

The fundamentals of hydro-clustering theory have been first exposed for spherical Brownian suspensions in function of the Péclet number [167]. For the low-shear structure, the shear viscosity was shown to be proportional to the Péclet number [221].

Different types of STFs can be effectively collapsed by scaling the shear rate with Péclet number, defined by Equation (3.6), and the suspension viscosity with medium viscosity η_s, at the respective temperature of each test. In Equation (3.6), a is the particle radius, m; k_B is the Boltzmann constant, 1.38×10^{-23} JK^{-1}; T is the temperature, K; $\dot{\gamma}$ is the shear rate, s^{-1} and η_s is the temperature dependent medium viscosity.

$$\mathrm{Pe} = \frac{a^2\dot{\gamma}}{D_0} = \pi r^2 \frac{6\,\pi\,\eta_s \dot{\gamma} a^3}{k_B \mathrm{T}} \qquad (3.6)$$

where D_0 is the Stokes-Einstein diffusion coefficient, k_BT is the thermal energy.

The number is useful because dispersion rheology is often measured by applied shear rates or shear stresses. Low *Pe* is close enough to equilibrium that Brownian motion can largely restore the equilibrium microstructure on the time scale of slow shear flow. At sufficiently high shear rates or stresses, though, deformation of the colloidal microstructure by the flow occurs faster than Brownian motion can restore it.

The *Pe* number expresses the ratio between shear forces and Brownian forces. Shear thinning is already evident around *Pe* ≈ 1 from Van der Werff and de Kruif [186]. If *Pe* > 1, Brownian motion can be neglected and there is a shear thinning transition from a Brownian dominated to a hydro-dynamically dominated regime. And higher shear rates or stresses (higher *Pe*) trigger the onset of shear thickening. Based on Boersma *et al*. [222] research, shear thickening has never been observed at P*é*clet number lower than one.

3.6.1.3 Equation for calculating the critical shear rate

On the basis of this assumption, we have recently deduced a criterion for the onset of shear thickening in a concentrated dispersion [222]. Like others in the past [21, 223] the starting point was a force balance between the different forces working on the particles. It was stated that when the shear forces overcome the repulsive interparticle forces there is a transition to shear thickening. For high volume fractions and thus small inter-particle distances, this leads to the following formula for the critical shear rate $\dot{\gamma}_s$, s^{-1}, at which shear thickening starts:

$$\dot{\gamma}_s = \frac{2\pi\epsilon_r\epsilon_0\,\varphi^2}{6\pi\eta_0 a}\frac{k}{2}\frac{h}{a} \qquad (3.7)$$

where ϵ_r is the relative dielectric constant of the medium and ϵ_0 is the permittivity of vacuum, 8.854×10^{-12} CV^{-1}; φ^2 is the surface potential, mV, which in many cases can be approximated by the potential of the particles in the medium; η_0 is the medium viscosity, Pa·s; a is the particle radius; $1/k$ is the reciprocal Debye double layer thickness, m^{-1}; and h is the distance between the particles, m.

Note that it is possible to write this critical shear rate is the form of a dimensionless number $N_{HE} = (12\,\pi\eta_0 a^2\dot{\gamma})\,/\,(2\pi\epsilon_r\epsilon_0\,\varphi^2 k\,h)$, which represents the balance between hydrodynamic and electrostatic forces. Shear thickening occurs when N_{HE} becomes

larger than order one. The ratio h/a is a function of the volume fraction and can be determined [168] from:

$$\frac{h}{a} = \left(\frac{8\pi}{3\sqrt{3\emptyset}}\right)^{\frac{1}{3}} \tag{3.8}$$

$\emptyset$ is the volume fraction. In the derivation of Equation (3.8), we assumed constant surface potential on the particles. As can be seen from Equation (3.7) the critical shear rate for shear thickening depends on a number of parameters of dispersion. A very important parameter is the volume fractions.

3.6.1.3 Equation for calculating the hydrodynamic lubrication force

The aggregation of microspheres is governed by the balance between forces enforcing them to approach and those making them move away from each other [224]. The hydrodynamic force, $F_{hydordynamic}$, enforces particles to approach. The inter-particle distance decreases with increasing the concentration of STF, which makes microspheres aggregate more quickly, and the critical shear rate decrease. As the equation (3.9) expressed, the decrease of inter-particle distance makes $F_{hydordynamic}$ increase, and more microspheres will be forced to aggregate. Given the frictional forces between microspheres is strong enough to maintain the aggregations, the increase of concentration will lead to more significant shear thickening behaviour [225].

$$F_{hydrodynamic} = \frac{6\pi\eta_0 a^2 \gamma}{h} \tag{3.9}$$

where, η_0 is the viscosity of the dispersing medium, a is the particle radius, γ is the shear rate and h is the distance between two particles.

3.6.1.4 Summary

Based on all the theories and equations, the critical shear rate mechanisms can be explained by P$\acute{e}$clet number theory, and shear thickening viscosity jump can be explained by $F_{hydrodynamic}$ equation.

3.5.2 Explanation of particle size associated with shear thickening behaviour

In Figure 3.3, the flow curves systematically shift to lower critical shear rates with increasing nanoparticle size, which can be explained by P$\acute{e}$clet number theory [181]. The larger particles are related to higher Péclet number which in turn would cause lower critical shear rate. Additionally, as expressed in Equation (3.6), larger particle size a would lead to lower critical shear rate $\dot{\gamma}$.

Moreover, STFs generating with larger particles lead to more dramatically change on STF's viscosity from critical viscosity to post-thickening viscosity, which can be explained by $F_{hydrodynamic}$ equation. According to the equation, larger particles a would result in higher hydrodynamic lubrication force $F_{hydrodynamic}$ which contribute to more obvious of the shear thickening effect.

3.5.3 Explanation of particle concentration associated with shear thickening behaviour

The critical shear rate decreases with the increasing particle concentrations, and the fact that higher particle concentrations are associated with lower critical shear rate can be explained by the Equation (3.6) and (3.7). Higher volume fraction $\emptyset$ leads to smaller h/a which results in lower critical shear rate $\dot{\gamma}_s$ which can be elucidated by the equations. It should be noted that particle concentration indicated here cover both volume fraction and weight fraction, and in this research weight fraction was used to characterize the STF production parameter.

As discussed in the calculation of $F_{hydordynamic}$, higher particle concentration is associated with a more dramatic increase of shear thickening viscosity. This is because the inter-particle distance h decreases with increasing the concentration of STF, which makes silica nanoparticles aggregate more quickly, and the critical shear rate decrease. As the equation expressed, the decrease of inter-particle distance makes $F_{hydordynamic}$ increase, and the more silica nanoparticles will be forced to aggregate and result in more significant shear thickening effect.

This finding is supported by Kang *et al*. [194] who reported that as the silica particle weight fraction increases, the interaction between particles will increase too. These further causes the hydrodynamic lubrication force between particles to be increased resulting in more and larger hydro-clusters to be formed thus creating improved shear thickening behaviour of the STF. Additionally, the higher silica nanoparticle weight fractions, the higher the solid content in the dispersion system and the fewer the dispersion medium. Then, the liquidity becomes poor, resulting in an increasing of initial viscosity in the system.

3.5.4 Explanation of dispersing medium associated with shear thickening behaviour

The change in η_s (medium viscosity) is achieved by varying the molecular weight of the PEG medium at constant volume fraction and same particle size. It has been indicated from the rheological tests that higher the molecular weight of the PEG medium higher the medium viscosity will be. As expressed by equation, medium viscosity η_s was found to scale with P*é*clet number. Increasing medium viscosity will cause increased P*é*clet number, which lead to lower critical shear rates. According to the equation (CSR calculation), higher medium viscosity η_0 will cause lower critical shear rate $\dot{\gamma}_s$ which means shear thickening phenomenon happened at relatively low shear rate.

The greater increase in shear thickening viscosity for higher medium viscosities (higher PEG molecular weight) can be explained from the calculation of hydrodynamic lubrication force $F_{hydordynamic}$. As expressed by equation, higher medium viscosity η_0 is associated with larger $F_{hydordynamic}$. The lubrication force between silica nanoparticles is increased as the viscosity of the PEG increased [225]. Both of them are beneficial for the aggregation of nanoparticles in the shear thickening region for high molecular weight PEG, leading to the enhanced shear thickening behaviour. The more dramatically increase of shear thickening viscosity due to higher medium viscosities can also be explained as follows.

For the same amount of silica nanoparticles added into the STFs, largest molecular weight PEG600 has the longest molecular chain and hence contains less hydroxyl, which leads to less hydrogen bonding are formed during the combination of silicon dioxide (from SiO_2) and hydroxyl, hence the bonding between solid and liquid is weak result in lower initial viscosity of STF comprising PEG600. Due to the weaker bonding between the solid particle and liquid, the particles in STF comprising PEG600 are easier to get rid of fluid phase bonding to form jamming particle clusters, hence the earlier increase in viscosity and more dramatic thickening behaviour than STF comprising with PEG200. The stronger hydrogen bond between PEG200 and silicon dioxide will make it hard for the nanoparticles to get rid of the hydrogen bond to form jamming hydro-clusters, which lead to higher critical shear rate marking the onset of shear thickening phenomenon and moderate viscosity changes.

3.5.5 Explanation of system temperature associated with shear thickening behaviour

The influence of system temperature on the shear thickening behaviour was studied. The critical shear rate increases with increasing of system temperature which can be explained by Péclet number theory. As expressed in equation (3.6), Péclet number

increases with decreasing system temperature T. As has been stated in Section 3.5.1.2, higher the *Pe* number is associated with lower critical shear rate $\dot{\gamma}_s$. Therefore, it can be concluded that lower system temperature T will cause lower critical shear rate $\dot{\gamma}_s$ which indicates shear thickening phenomenon is triggered with relatively low shear rate.

The shear thickening behaviour is enhanced with the decrease of system temperature. In this case, the system temperature influence on shear thickening behaviour can be explained by Brownian motion. The Brownian forces scale with k_BT/ a, where k_B is the Boltzman constant, T is the temperature of the system, and a is the particle radius [224]. It is clear that the Brownian force decreases with decreasing temperature. It addition, the Brownian motion forces nanoparticles to move away from each other [226]. Consequently, decreased system temperature is beneficial for the aggregation of nanoparticles and the enhancement of the shear thickening behaviour.

3.5.6 Summary

All of the rheological testing results presented in this research can be explained with the concept of hydro-cluster theory. The shear thickening phenomenon was caused by the formation of "particle cluster" due to the hydrodynamic lubrication force. From all the discussions and analysis, the agreement between theory and experiment was found to be equally good.

3.6 Conclusions

A systematical investigation on parametrical control of STF rheological properties has been explored in this Chapter. This research confirms that lower critical shear rate and amplified severity shear thickening viscosity of STFs can be achieved by using larger particle size, higher particle weight fraction and higher PEG molecular weight of

dispersing medium. In order of achieving higher critical shear rate, smaller particle size, lower particle weight fraction, and PEG with lighter molecular weight should be used, with the sacrifice of the reduced thickening effect of the STF. Furthermore, the mechanisms of shear thickening phenomenon were systematically discussed and analysed in this research.

Although all the rheological properties can be explained and predicted by the 'hydro-cluster' theory and the theoretical equations, the purpose of this research is to establish an experimental approach to define the certain range of critical shear rate and the magnitude of the shear thickening viscosity jump. As can be demonstrated from all the testing results, the range of C.S.R can be achieved is from 6.31 to 100 s^{-1}, and the amplitude of thickened viscosity is from 82 Pa·s to 3363 Pa·s.

As has been stated, the critical shear rate of STFs can be related to the particular impact shear rate and the degree of the shear thickening effect can affect the enhancement of impact energy dissipation. If use the proper STF compositions, the increase of shear thickening viscosity can exceed over several thousand Pa·s and the post-thickening viscosity can be more than forty times the value of the critical viscosity of STF.

All the rheological testing results indicated that different STFs with various compositions had regularly rheological properties and it should be meaningful to investigate the effects rheological properties of STFs on stabbing resistant performance and ballistic impact performance when it was impregnated into Twaron® fabrics, so that the impact resistant performance can be manipulated by the STF production parameters.

Chapter 4

Experimental Study of STF Impregnation on Stabbing Performance

4.1 Introduction

A detailed systemic investigation on control of rheological properties of STF has been done in Chapter 3. The outcome of the investigation indicated that the critical shear rate and the magnitude of the viscosity increase can be controlled by manipulating the STF parameters. This investigation confirms that critical shear rate and high critical shear thickening viscosity of STFs can be achieved by using large particle size, big particle weight fraction and high PEG molecular weight of the dispersing medium. In the case of achieving higher critical shear rate, smaller particle size, lower particle weight fraction, and PEG with lighter molecular weight will need to be used, with the sacrifice of reduced thickening of the STF.

This Chapter presents a quantitative investigation the use of STF and how STF can be efficiently utilised to improve the stabbing resistance of soft ballistic body armour. The effect of silica nanoparticle sizes and silica nanoparticle weight fractions of the STF were taken into consideration in order to explore the relationship between STF with different shear thickening behaviours and overall fabric panel response. Full impregnation processes of Twaron® fabrics with STF were proposed and the full STF

impregnation criterion was judged. Dynamic stabbing impact tests were carried out on different compositions of STFs impregnated Twaron® fabrics, comparing to untreated Twaron® fabrics. In addition, quasi-static impact tests were conducted to investigate impact behaviour more precisely.

The objective of this study is to understand and investigate how the rheological properties of STF work and affect impregnated into woven Twaron® fabric panels. The enhancing effect of STF was systematically discussed and the energy absorption mechanisms during the stabbing impact were analysed and revealed.

4.2 Optimise the full impregnation procedures of STF-fabric composites

4.2.1 Ballistic woven fabric

Aramids (Kevlar® and Twaron®), ultra-high molecular weight polyethylene fibres (Spectra®, Dyneema®), PBO fibres (Zylon®) and glass fibres are the examples of fibres used widely in ballistic fabrics [6].

The significantly higher tensile strength and modulus and lower fibre elongation make aramids offers great advantages compared with earlier synthetic fibres. These characteristics allow aramid yarns to be woven on looms more easily than those brittle fibres, like glass fibre, carbon fibre or ceramic. In addition, aramids have no melting point and only start to degrade at 500°C. The low flammability makes them behave well in fireproofing. These advantages make aramids extraordinarily suitable for producing ballistic body armour.

Therefore, aramid fibre was chosen and the aramid fibres used in this research was provided by Teijin called Twaron®, and Twaron® filament yarns were woven into plain weave structure. Additionally, the fabric specifications have been shown below:

Table 4.1 Details of Twaron® fabric specifications

Fabric structure parameter	**value**
Weave	Plain
Areal density (g/m^2)	160
Yarn count (tex)	93
Thread density (ends and picks per cm)	8
Fabric thickness (mm)	0.3

It needs to be said that the thread density 8 threads/cm was the optimised result from the previous study with the given yarn count, leading to best ballistic performance [227].

4.2.2 Preparation of STFs

Details for the preparation of STFs can be found in Chapter 3, and in this part of the research different particle sizes and different particle weight fractions were taken into consideration in order to explore the performance of STF upon shear load.

As have been discussed in Chapter 3, low critical shear rate and greater increase of shear thickening viscosity of STFs can be achieved by using large particle size, high particle concentration and high viscosity of dispersing medium. However, if the higher critical shear rate is required, the use of smaller particle size, lower particle concentration and lower viscosity of dispersing medium would help, with the sacrifice of the reduced thickening effect of STFs. As results of that, two different silica nanoparticle sizes (largest one is 650nm and smallest one is 12nm) and three different silica nanoparticle concentrations (20%, 25% and 30%) were chosen to prepare the STFs. All the silica nanoparticles used in this research were supplied by Sigma-Aldrich (Germany). 30% particle weight fraction was the maximum concentration that can be achieved for 12nm silica STF because of the higher free surface energy of the 12nm silica particles. The same particle weight fractions were chosen for the 650nm silica particles in order to carry out comparisons with the 12nm silica particle

STFs. According to the literature, different molecular weight PEG could be used and would not affect energy absorption of final product [204]. PEG200 was chosen because of its low viscosity for easier production of STFs and its density is 1.127g/cm^3 [220].

The rheological tests results of different types of STF samples are presented in the form of the double logarithmic plot of STF viscosity vs. shear rate to a quadratic curve shown in Figure 4.1.

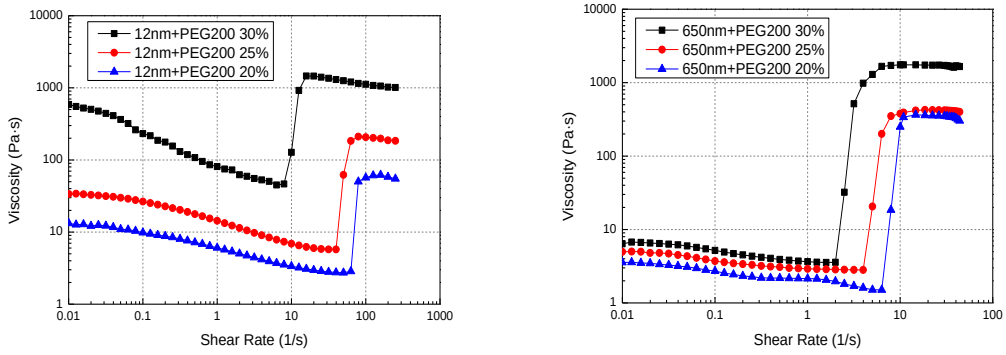

(a) (b)

Figure 4.1 (a). STF's Viscosities vs. shear rate for STFs generating with 12nm silica particle and PEG200 at different particle weight fractions

(b). STF's Viscosities vs. shear rate for STFs generating with 650nm silica particle and PEG200 at different particle weight fractions

Diagrams (a) and (b) in Figure 4.1 show the STFs made from 650nm and from 12nm silica particles with three particle concentrations clearly demonstrate viscosity jumps at certain shear rates, the typical shear-thickening phenomenon. In both cases, the viscosity of the STF became sharply increased. In the case of STF with 650nm silica particle at 30% concentration dispersed into PEG200 as shown in (a), the viscosity after a shear rate of 2 s^{-1} increased from 3 Pa·s to 1750 Pa·s. However, for the STF with 12nm silica particle at 30% concentration situation as depicted in (b), the viscosity of STF change from 46 Pa·s to 1459 Pa·s after the critical shear rate of 8 s^{-1}. From both (a) and (b), it is clear that the weight fraction increase of silica particle

causes decreased critical shear rate, which is the shear rate that triggers the shear thickening and more dramatically jumps of viscosity. The critical shear rate for 650nm STFs is between 2 and 7/s, and that for 12nm STFs between 8 and 70/s.

For the purpose of investigating the relationship between critical shear rate of STFs and shear rate of stabbing impact, the shear rate *S* created with the stabbing is calculated, using Equation (4.1) [212], to be about 1500/s, which will be sufficient to trigger the shear thickening of the STFs created in this research.

$$S = \frac{v}{d} \qquad (4.1)$$

In this equation, *v* is the impact velocity (3m/s in this exercise) and *d* is the thickness of the knife, which is 2mm.

This shear rate greatly exceeds the rate required for the onset of shear thickening in STF. Thus we expect the shear rates during the stabbing tests to be sufficient to transition the dispersion to its shear thickened state. STF should be rigid during high speed and high deformation events; therefore, STF would constrain the fabric yarns and pulling them through the fabric. As a result of that, more energy can be absorbed by the STF impregnated fabrics.

4.2.3 Manufacture procedures of STF-Twaron® composites

The composite fabric was prepared by the impregnating process. Preparation of the composite material could be used in two ways, one was the direct recombination of STF, the fabric was horizontally placed, STF was added into the fabric layer, and the wet fabrics were squeezed using a 2-roll mangle to get rid of the excess amount of the solution. After complete immersion, it was placed into the vacuum oven to remove the air bubbles. This method was suitable for the STF with low viscosity. The second

method was ethanol dilution method: before impregnation, STF was diluted with ethanol to reduce the viscosity of the scattered system. Then fabrics were immersed in the STF/ethanol solution. Since the viscosity of STF increased with the increase of the SiO_2 content, the liquidity of high concentrations of STF was decreased, and therefore it was very difficult to directly impregnate fabric. When the SiO_2 content was higher than 20%, STFs were difficult to impregnate the layer because they are highly viscous, the way of diluted with ethanol needed to be used. To make STFs uniformly impregnate into the fabric, they are diluted in ethanol at a 3:1 volume ratio of ethanol:STF to reduce the surface tension of the STF, i.e., to wet the fabric properly. Then the fabric was immersed in a diluted solution for one minute in order to apply this diluted dispersion uniformly on the fabric. Finally, it was placed in the oven, heated and dried at 70 °C for 8 hours, ethanol was volatilized to remove, and a composite material was obtained, shown in Figure 4.2. The detailed compositing steps were as follows:

(1) The fabric was cut into 12 centimetres in width and 24 centimetres in breadth, so one piece of fabric specimen weighs 4.6g.

(2) According to the 3:1 volume ratio, a certain amount of ethanol was weighed and added into the obtained STF, then stirred until fully diluted, and a mixed solution with lower viscosity and good fluidity was obtained.

(3) Each of these fabric layers was completely immersed in this diluted solution of STF for one minute, the fabric layer together with the container was together put into an oven, heated at 70 ℃, so the ethanol was evaporated, until the weight did not change. Alcohol was vaporised completely in the process of drying due to its low evaporation temperature, which has no effect on the final STF treated fabric.

(4) The STF impregnated fabric was removed from the container, and the wet fabric was squeezed by roller to get rid of the excess amount of the solution on the fabric

surface and around fabric, the composite material was weighed and saved in a sealed bag for the impact performance tests. In addition, the weights before shear thickening fluid impregnation and after impregnation were measured to control the quantity of STF that has impregnated into the fabrics. The percentage of STF weight adding is approximately 100% and the add-on weight ratio (wt %) STF was approximately 50% in the STF-Twaron® composites.

4.2.4 Weight control of STF-Twaron® composites

It is worth noting that the areal density of the STF-Twaron® fabric targets increases as particle weight fraction increases. In all the experiments performed in this study, the total target mass is kept constant by decreasing total STF weight as particle loading increases.

Table 4.2 Specimens prepared for stabbing tests

Target panels	No. of layers	Areal density (g/m^2)
Untreated fabric panels – 12L	12	1921.2
Untreated fabric panels – 24L	24	3842.4
20% 12nm + PEG200 STF treated fabric panels	12	3840.3
25% 12nm + PEG200 STF treated fabric panels	12	3844.2
30% 12nm + PEG200 STF treated fabric panels	12	3853.3
20% 650nm+ PEG200 STF treated fabric panels	12	3826.7
25% 650nm+ PEG200 STF treated fabric panels	12	3823.6
30% 650nm+ PEG200 STF treated fabric panels	12	3833.2

4.2.5 Thickness measurement of STF-Twaron® composites

Another concern of the fully impregnated woven fabrics is the thickness of the fabric specimens after the impregnation procedures. In the practical applications, the fabrics are mostly in the form of vertical, which means the STFs in the fabrics have the

tendency of dripping. In order to investigate the influence of gravity on the properties of STF-Twaron® fabrics, two sets of fabric specimens were prepared. One set of specimens were laid on a horizontal table for one month, the other were kept hanging up for one month before the thickness tests. All the specimens were kept under the ambient temperature (20°C) and they were sealed inside of polyethylene (PE) films individually for preventing leakage and contamination. Though the fabric specimens were sealed in the PE films, the STFs in the fabrics are still flowable, so this preparation procedure will not affect the final thickness measurement results.

Three different STF impregnation levels were used to investigate the STF-Twaron® specimen thickness and dripping effect of STF on STF-Twaron® specimen. Three add-on weights of STF (2g, 4g and 8g) added onto STF-Twaron® specimens were denoted as half impregnation, full impregnation and double impregnation.

The double full impregnation processes were achieved by double the quantity of STF amount which can be absorbed by the fabric impregnated into the fabric specimens, although there are a lot of excessive fluids around and on the surface of the fabric specimen, PE films were used to seal the STF and the fabric specimen in an enclosure.

Whether the STF impregnation would affect the thickness, and thickness of STF-Twaron® fabric specimens based on three STF impregnation criterions were explored. For investigating on the thickness distribution of STF-Twaron® fabric specimens, FAST-1 compression thickness meter with a sensitivity of 0.01mm was used, and the thickness was measured under the pressure energy of 0.5gf/cm^2. All the thickness distribution tests were conducted under a room temperature of 20°C.

Table 4.3 Thickness measurement of two sets of specimens

Sample Name	Add-on weight of STF (g)	Sample thickness placed horizontally (mm)	Thickness after hanging (mm)		
			Top Edge	Middle Part	Bottom Edge
12nm+PEG200 (30%)	2g	0.30	0.30	0.30	0.30
12nm+PEG200 (30%)	4g	0.47	0.46	0.47	0.48
12nm+PEG200 (30%)	8g	0.57	0.49	0.51	0.70
650nm+PEG200 (30%)	2g	0.30	0.30	0.30	0.30
650nm+PEG200 (30%)	4g	0.45	0.44	0.45	0.47
650nm+PEG200 (30%)	8g	0.54	0.47	0.48	0.67

In order to exclude the influence of PE films on the thickness of the specimens, the untreated fabric specimen was covered by the PE films and the thickness is 0.3mm.

Table 4.3 contrasts the thickness of STF-Twaron® specimens impregnated with two different particle sizes at 30% concentration placed horizontally with the specimen thickness after hanging for one month.

When add-on weight of STF is 2g, the thickness of all the specimens irrespective the particle size of STF kept same with hanging or without hanging. It can be postulated that 2g of STF well remain inside of the fibres of STF-Twaron® specimens, and wouldn't flow due to the gravity.

When the add-on weight of STF is 4g, the thickness of STF-Twaron® specimens present a little difference compared to the untreated Twaron® specimens. This means full impregnation of STF into STF-Twaron® specimens will cause a little increase in the thickness of the fabrics. For the two different particle sizes STF at 30% concentration impregnated Twaron® specimens, the increment of the fabric thickness

is 0.17mm and 0.15mm respectively than that of untreated Twaron® specimens. Nevertheless, all the specimens showed only a slight difference of the thickness between the horizontally laid specimens and hung up placed specimens. This is can be hypothesised that the gravity wouldn't cause the STF dripping inside of the STF-Twaron® specimens when the adding quantity of STF is 4g which is the full impregnation criterion.

When the add-on weight of STF is 8g which is the double full impregnation criterion, the thickness of both particle size STF impregnated Twaron® specimens are almost double of original untreated STF-Twaron® specimens thickness. Furthermore, there are significant differences in the thickness between the specimens horizontally placed and vertically placed. As have been demonstrated in the Table, both of the top edge of the specimens and middle part of the specimens after hanging have shown thinner thickness compared with the horizontally placed specimen thickness. Obviously, the bottom edge of the STF-Twaron® specimens after hanging have presented much thicker thickness than that of horizontal placed STF-Twaron® specimens. It can be determined that STFs in STF-Twaron® specimens are still flowable which causes the thicker thickness of the bottom edge of the STF-Twaron® specimens after hanging. Thus, it can be assumed that gravity could result in dripping of STF inside of the STF-Twaron® specimens if the adding quantity of STF reaches 8g.

Hence, if the full impregnation criterion can be controlled strictly and effectively, the STF would be well maintained inside of the STF-Twaron® specimens and won't be flowable upon the gravity or normal movement of the wearer. Besides, the addition of STF was shown to cause a little increase in the thickness of the Twaron® fabrics. Moreover, if have the right quantity of STF could be impregnated into the Twaron® fabrics, not only the dripping effect of STF can be eliminated, but also the STF can be well dispersed over the whole fabrics.

4.2.6 SEM observation of STF-Twaron® composites and untreated fabrics

During the process of impregnating the fabrics, when the add-on weight of STF is 2g, it was visible that the gaps between the yarns in the fabrics were not completely filled by the STF, which indicates that the fabric did not reach full impregnation at the add-on weight of 2g. This can also be proved by the thicknesses of the fabric, which were the same as that of the untreated fabric.

As the add-on weight of STF reached 4g, the almost the same weight as one trimmed (12cm×24cm) layer of untreated fabric, which has been stated as full STF impregnation into the fabrics. The STF visibly filled the gaps between the yarns, and there was no visible flowing STF on the surface of STF-Twaron® fabric.

The untreated Twaron® fabric and the STF fully impregnated Twaron® fabric were shown in Figure 4.2 (a and b). The morphologies of the untreated fabric targets and STF impregnated fabric targets were observed by scanning electron microscope (SEM, HITACHI, S-3000N). The SEM images have shown in Figure 4.2(c-f).

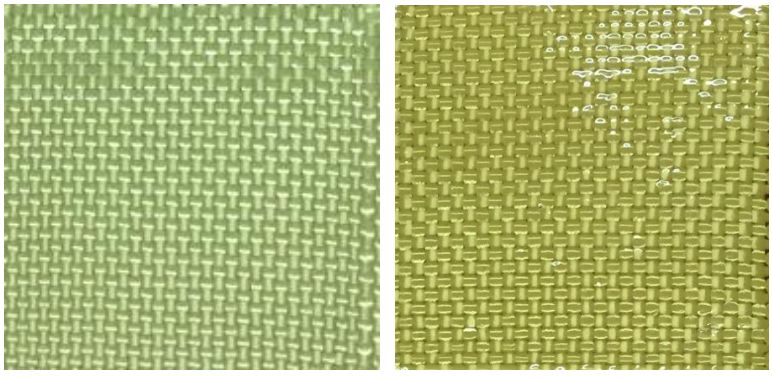

(a) Untreated fabric (b) STF impregnated fabric

Figure 4.2 (a-b) Untreated Twaron® fabric and fully STF impregnated Twaron®

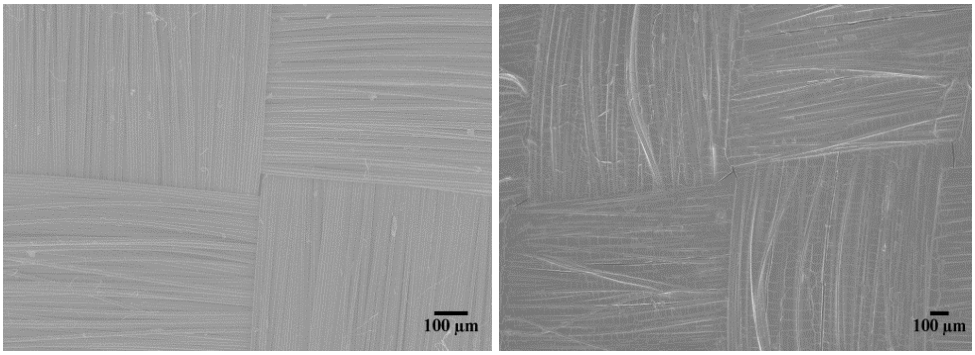

(c) Fabric before STF impregnation (d) Fabric after STF impregnation

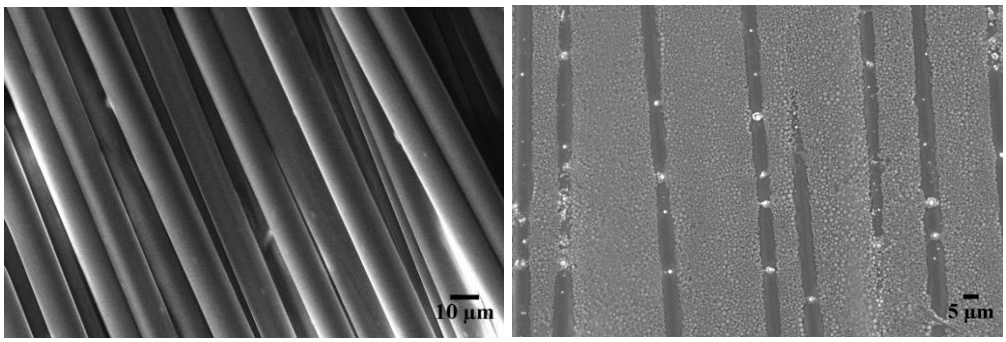

(e) Fibre tow in untreated fabric (f) fibre tow in STF-impregnated fabric

Figure 4.2 (c-f) SEM images of untreated and fully impregnated Twaron®

SEM images revealed that the STF was uniformly dispersed over the entire volume of Twaron® fabrics via fabric impregnation procedure. The SEM micrographs presented in Figure 4.2 (c-f) show pictures of untreated Twaron® fabric samples and STF treated Twaron® fabric samples at different magnifications. Compared to the SEM images of raw Twaron® fibres in the fabric presented in Figure (c), Figure (d) clearly had shown that STF was well dispersed over the entire surface of the Twaron® fabric. It can be seen in Figure (e) that Twaron® fibres were nice, clean and parallel to each other. As shown in Figure (f), it is clear that the gaps between the fibres in the STF-Twaron® fabric were filled with silica nanoparticles and the morphologies of spherical silica nanoparticles could be clearly seen, which revealed that the STF was completely immersed into the fibre surface and incorporated between fibres. It meant that STF impregnated Twaron® fabrics were prepared successfully. Thus, when add-on weight ratio of STF onto Twaron® fabrics is 1:1 which means the add-on weight of STF equals the Twaron® fabric weight, the STF-Twaron® fabric can be regard as reaching full impregnation. The full impregnation means the STF were continuous in the

impregnated Twaron® fabric, which is important and imperative for the STF to work at impact load.

When the add-on weight of STF was double of the Twaron® fabric weight, the Twaron® fabric cannot absorb the extra STF, hence the extra amount of STF is flowing on the surface of fabric which leads to the dripping problem described in the previous section. The SEM images of untreated Twaron® fabric and double impregnation Twaron® fabric have been shown below in Figure 4.3.

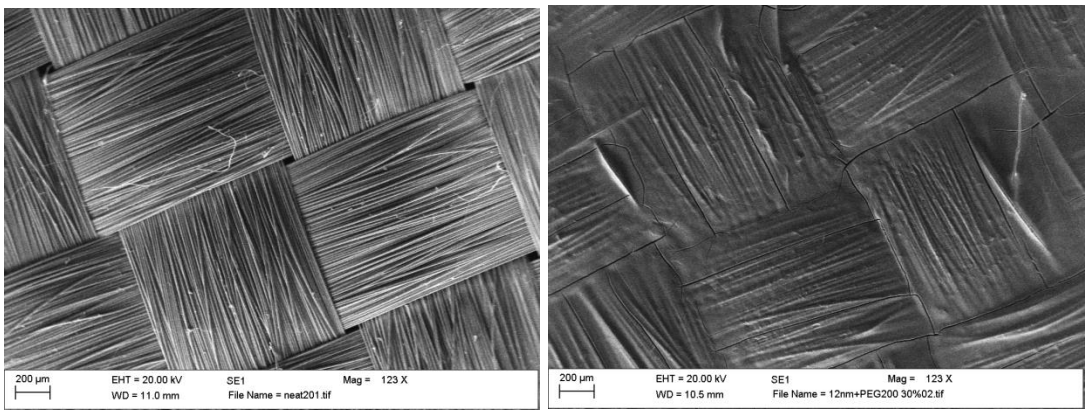

(a) (b)

Figure 4.3 The SEM images of untreated and double STF impregnated Twaron®

It can be seen from the (b) that if too much STF add on to the Twaron® fabric, there will have excessive fluid which cannot be absorbed by the Twaron® fabric and they will flow on the surface of the fabric. Therefore, longer time of the gold coating process would be needed to cover the excessive STF on the fabric surface. In consequence, the gold coating will form a shell-like coverage on the entire fabric surface which results in nothing can be seen even if raised the magnification. For all the reasons have been discussed, double STF impregnation into the Twaron® fabric is inadvisable.

4.3 Dynamic stabbing tests on fabric targets

4.3.1 Introduction

Untreated Twaron® fabric panels and different types of STF impregnated Twaron® fabric panels were tested a knife impactor for stabbing resistant performance based on the following test schemes: (1) untreated and impregnated panels with the same number of fabric layers, (2) untreated and impregnated panels with the same areal density, (3) fabric panels impregnated by STFs with different particle sizes, (4) panels impregnated by STFs with different weight fraction for an STF with a given particle size, and (5) untreated and pure dispersing medium (PEG) treated Twaron® fabric panels. The stabbing impact response and mechanisms analysis of different fabric targets were also studied.

Stab tests were carried out on untreated and different types of STF impregnated fabrics. As indicated in Table 4.2, impact panels are designed on two principles, i.e. the same number of layers and the same areal density. In the same areal density design, 24 layers of untreated Twaron® fabric panels and 12 layers of STF impregnated Twaron® fabric panels were found to have the closest areal density.

In order to study the influence of silica nanoparticle size and particle weight fraction on STF impregnated woven fabric panels' stabbing performance, two different silica nanoparticle sizes, i.e. 12nm and 650nm, were chosen to produce the STFs. For each particle size, 3 levels of particle weight fraction, i.e. 20%, 25% and 30%, were employed. The fabrics were fully impregnated using these STFs following the procedure described in Section 4.2.3.

4.3.2 Dynamic stabbing test equipment

The stabbing impact testing is performed on Instron Dynatup 8200 drop weight tester. Drop tower impact tests are commonly used to determine impact resistance of plastic,

metal composites, rubber, etc. This stab tests performed are based on the NIJ Standard 0115.0 for stab resistance of body armour. The NIJ-specified impactor "P1" knife was used (Figures 4.4). To perform a stab test, the impactor is mounted to the crosshead, which is then loaded with weights to a specific mass (5kg). The crosshead is dropped from a fixed height to impact the target. The velocity of the crosshead at impact is measured using fixed flags attached to the frame. Impact loads are measured using a load cell mounted on the base of the impactor. So the loading of the impactor is measured as the reaction force. The stab targets are placed on a multi-layer foams and elastomers backing, as specified by the NIJ standard to provide a damped target response similar to armour mounted on a human torso [228]. The backing materials consist of multiple layers of material: the strike face of four layers of neoprene sponge, a single layer of closed-cell polyethylene foam, and two layers of rubber at the bottom. The specimens were simply clamped at four edges using a steel frame fixture using the force of the fastening bolts. And the testing temperature is constant at 20°C.

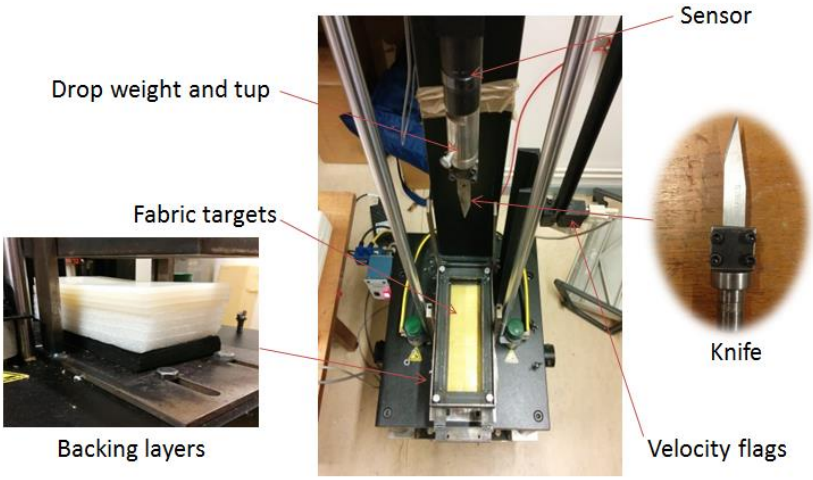

Figure 4.4 Stabbing test equipment

As the knife was driven into the fabric panel, the load and displacement data were recorded. The reaction forces were recorded by the pressure sensors mounted to the impactor, so the loading of the impactor was measured as the reaction force. In addition, the velocity of the crosshead during the impact process was measured as a verification using velocity flags attached to the frame, so the energy absorbed by the

targets can be calculated and recorded as a function of knife displacement. In this experiment, the impact velocity was set to be 3m/s representing 22.5J impact energy. For each test, three samples were stabbed in order to obtain the average stabbing behaviour. The corresponding shear rate of the impact was 1500/s as mentioned earlier, and this greatly exceeds the critical shear rate required for the onset of shear thickening of the STFs prepared in this research. Thickening was expected to be triggered by the knife impact.

4.3.3 Influence of STF impregnation

In order to investigate the effectiveness of STF impregnation with Twaron® fabrics, untreated impregnated panels with the same number of fabric layers were constructed. In parallel to the untreated panel, the 12-layers panels were impregnated with STFs made from 12nm and 650nm silica particles with different weight fractions, as described in Table 4.2. Stabbing test was carried out on these panels, and the panel performance was indicated by the maximum impact load and total energy absorption. Figure 4.5 compares the stabbing performance of the untreated and impregnated panels with 12 layers of Twaron® fabric. In this comparison, impregnated panels with the lowest 20% particle weight fraction were used, because of the fact that higher nanoparticle weight faction in STF leads to better stabbing performance.

It is evident from Figure 4.5 that the use of STF regardless of the particle size enhances the panel performance against stabbing impact. Figure 4.5 (a) suggests the maximum load associated to stabbing the STF impregnated panels is almost twice as big as that of the untreated panel. The increase in maximum load can be attributed to the STF hardening due to the shear introduced through the stabbing impact. The shear thickening of the STF made the impregnated panel to be more energy-absorbent, as illustrated in Figure 4.5 (b). This phenomenon can be explained as follows. The hardening of the STF turned the concentrated impact force created by knife stabbing

into a distributed force, causing an extended area of the panel to be involved in absorbing the impact energy. The untreated panel absorbed about a third of the energy that was taken up by the STF impregnated panels, implying an easy penetration of the knife through the panel. Considering the applied impact energy is 22.5J, the dry panel absorbed 20% of the impact energy. In comparison, the impregnated panels absorbed 64% (650nm STF) and 58% (12nm STF) of the impact energy, and were more likely to block the knife penetration because of the increased energy absorption.

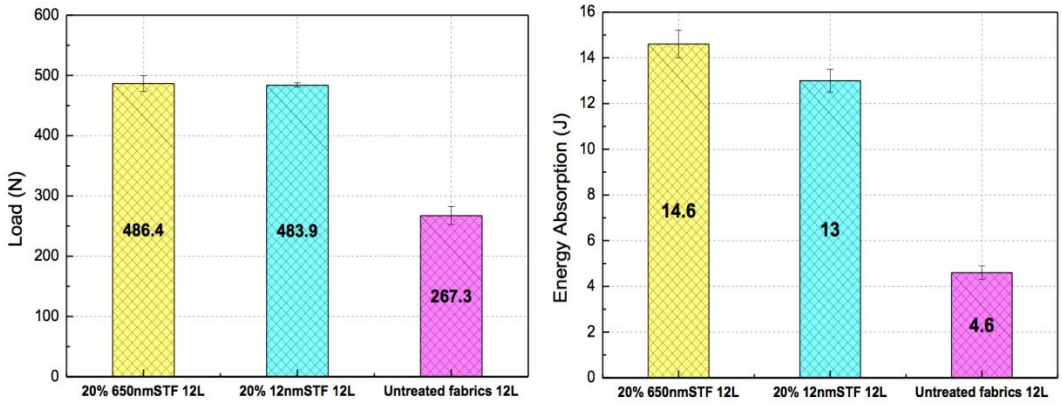

(a) Maximum load (b) Total energy absorption

Figure 4.5 Effectiveness of STF impregnation

Coupled with the increase of stabbing performance, attention has to be drawn to the fact that the STF impregnated panels became about twice as heavy as the untreated panel, as indicated in Table 4.2.

4.3.4 Reduction of fabric layers in panels

The purpose of involving STF in the stabbing panels was to increase the stabbing performance with lowest possible panel weight. The previous analysis and discussions indicated that for the panels with the same fabric layers, the impregnated greatly outperformed the untreated. In this exercise, untreated panel and impregnated panels were designed in such a way that they had the same panel weight. The untreated panel was constructed using 24 fabric layers, whereas the STF impregnated panels were

made up of 12 fabric layers with full impregnation. The weight of the panels was about 3850g/m^2, as listed in Table 4.2. Figure 4.6 displays the panel performance against stabbing impact, again using STFs of the lowest particle weight fraction for illustration.

It is clear from Figure 4.6 that for stabbing panels with same areal density, the STF impregnated panels demonstrated better performance over the untreated panel in terms of both the maximum load and the total energy absorption. This indicates that in stabbing panel design, the use of STF in the panels could lead to reduced fabric layers to achieve the same or even improved performance against stabbing. In this experiment, the untreated panel involved 24 fabric layers and the impregnated panel contained 12 fabric layers, and the impregnated panels demonstrated at least 31% increase in maximum load and at least 26% enhancement in total energy absorption.

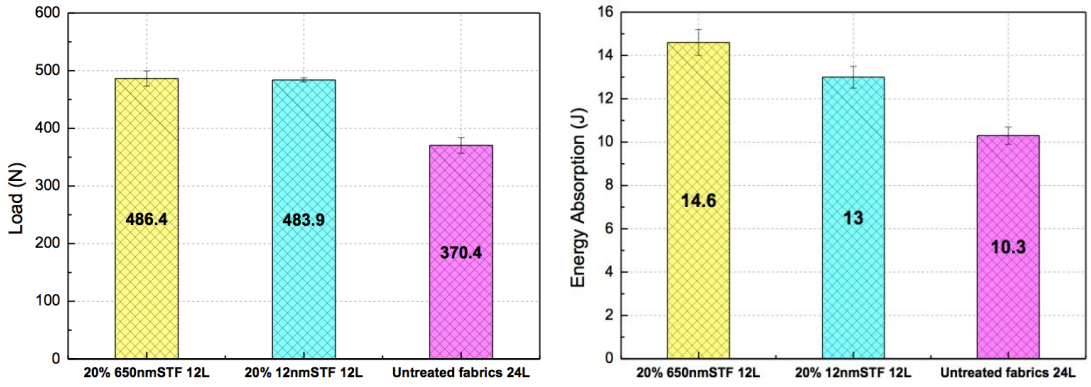

(a) Maximum load (b) Total energy absorption

Figure 4.6 Performance of panels with the same areal density

Irrespective of the particle size influences, although both of the STF impregnated Twaron® fabric targets have fewer fabric layers compared to untreated Twaron® fabric targets, they have shown enhanced stabbing resistant properties than that of untreated Twaron® fabrics even at their lowest particle concentrations.

Furthermore, 12 layers of untreated Twaron® fabric targets resist only 20% (4.6J) of

the total impact (22.5J) energy which performs worse than 24 layers of untreated Twaron® fabric targets which can absorb 44% (10J) of the total impact energy. Therefore, more Twaron® fabric layers can improve the stab resistant performance under stabbing impact while STF treated Twaron® fabric targets can offer more enhancement on stab resistant performance.

4.3.5 Nanoparticle size in STF versus performance of stabbing panels

The STFs used in this research were made from PEG200 and silica nanoparticles of 650nm and 12nm. In the discussion carried out in Section 3.4.1, it has been pointed out that STF with larger particle size related to smaller critical shear rate and a bigger increase in viscosity when triggered by shear loading. Figure 4.7 shows the performance of impregnated fabric panels with STFs containing 650nm and 12nm silica particles, all of which were composed of 12 layers of Twaron® fabrics.

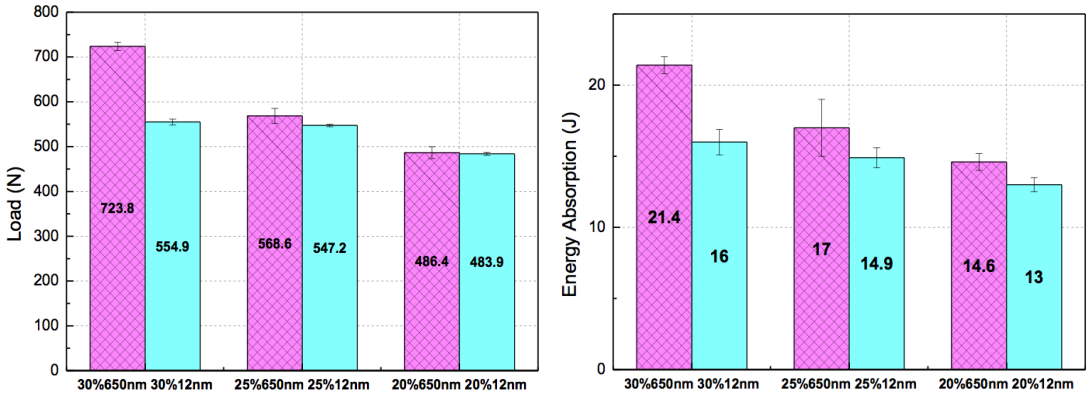

(a) Maximum load (b) Total energy absorption

Figure 4.7 Influence of nanoparticle size on panel performance

In terms of both the maximum load and the total energy absorption, 650nm STF leads to better performance than the 12nm STF regardless of the nanoparticle weight fraction, and the performance differences between the two types of panels become more notable when the nanoparticle weight fraction becomes higher, as clearly indicated in Figure 4.7(a) and (b). Take the total energy absorption for example. The

difference in energy absorption increases from 12%, 14%, to 34% as the particle weight fraction goes from 20%, 25%, to 30%. These results are believed to be associated with the more significant hardening effect of the 650nm STF at the particle weight fraction of 30% when it is triggered.

4.3.6 Particle weight fraction on performance of stabbing panels

The STF made from 650nm and 12nm silica nanoparticles were created with 3 levels of particle weight factions, i.e. 20%, 25% and 30%. For a given particle size, it has been seen from earlier discussions that the viscosity increase of the STF becomes more significant under a shear load with a shear rate equal to or above the critical shear rate. The STF impregnated fabric panels with different particle weight fractions were experimented on for their performance against knife impact. Figure 4.8 shows (a) the maximum load and (b) the total energy absorption. For both 12nm and 65nm STFs, the increase in particle weight fraction leads to an obvious increase in maximum impact load and total energy absorption, as depicted in Figure 4.8 (a) and (b) respectively.

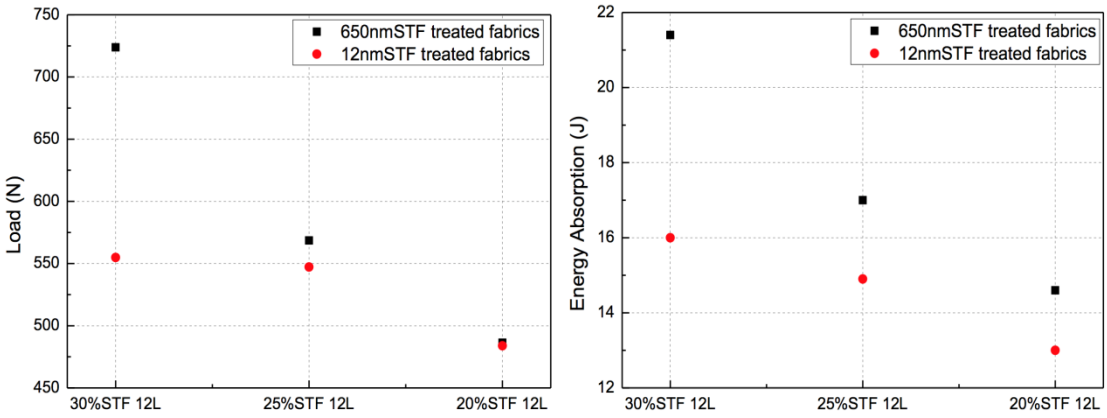

(a) Maximum load (b) Total energy absorption

Figure 4.8 Influence of nanoparticle weight fraction on panel performance

More specifically, as the total knife impact energy is 22.5J, STF producing with 650nm particle at 30% particle concentration treated 12 layers of Twaron® fabric

targets absorb almost all the impact energy which means successfully prevent knife from penetrating through the fabric targets, while 650nm particle STF at 25% particle concentration treated 12 layers of Twaron® fabrics absorb 75% of the whole impact energy and 66% of the total impact energy can be absorbed by 650nm particle STF with 20% particle concentration treated Twaron® fabric targets with 12 layers. Same situation for the 12nm particle treated Twaron® fabric targets. 12 layers of Twaron® fabric targets impregnated with 12nm STFs at different silica particle weight fraction of 30%, 25% and 20% absorb around 71%, 62% and 58% of the total impact energy.

In conclusion, higher silica particle concentrations irrespective silica particle sizes contribute to higher stabbing impact energy absorption of the STF treated fabric targets at the same areal density under impact.

In the case of higher particle concentration, more dramatically increase on shear thickening viscosity will make the STF more rigid under the impact. Note that the highest weight fraction of silica particles STF suspensions has the highest shear thickening viscosity, which can provide the highest protection performance due to the desired energy absorption effects. These results keep the consistent conclusion with former results discussions that the stabbing resistant performance of STF-Twaron® fabrics can be related to the rheological properties of the STF which has been used to treat on the fabrics.

4.3.7 The impact process

The histories of the impact force exerted onto the fabric targets and the fabric deformation from the dynamic stabbing impact tests have been shown below in Figure 4.9.

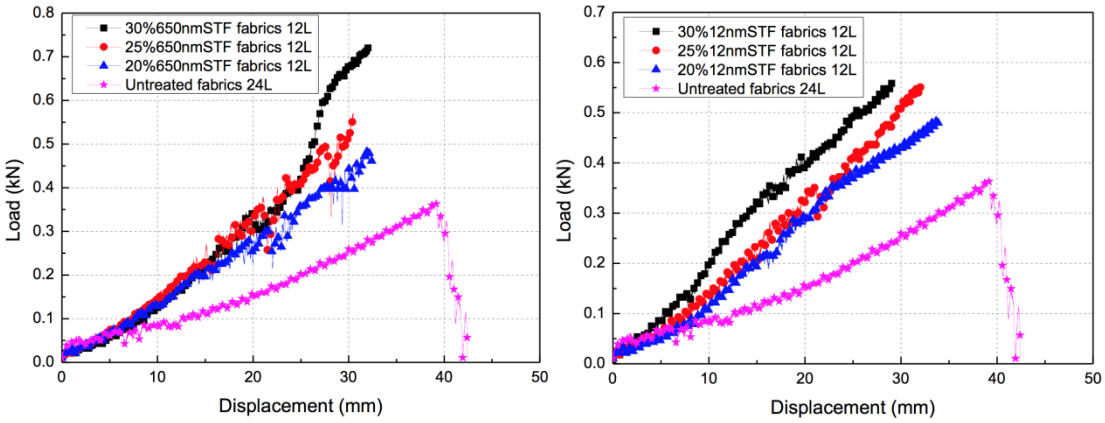

(a) 650nm STF panels vs. untreated panels; (b) 12nm STF panels vs. untreated panels

Figure 4.9 Load-deformation curves of STF impregnated panels and the 24-layer untreated panel

Figure 4.9 records the load-deformation process associated with the stabbing tests, with (a) showing the 12nm STF impregnated panels in comparison to the 24-layer untreated fabric panel, and (b) showing the 650nm STF impregnated panels in comparison to the same untreated fabric panel. All the curves have shown that impact loading of fabric targets increased linearly with the fabric displacement. It can be seen that the 24-layer untreated Twaron® fabric panel produced a maximum load 360N before the loading curves drop to zero which means the knife penetrated through all the fabric layers in the panel. Furthermore, in the case of untreated Twaron® fabrics, the displacement of the fabric participate in load resistance is larger than that of STF impregnated fabric targets, but the peak load is lower. The larger fabric displacement indicates that the deformation of untreated Twaron® fabrics is large after the impact. On the other hand, all the STF impregnated Twaron® fabric panels produced remarkably higher maximum load at the time of panel failure irrespective of the particle size and the particle weight fraction, and they were never punctured. Additionally, the presence of STF in treated fabrics enables less fabric deformation to participate in load resistance and higher modulus of STF-Twaron® fabrics are witnessed. As the slope of the loading vs. displacement curves steeper, this led the inference that this fabric targets exhibited higher stiffness under the impact. This is

related to the hardening of the STF depicted in the load-displacement curves.

In the initial stage of 650nm STF-Twaron® loading curves, there are no differences between the impregnated fabric targets with different particle concentrations but fluctuation can be observed on the last part of the curves. However, for the 12nm STF-Twaron® loading curves, they are more offset than 650nm STF-Twaron® do with different particle concentrations. The difference of their stab behaviours of the STF impregnated targets can be explained by their unique rheological properties of STFs which impregnated into them. 650nm STFs have similar initial viscosities before shear thickening phenomenon, while 12nm STFs have significant different initial viscosities at the lower shear rates.

Figure 4.9 also indicated that the deformation depth for the untreated fabric panel is 42mm, and that for the STF impregnated ones are all below 35mm. It is also found through the experiment that the untreated 24-layer fabric panels were fully penetrated by the knife, whereas only 9 layers were penetrated for the 12-layer panel impregnated with 650nm silica STF with 30% weight fraction. In addition, all the STF treated fabric panels stopped the knife as well and higher the particle concentration smaller the fabric displacement which lead to a fewer number of layers penetrated by the knife impactor. The penetrated fabric layers after the stabbing impact testing are presented in Table 4.4. Note that all these panels have the same areal density. This is a major evidence of improvement of stabbing resistant performance of the STF impregnated fabric panels.

Table 4.4 Layers of fabric penetrated by stabbing impact

Fabric panels	Total layers	Penetration layers
12nm 20% STF-Twaron®	12	11
12nm 25% STF-Twaron®	12	10
12nm 30% STF-Twaron®	12	10
650nm 20% STF-Twaron®	12	11
650nm 25% STF-Twaron®	12	10
650nm 30% STF-Twaron®	12	9
Untreated Twaron®	24	24

Improvements in back-face deformation of the STF impregnated panel were also evident in comparison with the untreated fabric panel. The deformation of 24-layer untreated fabric panel formed a cone with a 2.7cm depth, whereas the back-face deformation of the 650nm-30%-STF impregnated 12-layer panel was hardly noticeable. The comparison between the two is illustrated in Figure 4.10.

(a) 24-layer of Untreated panels (b) 12-layer STF-impregnated panel

Figure 4.10 Backface deformation comparisons of multilayer targets after impacted

Figure 4.10 presents the photos of the rear surfaces of 24 layered untreated Twaron® fabrics and 12 layered STF impregnated Twaron® fabric targets impacted by knife impactor. The deformation of untreated fabric targets acquired a dome-like shape and all the layers have been penetrated through by the knife impactor. While there is no obvious deformation on the back face of STF-impregnated fabric targets and the targets successfully prevent the knife impactor from penetrating through all the fabric layers. Lower back face deformation causes lower indentation which leads to less blunt trauma to the wearer and results in higher protection performance. In other words, the STF-impregnated fabrics can provide same stabbing protection with untreated fabrics using less fabric layer. Hence, more energy can be absorbed and dissipated by STF impregnated fabrics, which further proved the mechanism that how STF-impregnated prevent the stab impacting.

4.3.8 Influence of knife impact velocities

As 650nm-30%-STF impregnated 12-layer panel performs the best stabbing resistant performance, this panel was chosen to compare with 24-layer untreated Twaron® panel under different velocities for investigating the impact velocity influencing factor.

Since the velocity of 3m/s has been examined, in this section of research, the velocities of 1m/s and 2m/s were selected for exploring the effects.

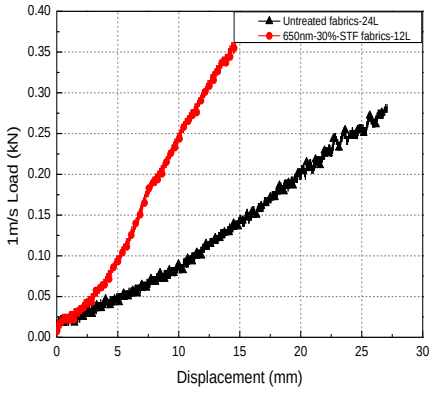

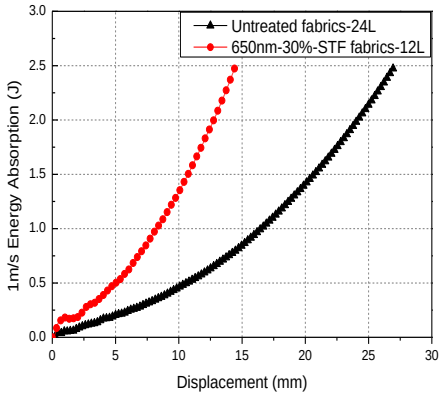

(a) Load-displacement (1m/s); (b) Energy absorption-displacement (1m/s)

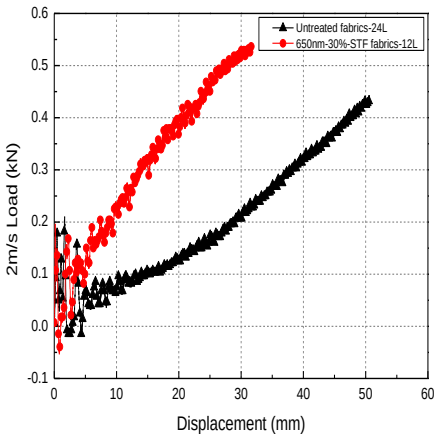

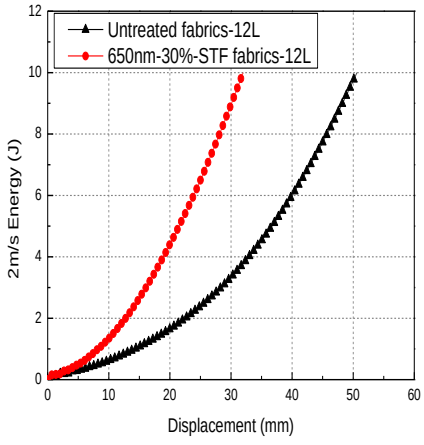

(c) Load-displacement (2m/s); (d) Energy absorption-displacement (2m/s)

Figure 4.11 12 layered 650nm-30%-STF impregnated Twaron® panels vs. 24 layered Twaron® untreated panels under different impact velocities

As can be observed in Figure 4.11, STF-Twaron® fabric panel show consistently less fabric displacement than the untreated Twaron® fabric panel under the same areal density. Higher stabbing resistance performance is demonstrated by smaller measured values of depth of indentation (fabric displacement). Total deflection is the total distance that the fabrics deform as a result of the impact force. Due to the lower velocities, both of the fabric panels were not penetrated by the knife impactor. And both of the fabric panels could absorb all the impact energy under the two different velocities. The STF-Twaron® panels constantly exhibit higher stiffness as compared with the untreated Twaron® panels. At each same value of displacement, STF-Twaron® fabrics show higher impact loading level and higher energy absorption than that of untreated Twaron® fabrics. It is observed that in the case of untreated Twaron® fabrics, the displacement of the fabrics participate in energy absorption is larger than that of STF impregnated fabric targets which indicate that the deformation of untreated Twaron® fabrics need to be larger to absorb the same level of impact energy as STF-Twaron® fabric panels do.

Consequently, STF impregnated Twaron® fabric targets have less fabric displacement undergo the same impact energy and perform significantly better stabbing resistance in the knife stabbing test than the untreated Twaron® fabric targets under different impact velocities.

4.3.9 Dynamic stabbing test on single layer fabric

Although in the practical applications, multi-layered fabric panels are used for manufacturing soft ballistic body armour. It is worthwhile to study the performance of single layer fabric in order to obtain more specific information on the stabbing mechanism of the fabrics. Because single layer fabric could absorb the limited level of impact energy, only 1m/s impact velocity was nominated to investigate the single layer fabric stabbing behaviours.

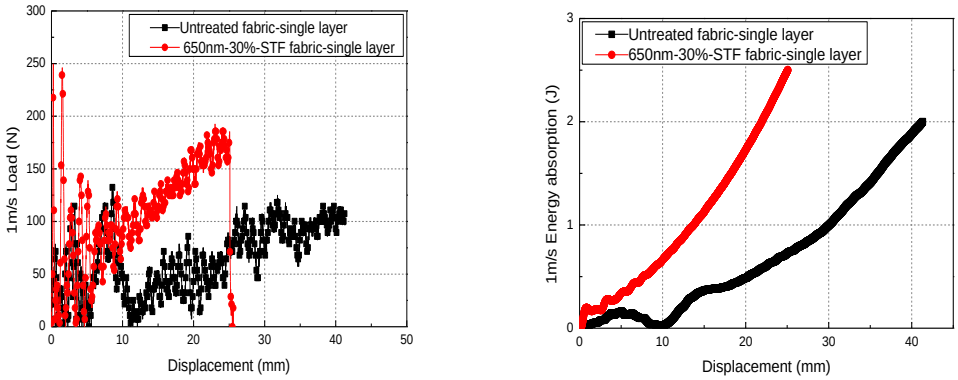

(a) load-displacement curves (b) energy absorption-displacement curves

Figure 4.12 Stabbing behaviours of single layer untreated Twaron® fabric vs. single layer STF-Twaron® fabric

As presented in Figure 4.12, single layer of STF-Twaron® fabric demonstrates higher loading results and higher energy absorption with the smaller fabric displacement compared with single layer Twaron® fabric. Though the testing results have shown a lot of fluctuations, the higher stiffness of STF-Twaron® fabric under impact still can be witnessed. Furthermore, both of the single layer fabric targets were easy to be penetrated by the knife impactor.

Consequently, stabbing tests on single layer fabric keep the consistent conclusions that STF impregnated Twaron® fabric performs better stabbing resistant performance with less fabric deformation.

4.3.10 Influence of the treatment by pure PEG medium

In addition, it need be demonstrated that the enhanced stabbing performance of impregnated fabric is due to the addition of STF to the fabric, not due to the increased target mass or solvent effects on the fabric weave. For this purpose, Twaron® fabric was impregnated with pure ethylene glycol. The objective of this section is to investigate if only treat the fabrics with a pure dispersing medium which is without

shear thickening behaviour, how would the fabric stabbing resistant performance be affected. A good comparison needs to be with the same areal density, and 21 layers PEG200 treated fabrics weigh the same as 20 layers of PEG600 treated fabrics and weigh the same as 24 layers of untreated fabrics.

Figure 4.13 shows the results of load-deformation and energy histories from the dynamic stabbing impact tests for the untreated Twaron® fabric targets and PEG-treated fabric targets.

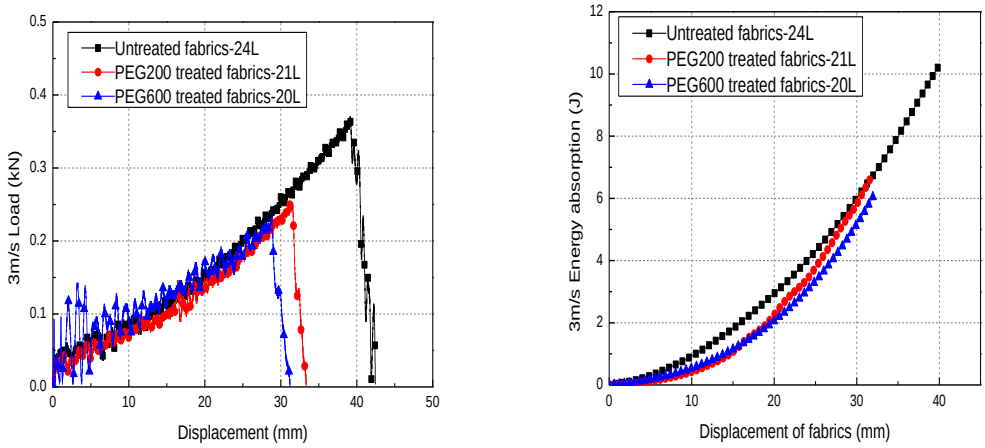

(a) Load-displacement curves (b) Energy absorption-displacement curves

Figure 4.13 Stabbing behaviours of multi-layer untreated Twaron® panel vs. PEG-treated Twaron® panel under the same areal density

As can be indicated from Figure 4.13 (a), all the fabric targets were impaled by the knife impactor under the impact velocity of 3m/s because all the loading curves dropped to zero in the end. After the treatment of PEG, no matter with the higher molecular weight PEG600 or lower molecular weight of PEG200, both of the fabric targets presented lower peak load and smaller energy absorption capability as compared with untreated Twaron® panel on the same areal density basis. Furthermore, PEG-treated fabric targets deform less than untreated fabric targets before they were penetrated by the knife impactor. This means PEG-treated fabric targets are easier to be penetrated before they deformed. The addition of pure PEG, even with relatively

high viscosities would generally decrease the stabbing resistant performance of the Twaron® fabric.

The reason for PEG-treated fabric targets support the lower load and absorb smaller impact energy than the untreated fabric targets may be attributed to the reduction of friction between fibres in the fabric due to the lubricating effects of the pure PEG. The decrease performance of PEG-treated Twaron® fabric panels clarified that shear thickening behaviour of STF is associated with the stabbing performance of the fabrics impregnated with STFs.

4.4 Mechanism analysis and discussions of fabric targets stabbing performance

4.4.1 Due to STF impregnation

From all the fabric targets designs, manufactures and dynamic tests on different types of fabric targets, it is learnt that STF impregnated Twaron® targets exhibit higher stabbing resistant performance compared with untreated Twaron® targets regardless the STF particle size or particle concentrations, or fabric targets areal densities, or fabric layers of the targets. The significant improvement of the stab properties is mainly due to the functions of the STF. The STF functions include binding the fibres together, protecting fibres from local damage and distributing the load to the fibres. Although STF by themselves generally have low mechanical properties compared to those of fibres, the STF influences the stab properties of the composite fabric.

As STF will be transformed from the liquid phase into the solid phase when it suffers intensive impacting, and the solidified STF greatly improves the coefficient of friction between adjacent filaments of yarns. Thus the yarn motion within the fabrics is restricted, which can prevent the yarns from being pushed away from the tip of knife impactor. Moreover, due to the treatment of Twaron® with STFs reduces yarn mobility, the resistance of yarn displacement increases and energy portion absorbed in

the processes related to yarn breakages inside the fabrics. Hence we can expect the increase of stabbing resistance of Twaron® fabrics to knife impactor were due to constraining the movement of the yarns and more portion of energy absorbed by yarn fracture.

In the case of STF impregnated fabric samples, it is postulated that at the time of impact, the STF is transformed into a solid-like material during impact. The transformed STF acts as a bridging matrix which converts the network of yarns in the fabric into a coherent structure as a result of solidification of the STF. Hence, even though the initial strike of the impactor takes place at the centre of the specimen initially engaging only the primary yarns, due to shear thickening phenomenon, the secondary yarns also get engaged and the entire fabric structure shares the impact as a single element. The failure of the STF treated structure is by rupture of fibres and yarns rather than their slippage. Thus the fabric can bear more impact force and absorbs more energy.

In the case of untreated fabric, almost all the force that the impactor transfers is taken up by the primary yarns. Since the force per yarn is high, the yarns slip forming long loops but the rest of the fabric remains undisturbed. Due to the participation of only a few yarns, the energy absorption is low.

4.4.2 Due to rheological properties of STF

The silica nanoparticle size of the STF and silica nanoparticle weight fraction of the STF are the dominant factors affecting shear thickening phenomena as discussed in former sections. The presence of different types of STFs in treated Twaron® fabrics have indicated that the effects of STF impregnation on stabbing resistant performance were associated with the silica weight fractions and silica nanoparticle sizes.

4.4.2.1 Due to different silica weight fractions of STF

From all the testing results related to the effect of the silica nanoparticle weight fraction production parameter of STF samples, higher silica nanoparticle weight fraction of STF samples used to impregnated into Twaron® fabric targets have shown higher rigidity than that of untreated Twaron® fabric panels under the dynamic knife impact. It is observed higher the concentration of STF impregnated onto the fabric, more energy can be absorbed by STF impregnated fabric targets. It can be concluded higher the particle concentrations of the STF lead to higher stabbing protection of the STF impregnated fabric samples. This improvement is due to the addition of STF to the fabric which leads to the enhancement of the fabric strength and properties. In the previous study [1] that higher concentration of silica in STF leads to higher STF add-on% on fabric. The higher amount of STF creates better bridging of yarns and thereby forms a coherent structure. However, there always has a limit amount of STF irrespective of the particle concentration could be impregnated into the fabrics and too much STF add onto the fabric would cause the fluid drip from the fabric when it is hung up upright. So this led to the inference that impact performance improvement is more likely caused by enhanced shear thickening phenomenon. As discussed before in Chapter 3, higher particle weight concentration leads to lower critical shear rate and a greater change of shear thickening viscosity. During the impact, STF works on improvement of impact performance due to its unique property which transfers its liquid state to solid-like state. In the case of higher particle concentration, more dramatically increase on shear thickening viscosity will make the STF more rigid under the impact. Note that the highest weight fraction of silica particles STF suspensions has the highest shear thickening viscosity, which can provide the highest protection performance due to the desired energy absorption effects. Additionally, it can be observed from the stabbing results that the STF impregnated fabric targets modulus increase with the STF concentrations, which is due to the viscosity and shear thickening effect of STF is more significant as the concentration increases. As a result of that, STF impregnated fabric samples with higher particle concentrations perform

better on impact resistant performance owing to the better bridging of yarns and forms better coherent structure.

4.4.2.2 Due to different silica nanoparticle sizes of STF

The larger nanoparticle size 650nm STF treated Twaron® fabric targets perform better on stabbing resistance than smaller nanoparticle size 12nm STF treated Twaron® fabric targets under the same areal density which can be correlated to the rheological properties of the STF which has been used to treat them. As has been discussed before, STFs synthesising with larger nanoparticle size 650nm exhibit a greater increase in viscosity and lower critical shear rate. From the calculation of stabbing shear rate, the influence of STF critical shear rate can be neglected. Additionally, although 650nm STF has a lower critical shear rate, at the early stage of knife stabbing impact, 650nm STF treated Twaron® fabric targets have shown less stiffness than 12nm STF Twaron® fabric targets under the same fabric targets areal density. It can be postulated that 650nm STF has lower initial viscosity which leads to lower stiffness the early stage of impact, however, 650nm STF treated fabric targets loading data performs more dramatically increment at the near end stage of the impact process compared with 12 STF treated fabric targets loading data, which means the larger particle size STF exhibits greater increase in viscosity can be related to higher impact resistance performance.

Nevertheless, it can be concluded that the major difference between 650nm STF impregnated fabric and 12nm STF impregnated fabric on stabbing performance indicated on STF particle weight fraction of 30%, while not noteworthy differences are observed for particle weight fraction of 20% and 30%. These results can be related to the rheological properties of which STFs has been impregnated into the fabric targets. As can be demonstrated in Table 4.5, the severity of shear thickening effect between 12nm STF and 650nm STF are quite similar at the particle weight fraction of

20% and 30%. Therefore, there are no obvious differences reflected on their stabbing performance which can be associated with the solidification effect of STFs. However, at the particle weight fraction of 30%, 650nm STF presents more dramatically increase on shear thickening viscosity, and 12nm STF displays less evident shear thickening phenomenon. This can result in more significant difference on stabbing performance between 650nm STF and 12nm STF at 30% particle weight fraction.

Table 4.5 Shear thickening viscosity jump of STF produced with two particle sizes at three particle concentrations

STF types	Critical viscosity (Pa·s)	Post-thickening viscosity (Pa·s)
12nm 20%	2.8	60
650nm 20%	1.5	250
12nm 25%	5.7	210
650nm 25%	2.8	425
12nm 30%	60	920
650nm 30%	3.6	1750

As a result, the rigidity of STF treated Twaron® fabric targets under impact can be correlated to the rheological properties of the STF which has been used to treat them. Impregnation with STF containing larger silica nanoparticle sizes yields better stabbing resistant performance than impregnation with smaller nanoparticle sizes the same STF particle concentrations.

For different rheological parameters effects on the stabbing behaviour of STF-Twaron® analysis, which will help to determine the particle size of STF is the most critical to achieving enhanced protection properties.

4.5 Quasi-static stab tests

4.5.1 Quasi-static stab testing equipment

In order to supplement the dynamic stabbing tests and to investigate more precisely the effect of STF impregnation on Twaron® fabrics stabbing resistant performance,

quasi-static stab tests of were conducted on Instron 3344 Tensile & Compression tester, as showed in Figure 4.14. The tester is equipped with 2 kN load capacity and 1067mm vertical test space. The NIJ-specified impactor "P1" knife was used.

To perform a stab test, the knife was mounted to the upper crosshead; the speed was 100 mm/min. The samples were tested in an environment of 20°C and 65% relative humidity. The specimens were clamped on the top of a hollow steel cylinder which fixed on the pedestal of the tester. At least three specimens were tested and an average compression force (load) vs. displacement curve could be obtained.

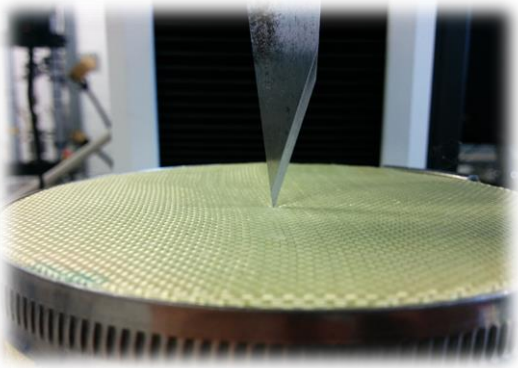

Figure 4.14 The quasi-static stab tests

4.5.2 Specimens preparation

The fabric targets used for quasi-static stab tests keep the same preparation standard as the fabric targets used for dynamic stab tests. All the tests were carried out on single layer fabric target irrespective the areal density. Three trimmed untreated Twaron® fabrics, 12nm STF at 30% particle concentration fully impregnated Twaron® fabrics and 650nm STF at 30% particle concentration fully impregnated Twaron® fabrics were prepared for the tests.

4.5.3 Quasi-static loading vs. displacement curves

As the knife impactor slowly penetrated into the fabric target at the speed of

100mm/min, the load and displacement of the knife can be recorded as the Figure 4.15.

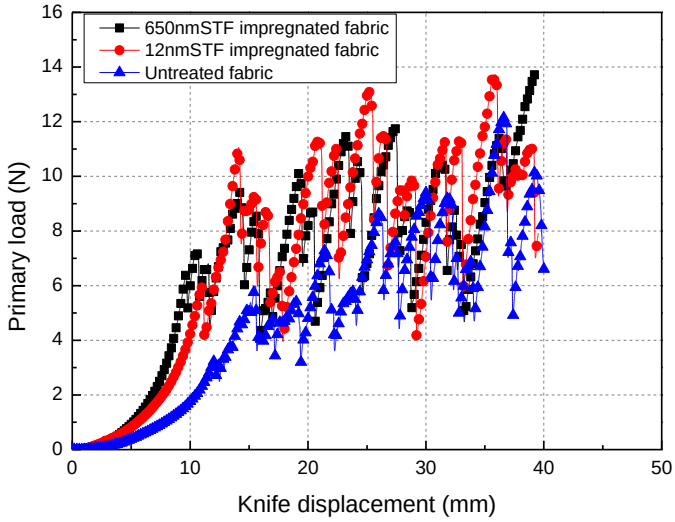

Figure 4.15 the load-displacement curves of quasi-static stab tests

Stabbing resistant performance of untreated fabric target and STF impregnated fabric target under quasi-static condition can by compared by the testing results curves. Figure 4.15 illustrates quasi-static load vs. displacement results for the untreated Twaron® and two categories of STF impregnated Twaron® targets against the knife threat. It can be indicated by the three curves that both of the untreated fabric targets and STF impregnated fabric targets have shown the same trend regardless the peak load or stiffness of the fabric targets. As can be demonstrated from the curves, the stages of knife penetration could be summarised as follows: 1) initial contact; 2) loading the fabric prior to initial puncture, resulting in a linear load increase with displacement. The yarns were pushed away by the knife and deformation of fabric is increasing, there were no yarn fracture occurred in the fabric; 3) initial puncture, resulting in the first peak load and initiation of fabric crack and cutting, 4) initial cut, as the knife move further down, the yarn contacted with the knife blade had been cut and the load decreased suddenly, 5) increasing loads as the impact knife contact area increased, widening the crack and cutting size, 6) the last peak load, when the fabric was cut and reached the maximum damage size.

In comparison the STF impregnated fabric targets regardless the STF particle sizes with the untreated fabric targets, the STF impregnated Twaron® fabric targets yielded a higher slope of impact load curve before the initial puncture of the fabrics, and higher peak loading values no matter how the load data fluctuated through the whole test. It is observed that both 12nm STF-Twaron® and 650nm STF-Twaron® loading curves are quite close to each other, while 12nm STF-Twaron® fabric targets exhibit a little higher loading resistance at the average load level through the whole penetration process than 650nm STF-Twaron® fabric targets. It can be concluded that STF impregnated Twaron® fabric targets support higher load than the untreated Twaron® fabric targets even though under the quasi-static stabbing speed condition.

4.5.4 Mechanism analysis

According to the equation (4.1) in section 4.2.2, the quasi-static stabbing shear rate can be calculated as $0.83s^{-1}$ which is smaller than the critical shear rate of shear thickening transition. Consequently, the quasi-static stab speed is not sufficient to initiate the onset of shear thickening phenomenon during the stab tests. As a result of that, the shear thickening effect cannot be used as an explanation for the enhancement of the quasi-static stabbing resistant performance on STF impregnated fabric targets. It can be hypothesised that STF impregnation had a particular effect on the inter-yarn friction due to its initial viscosity which could lead to superior stabbing resistant performance. This assumption of increased inter-yarn friction will be systematically studied and discussed in Chapter 5.

4.5.5 Damage observation of fabric targets

Following the test, untreated Twaron® fabric targets and STF impregnated fabric targets were visually inspected to compare the damage morphology.

(a) Untreated fabric (b) 650nm STF impregnated fabric

Figure 4.16 The failure of the untreated fabric and the STF impregnated fabric

Figure 4.16 displayed the damages in both cases were along the breadth of the knife from one cutting edge to the other cutting edge. In the case of untreated Twaron® target, several yarns were spread out by the knife instead of getting damaged. It can be observed that the yarns around the impact zone have been pulled out and have shown in form of trace line distributed to the edge of the fabric target. The reason why STF impregnated fabric target offered better stabbing resistance, as is evident from (b) as more yarns have been cut than being pull-out in the damage region. It looks like the STF held the fibre together during the impact process and the damage was in the form of a clear hole with fibre cut. This could be due to the presence of STF increases the inter-yarn friction of the STF-Twaron® which contributes to preferable stabbing performance.

4.6 Summary

This study demonstrated that the stabbing resistant behaviour of the STF impregnated Twaron® fabrics was strongly influenced by impregnation with STFs. It has demonstrated that silica nanoparticle size and particle weight fraction of STF are the dominant factors that can be manipulated to realise the benefits of STF impregnated Twaron® fabrics for enhanced stabbing resistant performance for soft ballistic body armour. Furthermore, substantial improvement in the performance-to-weight ratio, as well as performance-to-thickness of body armour can be achieved to fully utilise the

superiority of STF impregnated Twaron® fabrics for flexible body armour.

The significant enhancement of dynamic stabbing resistant performance in STF impregnated fabrics can be attributed to the shear thickening behaviour of STF which leads to increase in compactness of the fabric structures under the high speed impact. Nevertheless, the highest shear rate caused by quasi-static knife stabbing is lower than the critical shear rate which could trigger the shear thickening phenomenon. Therefore the defeat mechanisms of the low speed (quasi-static) test may be due to the increased inter-yarn friction caused by STF.

Hence, it is essential to investigate STF impregnation effect corresponding the strengthen mechanisms on STF impregnated fabrics. In Chapter 5, the STF impregnated fabric strength and properties under different shear rates conditions will be explored.

Chapter 5

Supplementary experimental investigation on STF corresponding stabbing resistance strengthen mechanisms

5.1 Introduction

Both of the dynamic stabbing impact and quasi-static stabbing tests clearly show that STF addition provides an enhancement to the stabbing resistant properties of Twaron® fabrics. However, the strengthen mechanisms of the STF impregnation under the different shear rates are different. In the case of dynamic stabbing tests, the shear rates during stabbing impact are high enough to trigger the shear thickening transition, thus STF can translate from liquid state to shear thickening state resulting in higher energy absorption. Whereas for the quasi-static stabbing tests, the impact shear rate is not large enough to exceed the onset shear rate that could induce the shear thickening phenomenon to the STF impregnated Twaron® fabrics. As results of that, the mechanisms of this improvement are not precisely known. Comprehensive testing and qualitative analysis are required, and the various parameters of the stab impact performance will be discussed and studied in this Chapter.

In order to develop a good understanding of STF effect on fabric impact resistance, this Chapter presents the evaluation of the inter-yarn friction for STF impregnated fabrics by using the yarn pull-out test, characterization of yarn property and fabric property with the treatment of STFs by conducting tensile tests. For each test, three

target specimens were tested in order to obtain the average performance.

5.2 Inter-yarn friction (yarn pull-out energy)

The inter-yarn friction of the fabric can be verified by yarn pull-out tests. Yarn pull-out test will be undertaken to determine the inter-yarn friction. Also, Yarn pull-out can be an important energy absorption mechanism of the stabbing resistance of woven Twaron® fabric.

The effect of STF impregnation on the interfacial friction of yarns under a quasi-static condition in Twaron® fabrics was evaluated by yarn pull-out tests. All tested fabric specimens were 50mm long × 50mm wide. The yarn pull-out tests were performed using a universal testing machine, an Instron 3344 Tensile & Compression Tester. The bottom part of the fabric was cut into 'bridge' shape with the centre part removed so that two sides of the fabric can be gripped by the bottom clamp and the single yarn in the middle part could be easily pulled out without elastic deformation or failure. The single yarn in the centre of the fabric was stick to the upper grip of the testing machine. The testing configuration has been shown in Figure 5.1. The single yarn was loaded by the crosshead at the speed of 100mm/min and to be pulled out from the fabric specimen. The tester is equipped with 10N load capacity and 1067mm vertical test space. All the tests are conducted at a constant temperature of 20°C.

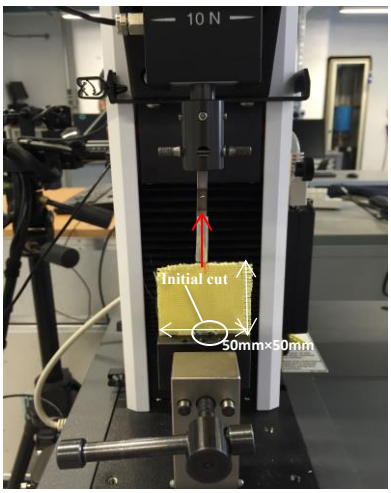

Figure 5.1 Quasi-static yarn pull-out testing configuration

The yarn pull-out tests under quasi-static testing speed have been conducted on 12nm-30% STF-fabric and 650nm-30% STF-fabric specimens compared with untreated Twaron® fabric specimens and the testing results are shown in Figure.

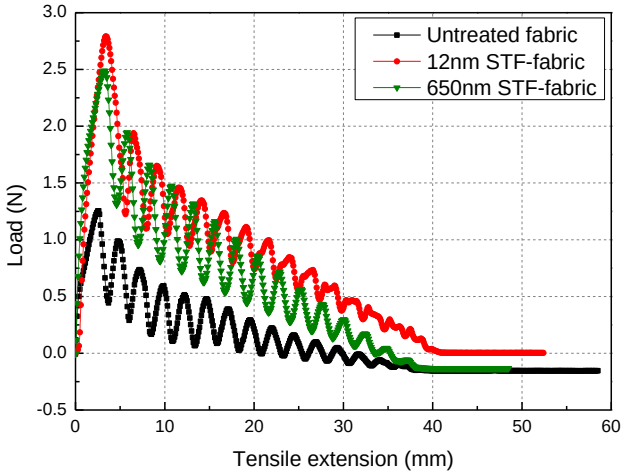

Figure 5.2 Load vs. displacement curves of quasi-static yarn pull-out test (100mm/min)

It can be indicated by Figure 5.2 that the data curves of all the fabric specimens irrespective STF treatment share the same trend. The data curves illustrate the yarn pull-out process as follows: During uncramping, the yarn undergoing pull-out force progressively straightens and locally disturbs the nominal woven architecture. This results in a nearly linear force-displacement curve. When the un-crimping zone reaches the edge of the specimen, the peak load point in reached. Finally, the entire yarn begins to translate within the fabric and the pull-out force gradually decreases. The oscillations in the force-displacement curve correspond to the subject yarn passing by woven structured yarns. Results indicate that both peak pull-out force and energy needed to pull an individual yarn increase with the friction between yarns.

In a comparison of the yarn pull-out properties between STF impregnated Twaron® fabrics and untreated Twaron® fabrics, STF impregnated fabrics exhibit higher peak load required to pull out a yarn than that of untreated fabric. Therefore, more force is

required to pull out each yarn from the STF-fabric, which leads to an increase in inter-yarn friction. Additionally, 12nm STF-fabric specimens demonstrate a little higher yarn pull-out force than that of 650nm STF-fabric specimens, which is can be postulated that 12nm STF has higher initial viscosity than that of 650nm STF resulting in higher inter-yarn friction. As have been stated in Chapter 2, the increased inter-yarn friction lead to improved impact resistant performance both in the stabbing and ballistic protections. It can be indicated from the yarn pull-out results that STF-fabric offers double of the peak load than that of untreated fabric specimens with the same knife displacements. Consequently, the mechanism of the quasi-static stabbing performance enhancement can be attributed to an increase of inter-yarn friction and decrease in yarn mobility within the fabric. The STF acts to restrict relative motion of the filaments and yarns, which provides higher energy dissipation capability.

5.3 STF impregnation effects on Twaron® yarn properties

As has been stated in section 2.5.1, yarn's strength is vital for enhancement of the fabric target knife stab resistance performance. The tensile modulus and tenacity of yarns are the key parameters affecting the stabbing resistant performance. In this section, the STF-Twaron® yarns were evaluated by tensile tests under the quasi-static state compared with the untreated Twaron® yarns.

The tensile properties of yarn specimens were carried out using Instron 44 yarn tensile strength tester. The special gauge length was set to be 250mm. A pre-tension of 0.5cN was employed in the tensile tests to make the yarn filament straight and parallel. All the tests were carried out at the temperature of 20°C and the humidity of 60%. The yarn specimen was stretched at a speed of 100mm/min and tensile testing results have shown below in Figure 5.3.

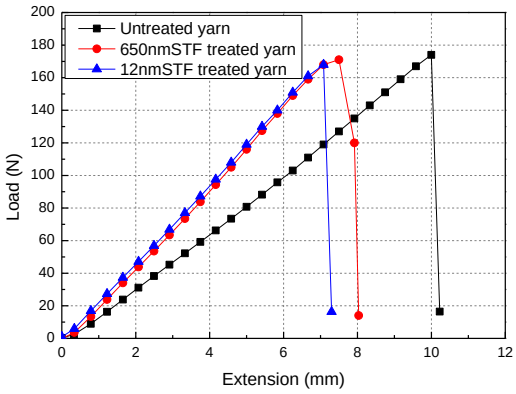

Figure 5.3 Tensile test results of yarn specimens

Figure 5.3 illustrated the yarn failure process undergoing the stretch force at the speed of 100mm/min. It can be observed from the tensile results curves that both 650nm STF and 12nm STF impregnated yarn specimens present earlier yarn breaking time and less yarn extension, which results in less failure strain than that of untreated Twaron® yarns. However, all the three different yarn specimens exhibit nearly same load results at the break. It can be assumed that the impregnation of Twaron® yarn with STFs doesn't affect its tensile strength while can offer improvement in tensile stiffness and modulus.

5.4 STF impregnation effects on Twaron® fabric tensile strength

The general features of impact resistant materials for higher energy dissipation are high tenacity and high tensile modulus. Fabric tensile strength is one of the major factors affecting the stabbing resistance performance of woven Twaron® fabric. Fabric tensile strength tests were carried out under both the dynamic and quasi-static conditions in order to characterise the fabric tensile properties with and without the STF treatment.

5.4.1 Fabric tensile tests under quasi-static speed

In order to compare the tensile properties of Twaron® fabrics with STF-Twaron® fabrics, an Instron 5569 Tensile & Compression Tester was used to evaluated the

tensile strength of the fabric specimens under the quasi-static state. All tested fabric specimens were 50mm long × 50mm wide which share the same dimensions with the yarn pull-out tests. Fabric specimens were prepared as two sets, one set is untreated Twaron® fabric strips, and the other one set is 650-30% STF impregnated Twaron® fabric strips. The top and bottom part of the fabric specimen were gripped by the upper clamp and lower clamp firmly in case of slippage. And the testing configuration has been shown in Figure 5.4. The upper load cell was loaded at the speed of 100mm/min and the load capacity is 50kN. The testing room temperature is kept constantly at 20°C.

Figure 5.4 Fabric tensile tests configuration

Three untreated fabric specimens and three STF-fabric specimens were stretched respectively under tensile loading speed of 100mm/min. And the tensile load results of the two sets of fabric specimens have presented in Figure 5.5.

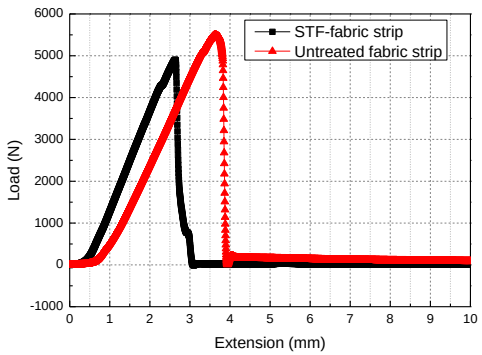

Figure 5.5 Tensile behaviour of STF impregnated fabric strip and untreated fabric strip under quasi-static

The standard load vs. extension of the fabric strip specimens during the testing were recorded as the plots shown in the Figure 5.5. The Figure 5.5 indicates that STF-fabric strip behaves less tensile strength than that of untreated fabric strip at quasi-static testing mode. In addition, STF-fabric strip demonstrates less fabric extension at the break than that of untreated fabric strips. Unlike the quasi-static yarn pull-out tests, the STF impregnated fabric strip didn't show enhanced tensile strength than that of untreated fabric strip as expected. Although STF-fabric strip exhibits higher stiffness which has shown in Figure 5.5 and higher inter-yarn friction in the fabric which has been proved in section 5.2.1, the tensile strength demonstrates lower peak load than untreated fabric strip. This behaviour should be correlated with the appearance of the targets after impact testing. The Figure has been shown below used to support the mechanisms analysis.

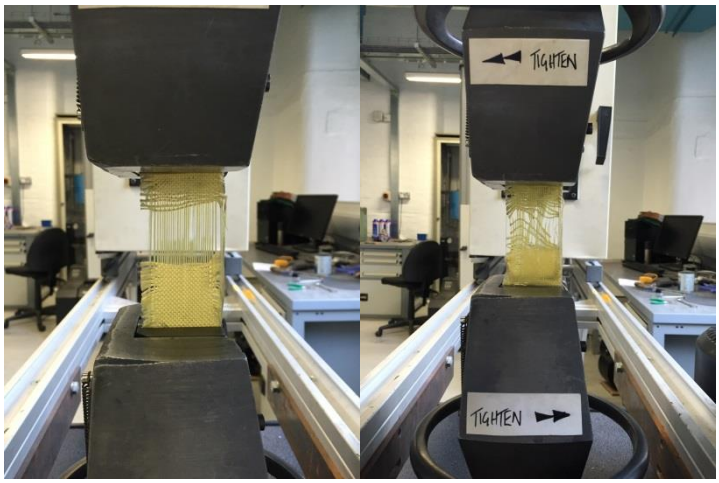

(a) Untreated fabric strip (b) STF-fabric strip

Figure 5.6 Photos of fabric fracture after quasi-static tensile tests

As can be seen in Figure 5.6 (a), all the yarns in fabric length direction are parallel to each other and all the yarn failure occur at nearly the same time for the untreated fabric strip specimens. It can be assumed that load stress was evenly distributed inside of the untreated fabrics and all the yarns along the length direction undertake the load stress uniformly to achieve better results of the load at break. In the case of STF-

fabric strips, Figure (b) displayed a relatively uneven breakage of the yarns along fabric length direction and the yarn failure happens at the different time. As has been discussed in section 5.3, STF impregnation into Twaron® yarns leads to higher modulus of the single STF-Twaron® yarn. During the process of stretching the STF-Twaron® yarn, the extension of the fabric may cause the STF unevenly distributed onto the surface of the STF-Twaron® yarns of the fabric, which leads to uneven load stress distribution on the STF-fabric. As a result of that, some part of the STF-Twaron® yarns needs to endure more stress which generates earlier yarn breakage. The yarns suffering more load stress appear to form the weakness part of the STF-Twaron® fabrics resulting in lower load at break.

The investigation of this section yields a better understanding of the tensile behaviour under quasi-static loading for STF-Twaron® fabrics. Although STF impregnated fabric demonstrates less tensile strength, it behaves higher stiffness than that of untreated fabric.

5.4.2 Fabric tensile tests under high strain rate

In the practical dynamic stabbing impact, the speed of the knife motion is around 3m/s. Therefore, it is meaningful to test the fabric tensile properties at such high loading speed corresponding to the dynamic stabbing impact speed. Furthermore, it is essential to building the relationship between fabric strength in dynamic state and the stabbing resistant performance.

Moreover, shear thickening is the non-linear response of the fluid triggered by large deformation or high stresses which are difficult to characterise using normal testing speed at low frequencies and deformation. In consequence, to gain a better understand dynamic response of STF at high shear rate, it is necessary to perform STF-fabric tensile tests under high strain rates.

STF impregnated fabrics were studied with high strain rate measurements techniques to characterise their mechanical properties. The high speed fabric tensile tests were carried out using Amsler HTM 5020 high strain rate testing machine (Zwick/Roell, Germany). The testing machine would carry out dynamic high speed testing with a load capacity of 50kN and at velocities up to 10m/s. All the fabric specimens were prepared with the same specifications as the specimens used for quasi-static fabric tensile tests, and the test configuration of the high strain rate fabric tensile tests have shown in Figure 5.7. All the tests are conducted at a constant temperature of 20°C.

Figure 5.7 Test configurations of high strain rate tensile tests of fabric strips

On account of the dynamic stabbing, tests have been conducted with the speed of 3m/s, the high strain rate tensile speed were set to be 3m/s. In this section, only 650nm-30% STF-fabric specimens were chosen as representative STF impregnated fabric specimens due to 650nm-30% STF-fabric has shown best stabbing performance during the dynamic stabbing tests out of all the types of STFs impregnated fabric targets. The testing results of high strain rate fabric tensile strength of STF-fabric specimens compared with untreated fabric specimens under the tensile speed of 3m/s have shown in Figure 5.8.

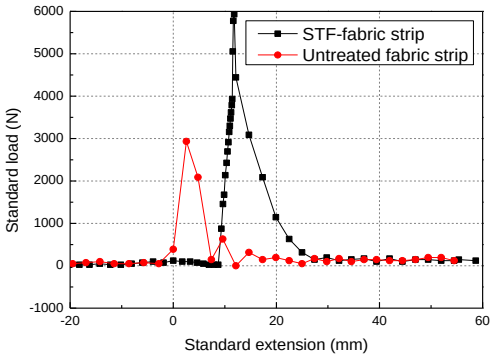

Figure 5.8 Tensile behaviour of STF impregnated fabric strip and untreated fabric strip under high strain rate

As can be seen in Figure 5.8, under the high strain rate yarn pull-out speed, the comparison data curves are different from the quasi-static fabric tensile loading curves. STF impregnated fabric strip showed slightly lower tensile strength than that of untreated fabric strip at quasi-static strain rate, while at high strain rate STF impregnated fabric strip exhibited significantly higher tensile strength compared to untreated fabric strip. At high strain rate level, STF impregnated fabric strip carried twice as high as the untreated fabric strip specimen tensile load. The high strain rate tensile testing results showed a major improvement in the tensile strength of the STF impregnated fabric specimens as compared to the untreated fabric specimens.

The noticeable peak load for STF-fabric specimens can be clearly spotted in the Figure, which indicated that dramatically change happened on the STF-fabric tensile strength during the tensile process. As has been stated, shear thickening transition occurs at the shear rate of $10^1 \sim 10^2$, and the shear rate of high strain rate fabric tensile tests can be calculated according to the equation in section 4.2.2. In the case of fabric tensile speed is 3m/s, yarn thickness is measured using an optical microscope and the measurement result is 0.144mm, so the shear rate of 3m/s fabric tensile test is $2.08 \times 10^4\ s^{-1}$. As a result of that, the shear rate of the speed for high strain rate fabric tensile test is much higher than the shear rate of STF which initiates the onset of shear thickening phenomenon. Subsequently, STF can transform from liquid to solid-like

during the high strain rate fabric tensile tests which lead to higher tensile strength. It can be concluded that tensile strength of STF impregnated fabric strip exhibit significantly enhancement undergo high strain rate tests. As a sufficiently high shear rate, STF exhibited shear thickening behaviour due to exceeded critical shear rate triggering the shear thickening phenomenon of STFs. These will provide the proof of shear thickening behaviour at high strain rate levels.

At the high strain rate testing, evidence of shear thickening phenomenon of STFs can be demonstrated from the results. It can determine that STF impregnation does have a positive effect on tensile properties at high strain rate. There is a good correlation between the shear rate of STF critical shear rate triggering the shear thickening phenomenon and the experimentally shear rate which provided by high speed testing machine. It was expected that at high strain rate which exceeded the critical shear rate of STFs, as a result of microstructural changes (hydro-cluster formation), the STF would manifest as an increase in viscosity and be able to carry more tensile strength.

Consequently, STF impregnated fabric strip can achieve better tensile behaviour than that of untreated Twaron® fabric. It should be noted that untreated fabric strip behaves much less tensile strength (3000N) under high strain rate than tensile strength (5500N) under the quasi-static state. Although STF-fabric resulted in higher tensile strength by the STFs, the tensile strength of STF-fabric is almost the same as untreated fabric at quasi-static state. Some valuable information can be obtained from the fracture photos of the STF-fabric strip and untreated fabric strip after the high strain rate tensile tests in Figure 5.9.

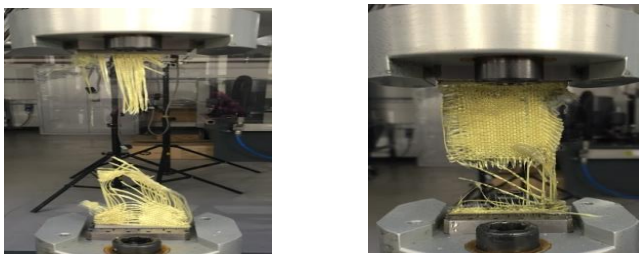

(a) Untreated fabric strip; (b) STF-fabric strip

Figure 5.9 Photos of fabric fracture after high strain rate tensile tests

It can be seen from Figure 5.9 (a) that most of the yarns in the untreated fabric strip were slipped and pulled out rather than fractured. Conversely, almost all the yarns in the STF-fabric strip were fractured after the high strain rate tensile load which can be observed in Figure 5.9 (b). As has been discussed in Chapter 4, yarn breakage can absorb more energy than yarn pull-out, and the function of STF addition is to prevent yarn from being pulled out from the fabric and contribute to more yarn fractured by the load. The reduced tensile strength of untreated fabric strip can be attributed to the increase of the yarn pull-out happened when subjected to high strain rate. The photos provide the evidence which supports the untreated fabric strip shows lower tensile strength than the STF-fabric strip tensile strength displays at under high strain rate state.

In comparison of untreated fabric strip tensile behaviour between quasi-static state and high strain rate state, from Figure 5.6 (a), it can be witnessed that all the yarns could have enough time to be fractured by the tensile load under quasi-static state; from Figure 5.9 (a), most the yarns were pulled out by the upper load which can be postulated that the yarns don't have sufficient time to be fractured and pulled out in a second. This is in agreement with the results of untreated fabric tensile behaviour under the quasi-static condition and high strain rate condition that more yarn breakage leads to higher load force than yarn pull-out in the fabric. Consequently, the untreated fabric strip shows lower tensile strength under high strain rate mode than the tensile strength displays at quasi-static state.

It can be concluded that the significant enhancement in stab and loading resistant properties in STF impregnated fabrics for knife threats which are attributed to the fact that the addition of STF to the fabric leads to the enhancement of the fabric strength and properties.

5.5 Summary

This Chapter enables the investigation of the relationship between STF impregnation into the fabrics associated with the inter-yarn friction, yarn and fabric properties under the quasi-static and high strain rate state with and without the shear thickening effect.

The performance enhancement in the dynamic stabbing impact tests and quasi-static impact tests provided by the STF is due to the increase in fabric tensile strength upon the transition of the STF to its rigid state, higher modulus of the yarns caused by presence of STF in the fabric, and increase in inter-yarn friction without the shear thickening effect under the quasi-static state owing to its relatively high initial viscosity.

Moreover, high speed tensile tests were implemented to evaluate the transient response of STF-Twaron® fabric at high strain rates. The results provided the evidence which supports the conclusion that the STFs exhibit shear thickening behaviour at high levels of strain rate.

Chapter 6

Experimental study of STF impregnation on ballistic performance

6.1 Introduction

The application of STFs results in enhancement of stabbing resistance of Twaron® fabrics, whether this STF impregnation will affect the ballistic performance positively or negatively will be explored in this Chapter.

In this Chapter, Twaron® fabric ballistic performance was determined by two evaluation methodologies: penetration and non-penetration tests. The former method is based on working out the projectile kinetic energy loss absorbed by fabric when it completely penetrates a fabric or panel target. For the latter method, the projectile does not penetrate the fabric panel and remains in it. Accordingly, the depth of back face signature is employed as an indicator of the ballistic performance.

High velocity ballistic impact tests were implemented on untreated Twaron® fabric targets compared with 12nm-30% STF-Twaron® fabric targets and 650-30% STF-Twaron® fabric targets with the same areal density in order to investigate the effect of STF impregnation on Twaron® fabric ballistic properties. The energy absorption characteristics of different fabric targets were discussed and analysed through different qualitative approaches.

6.2 Ballistic performance evaluation

Ballistic tests were conducted at the ballistic laboratory in the University of Manchester. A firing range used for impact tests was shown in Figure 6.3. A panel was placed between two couples of IR sensors. The clamp conditions for the panel depended on the ballistic performance evaluation methods. For perforation test, target specimens were clamped using a fixture, as shown in Figure 6.4. Perfect clamping conditions cannot be fully realised in experiments. Thus, efforts were made to reduce potential slippage and provide uniform clamping forces to all specimens. 12 sets of fasteners were applied to fasten the samples onto the steel fixture. Fabric samples were cut into square shape with the size of 24cm by 24cm and were placed under the steel frame with an aperture, then tightly clamped by the force of the fastening bolts. The effective area of the fabric samples is a circle with the diameter of 15cm. For the non-perforation test, target specimens were clamped using two rubber bands, as shown Figure 6.5 (b). The fabric layers were placed against a 225mm × 225mm × 100mm box filled with oil based Roma Plastilina® No.1 backing clay as shown in Figure 6.5 (a). The whole backing clay should be heated up to 37 degrees to simulate the mass properties of the human body before the non-perforation ballistic tests. The back layers of the fabric panel should be in contact with the clay surface as shown in Figure.

A blank cartridge (Figure 6.2 (c)) was used to propel the projectile held in a sabot (Figure 6.2 (b)). The projectile is a steel cylinder used as Fragment Simulation Projectiles (FSP) for impacting on panels in this study, with a diameter and a length of being both 5.5 mm, weighing 1g, as shown in Figure 6.2 (a). Pulling the trigger causes the projectile to be forced out from the barrel towards the target fabric at a high velocity, typically 490m/s. When the projectile passed through each pair of IR sensors, the responding time was recorded by the front and back timer. The time detectors then picked up the travelling time of the projectile before and after the fabric target, so the striking and residual velocity of the bullet can be measured. The loss of

kinetic energy carried by the projectile after going through the fabric can be calculated using Equation (6.3). In this set-up, the distances between the two pairs of time detectors were 46.84 cm (front) and 36.11 cm (rear) respectively. Figure 6.1 sketches the construction of this firing range.

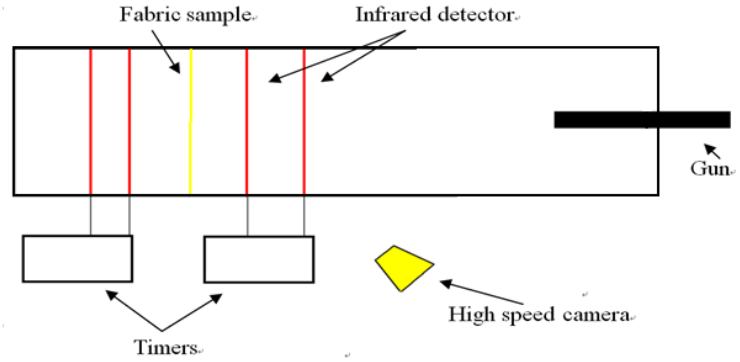

Figure 6.1 Schematic diagram of the ballistic tests configuration

Figure 6.2 (a) steel projectile (b) plastic sabot (c) cartridge

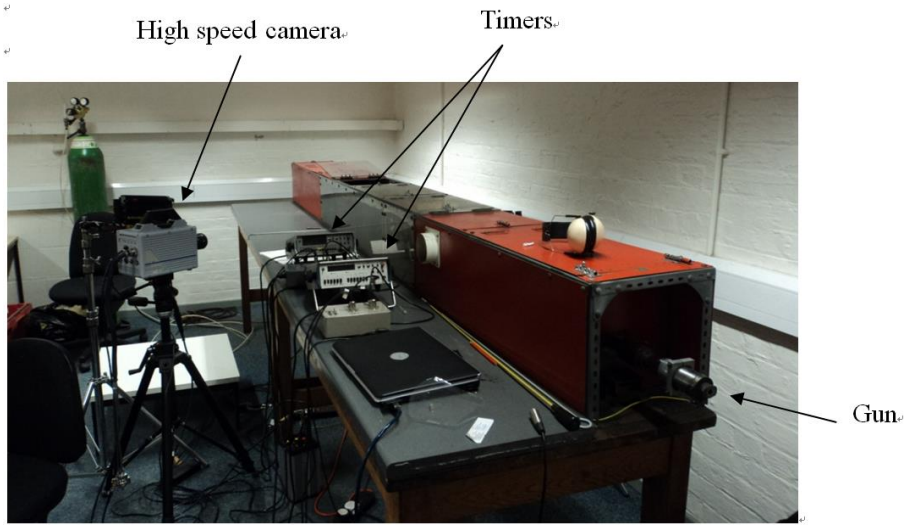

Figure 6.3 The ballistic range

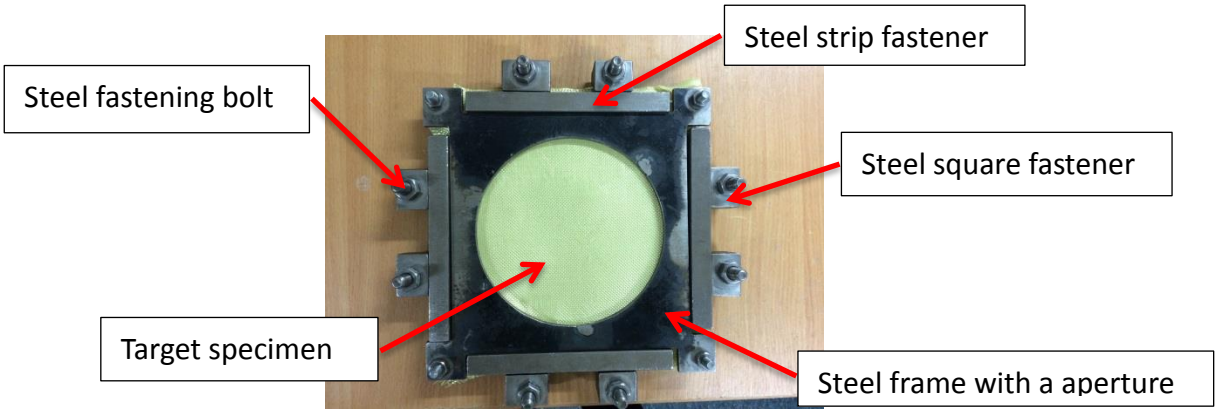

Figure 6.4 Clamp condition for the perforation test

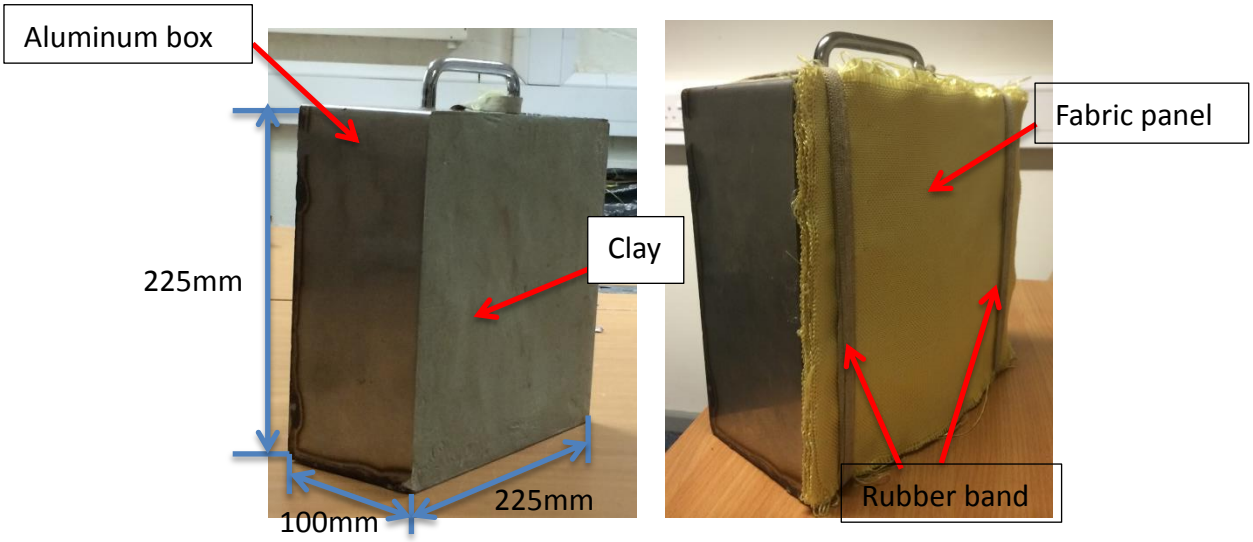

(a) (b)

Figure 6.5 (a) Roma Plastilina® oil-based backing clay; (b) Clamp condition for non-perforation tests

6.3 Ballistic penetration tests

Ballistic penetration tests are carried out on single layer fabrics or panels with small numbers of fabrics to measure the fabric or fabric panel's ability of absorb energy from the impacting projectile. The ballistic shooting test enables to have a direct understanding of how soft body armour dissipates and absorbs projectile energy. The velocity of the projectile propelled by a powder cartridge is in the range from 450 m/s to 500 m/s. The ballistic range is equipped with a high speed camera, which is able to show the ballistic impact upon fabric targets.

6.3.1 Striking velocity and residual velocity

According to the distance between IR sensors and the time of the projectile passing through, the striking velocity and residual velocity can be calculated based on the equations (6.1) and (6.2). The residual velocity is the exiting velocity through the panel.

$$v_s = \frac{s_1}{t_1} \tag{6.1}$$

$$v_r = \frac{s_2}{t_2} \tag{6.2}$$

where s_1 (46.84cm) and s_2 (36.11cm) is the distance between front and rear IR sensor pair respectively. v_s and v_r is the striking velocity and residual velocity respectively.

6.3.2 Energy absorption of the panel

The kinetic energy dissipation of the projectile can be calculated by the striking velocity and residual velocity of the projectile, Considering the amount of the striking velocity deceleration in the air even if without armour panels in the ballistic range, the loss of kinetic energy 0.21J was measured by ballistic tests. Suppose the energy dissipation due to the projectile deformation and acoustic losses are all negligible. The kinetic energy dissipation of the projectile is assumed to be equal to the energy absorption in the panel.

$$\Delta E = \frac{1}{2} m(v_s^2 - v_r^2) \tag{6.3}$$

where, ΔE is the kinetic energy dissipation of the projectile, m is the mass of the projectile, v_s and v_r is the striking velocity and residual velocity respectively. To compare the energy absorption capacity of different panels, the normalized energy absorption (SEA) was used to remove the effect of the areal density. This reflects the energy absorption capacity of the panel at unit areal density.

$$SEA = \frac{EA}{Ar} \tag{6.4}$$

where, *SEA* is the specific energy absorption, *EA* is the energy absorption of panel, *Ar* is the areal density of the panel. In this research, all the ballistic performance evaluations were based on same areal density of the panel. Therefore, all the energy absorption results can be treated as specific energy absorption results.

6.3.3 Ballistic properties of fabric targets

Ballistic perforation tests of different fabric targets results were listed in Appendix. Perforation tests aim to reflect the energy absorption (EA) performance of two layers of untreated Twaron® fabric targets, single layer of 12nm-30% STF impregnated Twaron® fabric targets and single layer of 650nm-30% STF impregnated Twaron® fabric targets with the same areal density. The ballistic performance of the fabric is evaluated by the energy loss of the projectile which equals to fabric energy absorption. Five specimens were used to obtain an average value. The testing data can be found in Appendix. The calculated absorbed energy values of fabric targets have been drawn in Figure 6.6 and standard deviations are shown in the form of error bars.

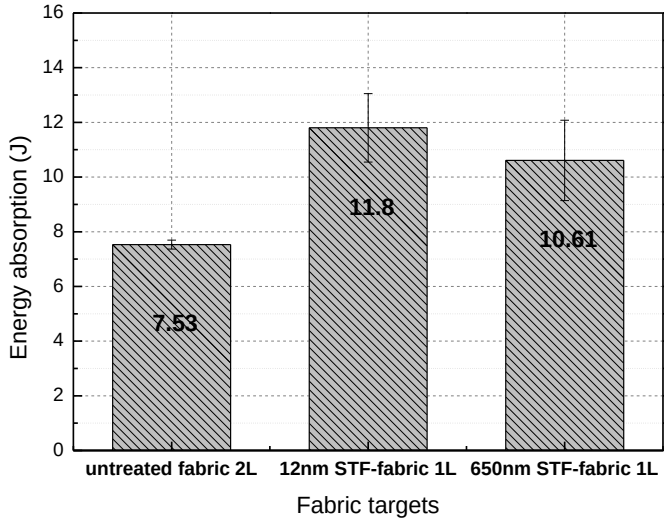

Figure 6.6 Energy absorption of untreated fabric targets and STF impregnated fabric targets at the ballistic tests

Figure 6.6 indicates that STF impregnated Twaron® fabric targets exhibit higher energy absorption capacity than that of untreated Twaron® fabric targets regardless STF particle sizes at highest particle concentration of 30%. The 12nm-30% STF impregnated Twaron® fabric targets showed 56.7% increase of the specific ballistic energy absorption capacity than that of untreated Twaron® fabric targets, and 650nm-30% STF impregnated Twaron® fabric targets demonstrated 40.9% increase of energy absorption capacity than that of untreated Twaron® fabric targets. It demonstrates that STF impregnation can achieve an enhancement in the fabric ballistic performance. Unlike the stabbing impact testing results that larger particle size 650nm STF displayed superior stabbing resistant performance than that of smaller particle size 12nm STF impregnated fabric targets with the same areal density, larger particle size 650nm STF showed inferior ballistic performance than that of smaller particle size 650nm STF impregnated fabric targets with the same areal density. Consequently, the perforation ballistic testing results are contradictory with the stabbing impact testing results on STF particle sizes associated with the impact performance. Whether this conclusion would be in consistent with the non-perforation ballistic testing results will be further studied in following non-perforation test investigations. The mechanisms of STF rheological properties related to ballistic performance will be analysed and discussed.

6.3.4 STF-fabric ballistic properties associated with STF behaviour

To couple the rheological properties of STFs and ballistic results, we need to estimate the shear rates encountered in the STF during the ballistic process. A characteristic shear rate can be estimated by normalizing the impact velocity 500 m/s and the projectile diameter 5mm, provides a lower bound shear rate of 1×10^5 according to the Equation (4.1). An upper bound shear rate could be defined based on the gap at the junction between crossed yarns, since yarn uncramping and pull-out are expected to occur during the ballistic impact process Although it is difficult to estimate the size of this vanishingly small gap, using an estimate of 30μm (the approximate filament

diameter) results in an upper bound shear rate of 1.7 $\times 10^7 s^{-1}$. These shear rates, if accurate, are well above the shear thickening transition points observed in the rheological behaviour of the STFs.

6.3.5 Impact process photographic observations

Some ballistic responses of armour panels under impact can be directly observed by a high speed camera. It records the impact process during ballistic impact. From the photographic observations, many ballistic characteristics of panels were revealed, such as the configuration of fabric transverse deformation at different times, the strain evolution on yarns, and the impact angle and trajectory of the projectile. This provides the physical evidence for the theoretical analysis. In this study, the impact process of penetration impact tests on fabric panels was recorded by the high speed camera Photron FASTCAM SA1. The high speed camera (Photron FASTCAM SA1) used in this study has frame rates from up to 675,000 per second (fps). At the least time interval, each frame can be taken every 5.5μs with the resolution 512 × 128 pixels. PFV (Photron FASTCAM SA1) software was used to control the camera from the computer, including setting camera options, shooting, and saving recorded data to the computer.

A clue regarding the mechanism for ballistic energy absorption comes from the high-speed video images of the fabric targets during impact. The comparison of high-speed images of a two layered of untreated Twaron® fabric and a single layer of 12nm-30% STF impregnated Twaron® fabric at the moment of ballistic impact have shown in Figure. It is clearly showed that impregnation with STF had significant effects on yarn pull-out behaviour at the ballistic impact occasion.

The high-speed images of untreated Twaron® fabric specimen show yarn pull-out on the bullet impact point at 2×10^{-5}s and yarn failure at 3×10^{-5}s on the impact point. In contrast, yarn pull-out was hardly observed in STF impregnated Twaron® fabric

specimen and yarn failure initiated at 3×10^5 in fragment form as indicated in the Figure. Deformation of untreated Twaron® specimens exhibited a domelike shape due to yarn pull-out and ravelling of yarns on the impact area, while STF impregnated Twaron® fabric specimens showed perforation hole straight away when a bullet penetrated through the fabric specimens. It is postulated that the shear thickening of STF was initiated at the early stage of ballistic impact and that the induced inter-yarn friction encouraged the neighbouring yarns to defend the projectile penetration. Consequently, more of the total fabrics were involved in energy dissipation, especially via inter-yarn friction and yarn breakage.

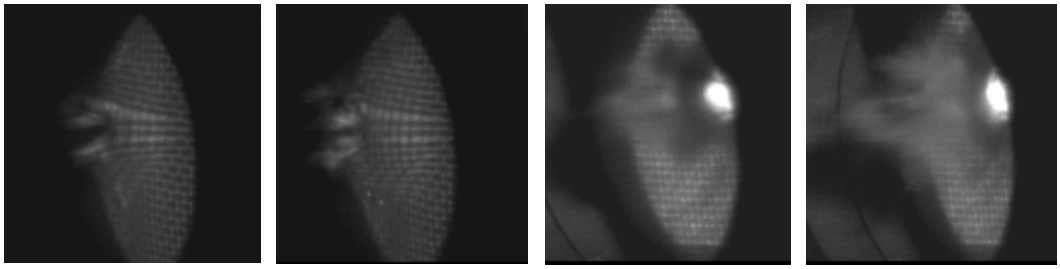

(a) $t = 2 \times 10^{-5}$s (b) $t = 3 \times 10^5$s (c) $t = 2 \times 10^{-5}$s (d) $t = 3 \times 10^5$s

(a) and (b) Untreated fabric targets; **(c) and (d)** STF impregnated fabric targets

Figure 6.7 High Ballistic impact process of fabric target

As can been seen in the Figure 6.7, untreated Twaron® fabric deforms larger than that of STF impregnated Twaron® fabric specimen and STF impregnated Twaron® fabric had more fractured yarns. STF impregnated Twaron® fabric performed like a composite due to the hardening effects as the primary yarns take the direct force and fail at the early stage of the impact. Primary yarns/fibres provide the force to resist the penetration of the projectile into the target. The strain is higher in these yarns/fibres compared with the strain in secondary yarns. These yarns fail under tension when the strain of these yarns exceeds the ultimate strain in tension at high strain rate. The tension in these yarns/fibres results in absorption of some energy. This composite-like may due to the shear thickening effect of STF which leading to hardening effect for the STF impregnated fabric targets. As for yarn/fibre failure would take place easier at the location of higher stress/strain concentration under the shear thickening effect. Although there were not much primary yarns fracture for the untreated Twaron®

fabric specimens as STF impregnated Twaron® fabric targets do, the secondary yarns of untreated Twaron® fabric targets deformed and could absorb some energy. The energy absorbed by secondary yarns depends on the strain distribution within the secondary yarns. So it can be postulated that STF impregnated Twaron® fabric targets lead to less BFS for non-perforation ballistic tests.

According to the images, at high velocity impact the ballistic resistance of STF impregnated Twaron® fabric targets were determined mainly by its ability to transform the kinetic energy of the bullet into energy for yarn breakage. Moreover, the STF in the fabrics undergoes a transition from liquid to solid-like during the impact.

6.3.6 Post-impact panels observations

To investigate failure modes of fabric layer after the ballistic impact and analyse failure mechanisms of fabric targets, the post-impact fabric targets were observed after ballistic tests, including untreated Twaron® fabric target and STF impregnated Twaron® fabric target. The mechanism of the energy absorption of the fabric panel can be investigated by visually damage area inspection. The global failure characteristics of post-impact panels were observed from the Figure 6.8.

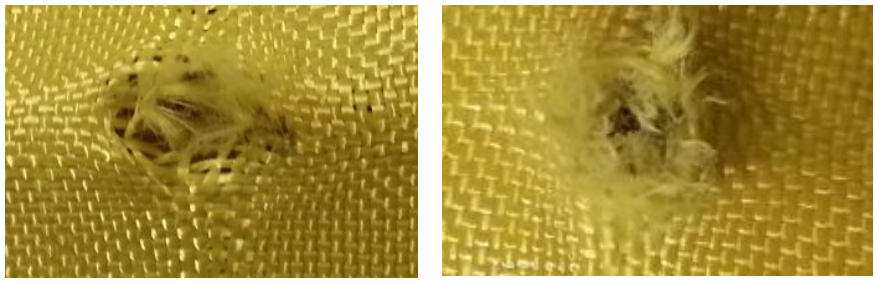

(a) Untreated Twaron® fabric (b) STF-Twaron® fabric

Figure 6.8 Fabric damage fabric targets after ballistic tests

Figure 6.8 shows the damaged area of untreated Twaron® double layered fabric and STF-Twaron® single layer fabric after bullet impact testing. Yarns which were directly impacted by the projectile in untreated Twaron® fabrics pulled out significantly from damage area, with yarn raveling there and formed a cross-patterned yarn pull-out

area. Only the primary yarns, which are engaged by the bullet participate the energy absorption. On the other hand, evidence of yarn pull-out was hardly observed in the area of fabric treated with STF. This can be explained by the fact that the impregnated STF serves as an additional constraint between yarns, resulting in less transverse deformation. Note that the fabric impregnated with STF occurred significant fibre breakage near the projectile impact area and the yarn failure at the damaged area of STF-Twaron® produced the formation of petal-like fibre extrusion and has more failure of the primary and secondary yarns in the impact zone. In addition, STF-Twaron® fabric target exhibited extensive fibre breakage near the projectile contact area and only very little yarn pull-out. Hence, unlike in untreated Twaron® fabrics, the entire STF-fabric rather than only primary yarns participates in energy absorption.

It should be noted that the yarns directly below the projectile are referred to as primary yarns. These yarns provide the resistive force to the projectile penetration into the target. The remaining yarns within the conical region are referred to as secondary yarns. These yarns deform and cause some energy absorption.

The yarns in the untreated Twaron® fabric did not show much damage while STF-fabric showed intensive yarn breakage. As a result of that, the improved impact resistant performance in STF-Twaron® fabrics can be attributed to yarn fracture.

6.4 Ballistic non-penetration tests

The non-penetration test for armour performance evaluation is based on the measurement of the back face signature depression produced on the backing clay. 24 layers of untreated Twaron® fabric targets, 12 layers of 12nm-30% STF impregnated Twaron® fabric targets and 12 layers of 650nm-30% STF impregnated Twaron® fabric targets trimmed with the size of 24cm by 24cm. In most cases, the fabric panels are not fully perforated, and the ballistic performance of the fabric panels is assessed by the number of fabric layers fractured and the depth of the back face signature. The

shape and volume of the back signature can be taken to study and residual energy carried by the projectile when it is checked. The average bullet impact velocity is 488m/s for the non-penetration tests.

6.4.1 Back face Signature (BFS)

BFS is one of the most important criteria to evaluate the ballistic performance of non-perforated panels. It is the perpendicular distance from the reference plane of the clay surface to the deepest point of the indentation. After ballistic tests, an indentation was produced in the clay behind armour panels. In this study, BFS can be directly measured by a Vernier calliper and the BFS of fabric panel after the ballistic impact have shown in Figure 6.9. The reference plane is the original surface of the clay.

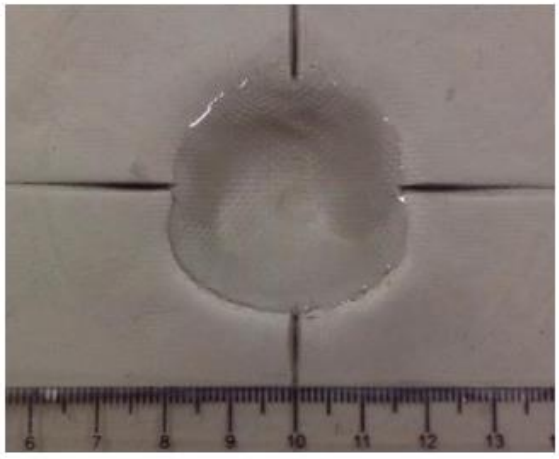

Figure 6.9 Back face signature on Roma Plastilina® No.1 backing clay

It this study, BFS was used as a complementary criterion to reflect the difference of energy absorption capacity between different non-perforated fabric panels. Smaller BFS reflects better ballistic resistant capacities of the non-perforated panel. To remove the effect of areal density between different panels, all the fabric panels are kept with the same areal density for non-penetration tests.

6.4.2 Quantification of the indentation in the clay

In the non-perforation case, the fabric targets are placed directly on the backing clay

and a projectile was stopped in a panel. Some transmitted kinetic energy of the projectile can produce an indentation in the clay behind the panel, and the clay does not spring back after impact, so it can memorize the shape of a dent. The width and depth of the BFS, together with the number of perforated layers were obtained to reflect ballistic resistance performance of fabric panels as shown in Table 6.1. Three types of fabric targets are compared and the final performance evaluation of BFS results were determined by three repeat ballistic tests on fabric targets in order to obtain average back face signature results.

Table 6.1 BFS measurement results of fabric panels

Fabric panels	Dent width	Dent depth	Number of perforated layers
24L untreated Twaron® fabrics	4.078cm	1.264cm	23
12L 30% 650nm STF-Twaron® fabrics	4.878cm	0.964cm	10
12L 30% 12nm STF-Twaron® fabrics	4.844cm	0.742cm	9

The table 6.1 shows the indent width and indent depth of the witness clay deformation for fabric systems with different fabric panel configurations. Generally, the STF treated Twaron® fabric panels showed significantly less indent depth than those of the untreated Twaron® fabrics. Also, STF-Twaron® fabric panels impregnated with smaller particle size produced STF exhibit shallower indent depth and wider indent width as compared to STF-Twaron® fabric panels impregnated with larger particle size produced STF. As the BFS of the non-penetration panel was mainly determined by the impact energy and energy absorption in the panel, lower BFS leads to higher energy absorption in the fabric panel with the same impact energy.

In terms of specific areal density and back face signature, Twaron® fabrics impregnated with 650nm particle size STF at 30% concentration exhibited 23.7% less indent depth than that of untreated Twaron® fabrics, while Twaron® fabrics impregnated with smaller nanoparticle size 12nm at 30% particle concentration could

achieve better ballistic performance that 41.3% less indent depth than untreated Twaron® fabrics had been observed. Both of the STF impregnated Twaron® fabric panels presented 19.6% wider indent width than that of untreated Twaron® fabric panels which means larger the stress distribution area participated the energy absorption when subjected the ballistic impact.

The residual deformation in the backing clay showed that STF impregnated Twaron® fabrics displayed significantly less indent depth than the untreated Twaron® fabrics. The results of Twaron® fabrics clearly demonstrated that impregnation with STF enhanced the ballistic performance of the fabric in terms of back face signature. More precisely, Twaron® fabrics treated with STF containing smaller silica nanoparticles decreased the transverse deformation and the size of the indented area of craters.

The number of the perforated fabric layers was used as validation criteria of ballistic performance. By adding STF into the Twaron® fabrics, the number of perforated fabric layers out of the total fabric panel layers is decreased.

The results indicated that the presence of STF in the Twaron® fabric panels result in significant influence on minimizing BFS.

6.5 Discussions on STF particle size associated with ballistic performance

Through the tests conducted in this section, it is concluded that the impregnation of Twaron® fabrics with STF containing 12nm silica particles enhanced the ballistic performance of those fabrics over that of untreated Twaron® fabrics, and in most cases also over that of Twaron® fabrics impregnated with larger silica nanoparticles 650nm, in terms of impact energy absorption under penetration tests and resistance to blunt trauma under non-perforation tests. This is maybe because the impregnation of STF containing 12nm silica particles resulted in higher inter-yarn friction that contributes to increased yarn pull-out energy during a ballistic event. Higher inter-yarn friction

enabled fabrics to dissipate more kinetic energy via greater yarn interaction. However, excessive inter-yarn friction would cause stress concentration in primary yarns contacting the projectile.

Additionally, the impregnation of STF increased the inter-yarn friction contributing to increasing the constraint of the yarns. This leads to rapid failure at the impact point and lower energy absorption. Thus, a large amount of constraint on the individual yarn induced by larger nanoparticle size 650nm STF because of its higher increase on shear thickening viscosity yielded high localized stresses at the impact zone, which could lead to earlier failure of yarns in the impact zone. Or perhaps due to STF producing with 12nm silica particles has a higher critical shear rate which is closer to the shear rate of the ballistic event.

Although this dramatic increment of frictional energy caused by STF impregnation made the fabrics stiff and could lead to earlier failure of the primary yarns, it is indicated that with appropriate STFs composition the impregnation of STF containing smaller silica particle 12nm contributed significantly to a larger transfer of the impact energy to interaction of individual yarns in the fabric, which resulted in much higher energy dissipation and less transverse deformation.

6.6 Summary

The penetration and non-penetration ballistic tests results have clearly shown that the STF addition provides an enhancement to the ballistic properties of Twaron® fabric. Prevention of yarn separation and yarn pull-out thanks to STF impregnation increases the ballistic performance due to changing the penetration mechanism.

Chapter 7

Conclusions and Future Work

7.1 Conclusions

This thesis has presented advancement in the development of STF enhanced soft ballistic body armour to achieve improved stabbing resistance with less fabrication material cost while without hindering flexibility of the fabrics. In order to accomplish efficient utilisation of STF for a particular new design of smart textiles equipped with both superior stabbing resistance and ballistic performance, the research routes of this project have been to (1) preparation and parametrical control of rheological properties of STF; (2) experimental investigation on use of STF to improve stabbing resistance of soft ballistic body armour; (3) mechanisms analysis of STF impregnation associated with fabric stabbing properties; (4) systematically study of STF impregnation effects on soft ballistic body armour ballistic performance. The methodology adopted for this research is based on interdisciplinary analytical methodologies predominantly derived from physics and chemistry to provide theoretical background and assist the mechanism analysis.

In the light of the work carried out in this thesis, a number of original contributions and achievements have been drawn. These are summarised below.

1. Realisation of parametrical control over rheological properties of STFs made from SiO_2 and polyethylene glycol

This research has indicated that shear thickening transition occur and the magnitude of the viscosity increase can be controlled by changing the particle size, particle concentrations and dispersed medium viscosity. All the results suggest that if all other parameters of the STFs production are held constant, the critical shear rate is independent of each production parameter.

a) For different particle sizes chosen to produce STF, larger particle size leads to lower critical shear rates and the thickening effect is more obvious at the critical shear rate for STF with larger particles. The absolute viscosities of STFs increase when the particle size changes from small to large. Additionally, the critical shear rate is much more sensitive for STF with smaller particle sizes.

b) For different dispersion concentrations chosen to produce STF, the critical shear rates appear at lower shear rates as the particle concentrations increase and greater change in viscosity at the critical shear rate for STF with larger particle concentrations. The absolute viscosities of STFs increase remarkably with the increase of the particle concentrations. It should be noted that a certain minimum level of particle concentration is required to create the shear thickening behaviour and 33% is the maximum concentration for 12nm silica nanoparticles can be achieved to produce STFs. Moreover, at the maximum weight fraction 33%, the initial viscosity is even higher than the post-thickening viscosity. The relationship between particle concentrations and CSR is almost linear from 15% to 30%, while the decrease in critical shear rate becomes less obvious when the particle concentration is increased from 30% to the maximum 33%.

c) For different dispersing medium chosen to produce STF, shear thickening behaviour occur at the lower shear rates for STF with the higher molecular weight of

PEG dispersing medium, and shear thickening phenomenon happens more sharply with the higher molecular weight of PEG. The absolute viscosities of STFs systematically increase with the increasing molecular weight of PEG. Furthermore, PEG with lower molecular weight causes the critical shear rate to change more effectively.

In summary, the success of this tailoring method can produce lower CSR of STFs and amplified severity shear thickening viscosity of STFs by using larger particle size, higher particle concentrations, and higher PEG molecular weight of dispersing medium. Meanwhile, the too large particle size will make it hard to be embedded into other materials, too high particle concentration will cause really high initial viscosity, and too high molecular weight of PEG can cause the problem of producing STFs.

The findings open up possibilities for new designs of smart colloidal suspensions that could combine shear thickening with control of production parameters, thus producing specific STFs for different applications, and certainly widening the potential impact resistance applications of STFs.

2. Fulfilment of enhanced stabbing resistance through STF impregnation

From the investigations on influences of STF rheological properties on stabbing impact resistance of STF impregnated Twaron® fabrics by using two different silica nanoparticle sizes with three different particle weight fractions, it can be concluded that STF rheological properties do affect the stabbing protection performance of STF impregnated Twaron® fabrics and the performance can be correlated to the whole shear thickening phenomena.

a) In order to fulfil efficient utilisation of STF to attain optimal impact resistance, full impregnation process of the STF-fabric composite was optimised in this research. Accordingly, the addition of STF was shown to cause little or no increase in the

thickness or stiffness of the fabric. Moreover, the gravity will not induce the dripping effect to the fully impregnated STF-fabric composite.

b) To couple the rheological properties of STFs and STF treated Twaron® fabric targets stabbing impact resistant testing results, it can be confirmed that greater increased shear thickening viscosity of STFs result in higher stabbing resistant performance in STF impregnated Twaron® fabrics.

c) The work revealed that the STF impregnation provides substantial stabbing load resistance and energy absorption enhancement in terms of areal density, volume and fabrication material cost. Thinner shielding configurations with equivalent or higher stabbing resistant performance were found to be possible through STF impregnation as the 12 layer STF impregnated Twaron® fabrics configuration showed 100% higher energy absorption as the 24 layer untreated Twaron® fabrics while the energy absorption normalised for same areal density. In addition, STF impregnated Twaron® fabrics provides an approximately 300% enhanced specific energy absorption performance over untreated Twaron® fabrics with the same number of layers.

d) It is clear that STF impregnation offers a volume advantage as less number of fabric layers if necessary to give equal or greater absorption performances. The decreased number of Twaron® layers leads directly to a decrease in overall target thickness and an increase in flexibility.

e) The employment of STF in the panels also significantly reduced the back-face deformation caused by the knife impact.

The work in this research has determined that fully impregnated panels with STFs having larger nanoparticle size and higher weight fraction resulted in better stab resistant performance in terms of maximum load and total energy absorption. These findings indicate the feasibility of achieving more protective stabbing panels with

lower weight and less bulkiness when STF impregnated panels are used against stabbing impact.

3. Development of lightweight armour panels for knife and ballistic protection

STF impregnated Twaron® fabric targets are observed to have superior ballistic resistance as compared to the untreated Twaron® fabric targets. However, STF produced with smaller nanoparticle size impregnated fabric targets demonstrate better energy absorption capability than that of STF synthesised with larger nanoparticle size impregnated fabric targets. This conclusion is contrary to the stabbing performance on STF particle sizes, whereas the improved stabbing resistance is the major concern in this research. As a result of that, 30%-650nm STF fully impregnated Twaron® fabrics are the prime combination of conventional soft ballistic body armour with STF to achieve both knife and ballistic protection.

This research has opened up a new opportunity for designing soft ballistic body armour with improved protection and reduced panel weight, while without hindering the flexibility of the panel. This approach could be used to achieve better stabbing and ballistic protection in soft body armours.

7.2 Further work

The aim of this research was to establish an approach to improve the stabbing resistance of soft ballistic body armour. It has been shown that the combination of STF and soft ballistic body armour created new opportunities to improve the stabbing and ballistic impact resistance. Based on the achievements made through this research, the following future work for further refinement and improvement are recommended.

1) The main factors influencing the rheological properties of SiO_2/PEG system were studied and the shear thickening mechanism was analysed. Although it is the synergistic effect of various factors to have the impact rather than single factor does, in fact, there is still a need to understand which characteristic of the fluid rheology is necessary to obtain the desired response.

2) SiO_2 and PEG is not the only formula to produce STF, so other recipe possibilities should be explored. To find the possibility to increase the range of critical shear rate and the amplitude of shear thickening viscosity, in addition, the weight of the STF may be reduced.

3) The work that has been done in this research suggests that application of STF systems on textiles leads to improvement in impact resistance behaviour. However, further fundamental understanding still needs to be established through systemic investigation on determining which rheological parameters are most critical to achieving enhanced protection properties.

4) STF has been proved to have a significant improvement on impact resistance performance and has been used in protective applications. It is believed that this improvement is related to the resistance of STF to deformation at high strain rates. Nevertheless, the precise role of STF and its rheological properties in the impact process are not known. Numerical simulation can obtain additional mechanism information through computer modelling. The behaviour of STF can be expressed using the Bingham fluid model which STF has the characteristics of where a characteristic stress or yield stress below which the material behaves like a solid is incorporated. The nonlinear explicit finite element analysis is used to simulate the response of STF impregnated fabric subjected to the impact. The computational analysis can contribute to a better understanding of the mechanism involved in the impact and the perforation process of the modelled STF impregnated fabrics.

References

1. Srivastava, A., Majumdar, A., and Butola, B., *Improving the impact resistance of textile structures by using shear thickening fluids: a review.* Critical Reviews In Solid State And Materials Sciences, 2012. **37**(2): p. 115-129.
2. Hasanzadeh, M. and Mottaghitalab, V., *The role of shear-thickening fluids (STFs) in ballistic and stab-resistance improvement of flexible armor.* Journal Of Materials Engineering And Performance, 2014. **23**(4): p. 1182-1196.
3. Ding, J., Tracey, PJ., Peng, Li, W., , Whitten, G., , Wallace, PG., *Review on shear thickening fluids and applications.* Textiles and light industrial science and technology, Volume 2 Issue 4, 2013: pp. 161-170.
4. Briscoe, B.J. and Motamedi, F., *The Ballistic Impact Characters of Aramid Fabrics: The Influence of Interface Friction.* Text Res J, 1992. **158**: p. 229-247.
5. Hoffman, R.L., *Explanations for the cause of shear thickening in concentrated colloidal suspensions.* Journal of Rheology (1978-present), 1998. **42**(1): p. 111-123.
6. Hearle, J.W., *High-performance fibres*. 2001, Woodhead Publishing Limited, Cambridge, England : pp. 49.
7. Cheeseman, B.A. and Bogetti, T.A., *Ballistic impact into fabric and compliant composite laminates.* Composite structures, 2003. **61**(1): p. 161-173.
8. Horsfall, I., *Stab Resistant Body Armour.* PhD thesis, Cranfield Defence and Security, Shrivenham, Mar 2000 : pp. 51-52.
9. Chadwick, E., Nicol, A.C., Lane, J.V., Gray, T.G., *Biomechanics of knife stab attacks.* Forensic Science International, 1999. **105**(1): pp. 35-44.
10. Zhou, Y., Chen, X., and Wells, G., *Influence of yarn gripping on the ballistic performance of woven fabrics from ultra-high molecular weight polyethylene fibre.* Composites Part B: Engineering, 2014. **62**: p. 198-204.
11. Gadow, R. and Niessen, K.v., *Lightweight ballistic structures made of ceramic and cermet/aramide composites.* Ceramic Armor and Armor Systems, Volume 151, 2003: p. 1-18.
12. Egres Jr, R., Halbach, CJ., Decker, MJ., Wetzel, ED., Wagner, NJ., *Stab performance of shear thickening fluid (STF)–fabric composites for body armor applications.* development, Proceedings to SAMPE 2005: New horizons for materials and processing technologies, Long Beach, CA. 2005.
13. Chiou, M. *Development of protective body armour for puncture, stab and multi-threat protection*. in *Proc Sharp Weapons Armour Technology Symposium*. 1999.
14. Tan, V., Tay, T., and Teo, W., *Strengthening fabric armour with silica colloidal suspensions.* International journal of solids and structures, 2005. **42**(5): p. 1561-1576.
15. Barnes, H., *Shear-thickening ("Dilatancy") in suspensions of nonaggregating solid particles dispersed in Newtonian liquids.* Journal of Rheology (1978-

present), 1989. **33**(2): p. 329-366.
16. Maranzano, B.J. and Wagner, N.J., *The effects of interparticle interactions and particle size on reversible shear thickening: Hard-sphere colloidal dispersions.* Journal of Rheology (1978-present), 2001. **45**(5): p. 1205-1222.
17. Lee, Y.S. and Wagner, N.J., *Dynamic properties of shear thickening colloidal suspensions.* Rheologica Acta, 2003. **42**(3): p. 199-208.
18. Wagner, N.J. and Wetzel, E.D., *Advanced body armor utilizing shear thickening fluids*. United States patent US 7,498,276. 2009 Mar 3.
19. d'Haene, P., Mewis, J., and Fuller, G., *Scattering dichroism measurements of flow-induced structure of a shear thickening suspension.* Journal of colloid and interface science, 1993. **156**(2): p. 350-358.
20. Brown, E. and Jaeger, H.M., *The role of dilation and confining stresses in shear thickening of dense suspensions.* Journal of Rheology (1978-present), 2012. **56**(4): p. 875-923.
21. Hoffman, R., *Discontinuous and dilatant viscosity behavior in concentrated suspensions. II. Theory and experimental tests.* Journal of colloid and interface science, 1974. **46**(3): p. 491-506.
22. Xu, Y.l., Gong, XL., Peng, C., Sun, YQ., Jiang, WQ., Zhang, Z., *Shear thickening fluids based on additives with different concentrations and molecular chain lengths.* Chinese Journal of Chemical Physics, 2010. **23**(3): p. 342-346.
23. Maranzano, B.J. and Wagner, N.J., *The effects of particle size on reversible shear thickening of concentrated colloidal dispersions.* The Journal of chemical physics, 2001. **114**(23): p. 10514-10527.
24. Lee, B.W., Kim, I.J. and Kim*, C.G. , *The Influence of the Particle Size of Silica on the Ballistic Performance of Fabrics Impregnated with Silica Colloidal Suspension.* Journal of Composite Materials, 2009. **43**: p. 2679-2698.
25. Mahfuz, H., Clements, F, Rangari, V., Dhanak, V., Beamson, G., *Enhanced stab resistance of armor composites with functionalized silica nanoparticles.* Journal of Applied Physics, 2009. **105**(6): p. 064307.
26. Wang, Y., Li, S.K., and Feng, X.Y.., *The Ballistic Performance of Multi-Layer Kevlar Fabrics Impregnated with Shear Thickening Fluids*. in *Applied Mechanics and Materials*. 2015. Trans Tech Publ.
27. Majumdar, A., Butola, B.S., and Srivastava, A., *An analysis of deformation and energy absorption modes of shear thickening fluid treated Kevlar fabrics as soft body armour materials.* Materials & Design, 2013. **51**: p. 148-153.
28. Park, Y., Kim, Y., Baluch, AH., Kim, CG., *Empirical study of the high velocity impact energy absorption characteristics of shear thickening fluid (STF) impregnated Kevlar fabric.* International Journal of Impact Engineering, 2014. **72**: p. 67-74.
29. Park, J.L., Yoon, BI., Paik, JG., Kang, TJ., *Ballistic performance of p-aramid fabrics impregnated with shear thickening fluid; part I–effect of laminating sequence.* Textile Research Journal, 2011: p. 0040517511420753.

30. Cavallaro, P.V., *Soft body armor: an overview of materials, manufacturing, testing, and ballistic impact dynamics*, 2011, DTIC Document.
31. Parker, G., *PSDB stab resistant body armour test procedure*. 1993: Home Office, Police Scientific Development Branch.
32. *http://www.hellotrade.com/high-speed-and-carbide/hosdb-psdb-stab-test-knives-and-spikes.html*. [cited 10th, Nov 2016.].
33. Murray, L. and Green, M., *Hilts and knives: a survey of ten years of fatal stabbings.* Medicine, Science and the Law, 1987. **27**(3): p. 182-184.
34. Brown, B., *Assaults on police officers: an examination of the circumstances in which such incidents occur*. 1994: Citeseer.
35. Green, M., *Stab wound dynamics—a recording technique for use in medico-legal investigations.* Journal of the Forensic Science Society, 1978. **18**(3): p. 161-163.
36. Rouse, D., *Patterns of stab wounds: a six year study.* Medicine, Science and the Law, 1994. **34**(1): p. 67-71.
37. Fligelstone, L., Johnson, RC., Wheeler, MH., Salaman, JR., *An audit of stab wounds in Cardiff.* Journal of the Royal College of Surgeons of Edinburgh, 1995. **40**(3): p. 167-170.
38. Miller, S. and Jones, M., *Kinematics of four methods of stabbing: a preliminary study.* Forensic Science International, 1996. **82**(2): p. 183-190.
39. Horsfall, I., Watson, C., Champion, S., Prosser, P., Ringrose, T., *The effect of knife handle shape on stabbing performance.* Applied Ergonomics, 2005. **36**(4): p. 505-511.
40. Termonia, Y., *Puncture resistance of fibrous structures.* International Journal Of Impact Engineering, 2006. **32**(9): p. 1512-1520.
41. Shin, H.S., Erlich, DC., Simons, JW., Shockey, DA., *Cut resistance of high-strength yarns.* Textile Research Journal, 2006. **76**(8): p. 607-613.
42. Grujicic, M., Glomski, PS., He, T., Arakere, G., Bell, WC., Cheeseman, BA., *Material modeling and ballistic-resistance analysis of armor-grade composites reinforced with high-performance fibers.* Journal of materials engineering and performance, 2009. **18**(9): p. 1169-1182.
43. Dudde, F.P., Feldhusen PP, Abdelsadek GG, Parker AM, Xu J, Allen SD, Palazzola M, inventors; Dudde Frank P, Feldhusen Peter P, Abdelsadek Gomaa G, Parker Alan M, assignee, *Elevator suspension and transmission strip*, 2011, Google Patents.
44. Shin, H.-S., D. Erlich, and D. Shockey, *Test for measuring cut resistance of yarns.* Journal of materials science, 2003. **38**(17): p. 3603-3610.
45. Mayo, J.B., Feldhusen, PP., Abdelsadek, GG., Parker, AM., Xu, J., Allen, SD., Palazzola, M., inventors; Dudde Frank, P., Feldhusen Peter, P., Abdelsadek Gomaa, G., Parker Alan, M., *Stab and puncture characterization of thermoplastic-impregnated aramid fabrics.* International Journal of Impact Engineering, 2009. **36**(9): p. 1095-1105.
46. Kirkwood, K.M., Kirkwood, JE., Lee, YS., Egres, RG., Wagner, NJ., Wetzel, ED., *Yarn pull-out as a mechanism for dissipating ballistic impact energy in*

Kevlar® KM-2 fabric part I: quasi-static characterization of yarn pull-out. Textile Research Journal, 2004. **74**(10): p. 920-928.
47. Kirkwood, J.E., Kirkwood, KM., Lee, YS., Egres, RG., Wagner, NJ., Wetzel, ED., *Yarn pull-out as a mechanism for dissipating ballistic impact energy in Kevlar® KM-2 fabric part II: predicting ballistic performance.* Textile Research Journal, 2004. **74**(11): p. 939-948.
48. Dischler, L., Moyer, T.T., and Henson, J.B., *Dilatant powder coated fabric and containment articles formed therefrom*, 1998, Google Patents.
49. Baucom, J. and Zikry, M., *Evolution of failure mechanisms in 2D and 3D woven composite systems under quasi-static perforation.* Journal of composite materials, 2003. **37**(18): p. 1651-1674.
50. Sun, B., Wang, Y., Wang, P., Hu, H., Gu, B., *Investigations of puncture behaviors of woven fabrics from finite element analyses and experimental tests.* Textile Research Journal, 2011. **81**(10): p. 992-1007.
51. Watson, C., Horsfall, I., and Robertson, A., *Stacking Sequence Effects in Multi-Purpose Body Armour*. in *Proceedings Sharp Weapons Armour Technology Symposium, Cranfield University, UK*. 1999.
52. Wang, P., Sun, B., and Gu, B., *Comparison of stab behaviors of uncoated and coated woven fabrics from experimental and finite element analyses.* Textile Research Journal, 2012: p. 0040517511418560.
53. *Stab Resistance of Personal Body Armour.* National Institute of Justice Standard-0115.00, 2000.
54. Croft, J. and Longhurst, D., *HOSDB Body Armour Standards for UK Police (2007) Part 3: Knife and Spike Resistance.* St Albans: Home Office Scientific Development Branch, 2007.
55. Croft, J. and Longhurst, D., *HOSDB Body Armour Standards for UK Police (2007) Part 2: Ballistic Resistance.* C) Crown Copyright, 2007.
56. Horsfall, I., Prosser, PD., Watson, CH., Champion, SM., *An assessment of human performance in stabbing.* Forensic Science International, 1999. **102**(2): p. 79-89.
57. Pettit, M. and Croft, J., *PSDB Stab resistance standard for body armour (1999).* Police Scientific Development Branch, Publication, 1999(6/99).
58. Brooker, D.C., *Numerical modelling of pipeline puncture under excavator loading. Part I. Development and validation of a finite element material failure model for puncture simulation.* International Journal Of Pressure Vessels And Piping, 2003. **80**(10): p. 715-725.
59. Brooker, D.C., *Numerical modelling of pipeline puncture under excavator loading. Part II: parametric study.* International Journal Of Pressure Vessels And Piping, 2003. **80**(10): p. 727-735.
60. Ursenbach, D.O., *Penetration of CFRP Laminates by Cyclindrical Indenters*, 1995, the University of British Columbia.
61. Cantwell, W.J. and Morton, J., *Comparison of The Low And High Velocity Impact Response of CFRP.* Composite, 1989. **20**(6): p. 545-551.
62. Cantwell, W.J. and Morton, J., *Impact Perforation of Carbon Fibre Reinforced*

Plastic. Composite, 1990. **38**(2): p. 119-141.
63. Carr, D.J., *Failure Mechanisms of Yarns Subjected to Ballistic Impact.* Mater Sci J, 1995. **18**: p. 585-588.
64. Roylance, D., Wilde, A and Tocci, G., *Ballistic Impact of Textile Structures.* Textile Research Journal, 1973. **43**: p. 34-41.
65. Roylance, D., *Stress Wave Propagation In Fibres: Effect of Crossoves.* Fibre science and technology 1980. **13**: p. 385-395.
66. Carr, D., *Failure mechanisms of yarns subjected to ballistic impact.* Journal of materials science letters, 1999. **18**(7): p. 585-588.
67. Cunniff, P.M., *An analysis of the system effects in woven fabrics under ballistic impact.* Textile Research Journal, 1992. **62**(9): p. 495-509.
68. Gu, B., *Analytical Modeling for The Ballistic Perforation of Planar Plain-Woven Fabric Target by Projectile.* Compos Pt B, 2003. **34**: p. 361-371.
69. Cheeseman, B.A. and Boggeti, T.A., *Ballistic Impact Into Fabric and Compliant Composite Laminates.* Composite Structure, 2003. **61**: p. 161-173.
70. Tabiei, A., *Ballistic Impact of Dry Woven Fabric Composites: A Review.* Applied Mechinics, 2008. **61**.
71. Shahkarami, A., Cepus, E., Vaziri, R. and Poursartip, A., *Material Responses To Ballistic Impact*, in *Lightweight Ballistic Composite*, A. Bhatnagar, Editor. 2006, Woodhead Publishing Limited and CRC Press LLC: Cambridge. p. 82-95.
72. Prosser, R.A., Cohen, S.H. and Segars, R.A., *Heat as A Factor in the Penetration of Cloth Ballistic Panels by 0.22 Caliber Projectiles.* Textile Research Journal, 2000. **70**(8): p. 709-722
73. Roylance, D., *Influencee of Fibre Propeerties On Ballistic Penetration of Textile Panels* Fibre science and technology, 1981. **14**: p. 183-190.
74. Lee, B.L., Walsh, T.F., Won, S.T., Patt, H.M., Song, J.W and Mayer A.H., *Penetration Failure Mechanisms of Armour-Grade Fibre Composite Under Impact.* Journal of Composite Material 2001. **35**: p. 1605-1633.
75. Smith, J.C., McCrackin, F.L. and Schniefer, H.F, *Stress-Strain Relationships in Yarns Subjected to Rapid Impact Loading (Part 5: Wave Propagation in Long Textile Yarns Impacted Transversely).* Textile Research Journal, 1956. **28**(4): p. 288-302.
76. Field, J.E. and Sun, Q., *A High Speed Photographic Study of Impact On Fibres and Woven Fabrics*. in *proceedings of the 19th international congress on high speed photography and photonics*. 1990.
77. Roylance, D., *Ballistic of Transversely Impacted Fibres.* Textile Research Journal, 1977. **47**: p. 697.
78. Cunniff, P.M. *Dimensionless Parameters for Optimization of Textile Based Body Armour Systems*. in *Proceedings of the 18th International Symposium on Ballistics*. 1999. San Antonio, Texas.
79. Cunniff, P.M., *An Analysis of The System Effects of Woven Fabrics Under Ballistic Impact.* Textile Research Journal, 1992: p. 495-509.
80. Rao, Y. and Farris, R., *A Modeling and Experimental Study of the Influence of*

Twist on and Mechanical Properties of High-Performance Fibre Yarns. Journal of Applied Polymer Science, 2000. **77**: p. 1938-1949.
81. Song, W.J., *Fabrics and Composites for the Ballistic Protection of Personnel*, in *Lightweight Ballistic Composite*, A. Bhatnagar, Editor. 2006, Woodhead publishing and Maney publishing limited.
82. Yang, D., *Design, Performance And Fit of Fabric For Female Body Armour* in *School of materials*2010, university of manchester: manchester.
83. Shi, W., Hu,H., Sun,B. and Gu, B., *Energy Absorption of 3D Orthogonal Woven Fabric Under Ballistic Penetration of Hemispherical-Cylindrical Projectile.* The journal of textile institute, 2011. **102**: p. 875-889.
84. Shockey, D.A., Erlich, D.C. and Simons, J.W., *Improved Barriers to Turbine Engine Fragments, Interm Report III*, 2001.
85. Chen, X., Zhou, Y., Wells, G., Numerical and experimental investigations into ballistic performance of hybrid fabric panels. Composites Part B: Engineering. 2014 Mar 31;58:35-42.
86. Shockey, D.A., Erlich, D.C. and Simons, J.W., *Improved Barriers to Turbine Engine Fragments: Interim Report IV*, 2002.
87. Lim, C.T., Tan, V.B.C. and Cheong, C.H., *Perforation of High-Strength Double-Ply Fabric System by Varying Shape Projectiles.* Journal of Impact Science, 1989. **28**: p. 160-172
88. Porwal, P.K. and Phoenix, S.L., *Effect of Layer Stacking Order on the V50 Velocity of a Two-Layered Hybrid Armour System* Journal of Mechanics of Materials and Structures, 2008. **3**: p. 627-639.
89. Nader, J. and Dagher, H., *3D Hybrid Ballistic Fabric Testing Using A 3D Dgital Image* Experimental Techniques, 2011: p. 55-60.
90. Duan, Y., Keefe, M., Bogetti, T.A., Cheeseman, B.A. and Powers, B, *A Numerical Investigation of Influence of Friction on Energy Absorption by A High-Strength Fabric Subjected to Ballistic Impact.* International Journal of Impact Engineering, 2006. **32**(8): p. 1299-1312.
91. Shahkarami, A., Cepus, E., Vaziri, R. and Poursartip, A., *Material Responses To Ballistic Impact*, in *Lightweight Ballistic Composite*, A. Bhatnagar, Editor. 2006, Woodhead Publishing Limited and CRC Press LLC: Cambridge. p. 77.
92. Bazhenov, S., *Dissipation of Energy by Bulletproof Aramid Fabric.* Journal of Material Science, 1997. **32**: p. 4167-4173.
93. Starratt, D., Pageau, G., Vaziri, R and Pourartip A. *An Instrumented Experimental Study of the Ballistic Impact Response of Kevlar Fabric*. in *Proc. 18th international symposium on ballistics*. 1999.
94. Kirkwood, K.M., Wetzel, E.D. and Kirkwood, J.E., *Yarn Pull-Out as A Mechanism for Dissipating Ballistic Impact Energy in Kevlar KM-2 Fabric, Part 1: Quasi-Static Characterization of Yarn Pull-Out.* Textile Research Journal, 2004. **74**: p. 920-928.
95. Kirkwood, K.M., Wetzel, E.D. and Kirkwood, J.E., *Yarn Pull-Out as A Mechanism for Dissipating Ballistic Impact Energy in Kevlar KM-2 Fabric, Part 2: prediction of ballistic performance.* Text Res J, 2004. **74**: p. 939-948.

96. Chitrangad, M., *Ballistic Structure*, in *United States Patent*1994, E.I.Du pont de Nemours and Company, Wilmington, Del U.S.
97. Zeng, X.S., Shim,V.W., and Tan, V.B.C., *Influence of Boundary Conditions On The Ballistic Performance Of High-Strength Fabric Targets.* International Journal of Impact Engineering, 2005. **32**: p. 631-642.
98. Zee, R.H. and Hsieh, C.Y., *Energy loss partitioning during ballistic impact of polymer composites.* Polymer Composites, 1993. **14**(3): p. 265-271.
99. Lee, B., Song, J., and Ward, J., *Failure of spectra® polyethylene fiber-reinforced composites under ballistic impact loading.* Journal of Composite Materials, 1994. **28**(13): p. 1202-1226.
100. Shim, V., Tan, V., and Tay, T., *Modelling deformation and damage characteristics of woven fabric under small projectile impact.* International Journal of Impact Engineering, 1995. **16**(4): p. 585-605.
101. Sun, C. and Potti, S., *A simple model to predict residual velocities of thick composite laminates subjected to high velocity impact.* International Journal of Impact Engineering, 1996. **18**(3): p. 339-353.
102. Starratt, D., Sanders T, Cepuš E, Poursartip A, Vaziri R, *An efficient method for continuous measurement of projectile motion in ballistic impact experiments.* International Journal of Impact Engineering, 2000. **24**(2): p. 155-170.
103. Duan, Y., Sanders, T., Cepuš, E., Poursartip, A., Vaziri, R., *Modeling friction effects on the ballistic impact behavior of a single-ply high-strength fabric.* International Journal of Impact Engineering, 2005. **31**(8): p. 996-1012.
104. Duan, Y., Keefe, M., Bogetti, TA., Cheeseman, BA., Powers, B. , *A numerical investigation of the influence of friction on energy absorption by a high-strength fabric subjected to ballistic impact.* International Journal of Impact Engineering, 2006. **32**(8): p. 1299-1312.
105. Zeng, X., Tan, V., and Shim, V., *Modelling inter-yarn friction in woven fabric armour.* International Journal for Numerical Methods in Engineering, 2006. **66**(8): p. 1309-1330.
106. Gogineni, S., Gao, XL., David, NV., Zheng, JQ., *Ballistic impact of Twaron CT709® plain weave fabrics.* Mechanics of Advanced Materials and Structures, 2012. **19**(6): p. 441-452.
107. Grujicic, M., Bell, WC., Arakere, G., He, T., Xie, X., Cheeseman BA *Development of a meso-scale material model for ballistic fabric and its use in flexible-armor protection systems.* Journal of materials engineering and performance, 2010. **19**(1): p. 22-39.
108. Zhou, Y., *Development of lightweight soft body armour for ballistic protection*, in *School of Mateials*2013, The University of Manchester: Manchester.
109. Duan, Y., Keefe, M., Bogetti, TA., Powers, B., *Finite element modeling of transverse impact on a ballistic fabric.* International Journal of Mechanical Sciences, 2006. **48**(1): p. 33-43.
110. National Institue of Justice, U.S.D.o.J., *Ballistic resistance of body armor NIJ Standard-0101.06*, 2000.

111. Croft, J. and Longhurst, D., *HOSDB body armour standards for UK police (2007) Part 2: ballistic resistance*, 2007: Sandridge, St Albans, Herfordshire
112. Ahmad, M., Ahmad, WY., Samsuri, A., Salleh, J., Abidin, MH., *Blunt Trauma Performance of Fabric Systems Utilizing Natural Rubber Coated High Strength Fabrics*. in *International Conference on Advancemetn of Materials and Nanotechnology:(ICAMN-2007)*. 2010. AIP Publishing.
113. Lee, Y.S., Wetzel, E.D., and Wagner, N.J., *The ballistic impact characteristics of Kevlar® woven fabrics impregnated with a colloidal shear thickening fluid.* Journal of materials science, 2003. **38**(13): p. 2825-2833.
114. Metker, L.W., Prather, R.N., and Johnson, E.M., *A method for determining backface signatures of soft body armors*, 1975, DTIC Document.
115. Prather, R.N., Swann, C.L., and Hawkins, C.E., *Backface signatures of soft body armors and the associated trauma effects*, 1977, Army Armament Research and Development Command Aberdeen Proving Ground MD Chemical Systems LAB.
116. Gower, H., Cronin, D., and Plumtree, A., *Ballistic impact response of laminated composite panels.* International Journal of Impact Engineering, 2008. **35**(9): p. 1000-1008.
117. Lomakin, E., Mossakovsky, PA., Bragov, AM., Lomunov, AK., Konstantinov, AY., Kolotnikov, ME., Antonov, FK., Vakshtein, MS., *Investigation of impact resistance of multilayered woven composite barrier impregnated with the shear thickening fluid.* Archive of applied mechanics, 2011. **81**(12): p. 2007-2020.
118. Bilisik, K. and Korkmaz, M., *Multilayered and multidirectionally-stitched aramid woven fabric structures: experimental characterization of ballistic performance by considering the yarn pull-out test.* Textile Research Journal, 2010. **80**(16): p. 1697-1720.
119. Karahan, M., *Comparison of ballistic performance and energy absorption capabilities of woven and unidirectional aramid fabrics.* Textile Research Journal, 2008. **78**(8): p. 718-730.
120. Tam, T. and Bhatnagar, A., *Chapter 7 High-performance ballistic fibers*, in *Lightweight ballistic Composites*, A. Bhatnagar, Editor. 2006, Woodhead Publishing Limited, Abington Hall, Abington, Cambridge CBI 6AH, England. p. 189-209.
121. Pandya, K.S., Pothnis, JR., Ravikumar, G., Naik, NK., *Ballistic impact behavior of hybrid composites.* Materials & Design, 2013. **44**: p. 128-135.
122. Reyes Villanueva, G. and Cantwell, W., *The high velocity impact response of composite and FML-reinforced sandwich structures.* Composites Science and Technology, 2004. **64**(1): p. 35-54.
123. Department of Defense, U.S.o.A., *V_{50} Ballistic Test for Armour*.
124. Nilakantan, G. and Gillespie, J.W., *Ballistic impact modeling of woven fabrics considering yarn strength, friction, projectile impact location, and fabric boundary condition effects.* Composite Structures, 2012. **94**(12): p. 3624-3634.
125. Tabiei, A. and Nilakantan, G., *Ballistic impact of dry woven fabric*

composites: a review. Applied Mechanics Reviews, 2008. **61**(1): p. 1-12.
126. Backman, M.E. and Goldsmith, W., *The mechanics of penetration of projectiles into targets.* International Journal of Engineering Science, 1978. **16**(1): p. 1-99.
127. Cunniff, P.M., *A semiempirical model for the ballistic Impact performance of textile-based personnel Armor.* Textile Research Journal, 1996. **66**(1): p. 45-58.
128. Tan, V. and Khoo, K., *Perforation of flexible laminates by projectiles of different geometry.* International Journal of Impact Engineering, 2005. **31**(7): p. 793-810.
129. Cork, C. and Foster, P., *The ballistic performance of narrow fabrics.* International Journal of Impact Engineering, 2007. **34**(3): p. 495-508.
130. Drodge, D.R., Mortimer, B., Holland, C., Siviour, CR., *Ballistic impact to access the high-rate behaviour of individual silk fibres.* Journal of the Mechanics and Physics of Solids, 2012. **60**(10): p. 1710-1721.
131. Sakaguchi, S., Sakaguchi, S., Carr, D., Horsfall, I., Girvan, L., *Protecting the extremities of military personnel: fragment protective performance of one-and two-layer ensembles.* Textile Research Journal, 2012. **82**(12): p. 1295-1303.
132. Majumdar, A., Butola, B.S., and Srivastava, A., *Development of soft composite materials with improved impact resistance using Kevlar fabric and nano-silica based shear thickening fluid.* Materials & Design, 2014. **54**: p. 295-300.
133. Park, J.L., Park, JL., Yoon, BI., Paik, JG., Kang, TJ., *Ballistic performance of p-aramid fabrics impregnated with shear thickening fluid; Part I - Effect of laminating sequence.* Textile Research Journal, 2012. **82**(6): p. 527-541.
134. Park, J.L., Park, JL., Yoon, BI., Paik, JG., Kang, TJ., *Ballistic performance of p-aramid fabrics impregnated with shear thickening fluid; Part II - Effect of fabric count and shot location.* Textile Research Journal, 2012. **82**(6): p. 542-557.
135. Smith, J.C., McCrackin, F.L., and Schiefer, H.F., *Stress-Strain Relationships in Yarns Subjected to Rapid Impact Loading Part V: Wave Propagation in Long Textile Yarns Impacted Transversely.* Textile Research Journal, 1958. **28**(4): p. 288-302.
136. Vinson, J.R. and Taylor, W.J., *Modeling ballistic impact into flexible materials.* AIAA journal, 1990. **28**(12): p. 2098-2103.
137. Vinson, J. and Zukas, J., *On the ballistic impact of textile body armor.* Journal of Applied Mechanics, 1975. **42**(2): p. 263-268.
138. Parga-Landa, B. and Hernandez-Olivares, F., *An analytical model to predict impact behaviour of soft armours.* International Journal of Impact Engineering, 1995. **16**(3): p. 455-466.
139. Hetherington, J., *Energy and momentum changes during ballistic perforation.* International Journal of Impact Engineering, 1996. **18**(3): p. 319-337.
140. Chocron-Benloulo, I.S., Rodriguez, J., and Sanchez-Galvez, V., *a simple analytical model to simulate textile fabric ballistic impact behavior* Textile Research Journal, 1997. **67**(7): p. 520-528.

141. Billon, H. and Robinson, D., *Models for the ballistic impact of fabric armour.* International Journal of Impact Engineering, 2001. **25**(4): p. 411-422.
142. Gu, B., *Analytical modeling for the ballistic perforation of planar plain-woven fabric target by projectile.* Composites Part B: Engineering, 2003. **34**(4): p. 361-371.
143. Porwal, P.K. and Phoenix, S.L., *Modeling system effects in ballistic impact into multi-layered fibrous materials for soft body armor.* International journal of fracture, 2005. **135**(1-4): p. 217-249.
144. Porwal, P. and Phoenix, S., *Effects of layer stacking order on the V 50 velocity of a two-layered hybrid armor system.* Journal of Mechanics of Materials and Structures, 2008. **3**(4): p. 627-639.
145. Phoenix, S. and Porwal, P.K., *A new membrane model for the ballistic impact response and V_{50} performance of multi-ply fibrous systems.* International Journal of Solids and Structures, 2003. **40**(24): p. 6723-6765.
146. Mamivand, M. and Liaghat, G., *A model for ballistic impact on multi-layer fabric targets.* International Journal of Impact Engineering, 2010. **37**(7): p. 806-812.
147. Chen, X., Zhu, F., and Wells, G., *An analytical model for ballistic impact on textile based body armour.* Composites Part B: Engineering, 2013. **45**(1): p. 1508-1514.
148. Ha-Minh, C., Imad, A., Boussu, F., Kanit, T., *On analytical modelling to predict of the ballistic impact behaviour of textile multi-layer woven fabric.* Composite Structures, 2013. **99**: p. 462-476.
149. Instruments, T., *Understanding Rheology of Structured Fluids.* Paper revised by Franck, AJ in TA Instruments, 2004.
150. Wagner, N., Kirkwood, J., and Egres, R., *Shear thickening fluid containment in polymer composites*, 2005, Google Patents.
151. Wagner, N.J. and Brady, J.F., *Shear thickening in colloidal dispersions.* Physics Today, 2009. **62**(10): p. 27-32.
152. Lee, Y.S. and Wagner, N.J., *Rheological properties and small-angle neutron scattering of a shear thickening, nanoparticle dispersion at high shear rates.* Industrial & Engineering Chemistry Research, 2006. **45**(21): p. 7015-7024.
153. Kaldasch, J. and Senge, B., *Shear thickening in polymer stabilized colloidal suspensions.* Colloid And Polymer Science, 2009. **287**(12): p. 1481-1485.
154. Egres, R.G. and Wagner, N.J., *The rheology and microstructure of acicular precipitated calcium carbonate colloidal suspensions through the shear thickening transition.* Journal of Rheology (1978-present), 2005. **49**(3): p. 719-746.
155. White, E.E.B., Chellamuthu, M., and Rothstein, J.P., *Extensional rheology of a shear-thickening cornstarch and water suspension.* Rheologica Acta, 2010. **49**(2): p. 119-129.
156. Hu, Y., Boltenhagen, P., and Pine, D., *Shear thickening in low-concentration solutions of wormlike micelles. I. Direct visualization of transient behavior and phase transitions.* Journal of Rheology (1978-present), 1998. **42**(5): p.

1185-1208.
157. Frith, W.J., d'Haene, P., Buscall, R., Mewis, J., *Shear thickening in model suspensions of sterically stabilized particles.* Journal of Rheology (1978-present), 1996. **40**(4): p. 531-548.
158. Metzner, A. and Whitlock, M., *Flow behavior of concentrated (dilatant) suspensions.* Transactions of The Society of Rheology (1957-1977), 1958. **2**(1): p. 239-254.
159. Hoffman, R., *Discontinuous and dilatant viscosity behavior in concentrated suspensions. I. Observation of a flow instability.* Transactions of The Society of Rheology (1957-1977), 1972. **16**(1): p. 155-173.
160. Bazhenov, S., *On the role of friction in energy dissipation upon transverse ballistic impact on fabric.* Polymer Science Series B, 2006. **48**(5): p. 282-286.
161. Bergström, L., *Shear thinning and shear thickening of concentrated ceramic suspensions.* Colloids and Surfaces A: Physicochemical and Engineering Aspects, 1998. **133**(1): p. 151-155.
162. Woodcock, L.V., *Origins of shear dilatancy and shear thickening phenomena.* Chemical Physics Letters, 1984. **111**(4): p. 455-461.
163. Durlofsky, L., Brady, J.F., and Bossis, G., *Dynamic simulation of hydrodynamically interacting particles.* Journal Of Fluid Mechanics, 1987. **180**: p. 21-49.
164. Bender, J.W. and Wagner, N.J., *Optical measurement of the contributions of colloidal forces to the rheology of concentrated suspensions.* Journal of colloid and interface science, 1995. **172**(1): p. 171-184.
165. Kalman, D.P. and Wagner, N.J., *Microstructure of shear-thickening concentrated suspensions determined by flow-USANS.* Rheologica Acta, 2009. **48**(8): p. 897-908.
166. Kaffashi, B., O'Brien, VT., Mackay, ME,, Underwood, SM., *Elastic-like and viscous-like components of the shear viscosity for nearly hard sphere, Brownian suspensions.* Journal of colloid and interface science, 1997. **187**(1): p. 22-28.
167. Bossis, G. and Brady, J.F., *The rheology of Brownian suspensions.* The Journal of chemical physics, 1989. **91**(3): p. 1866-1874.
168. Boersma, W.H., Laven, J., and Stein, H.N., *Shear thickening (dilatancy) in concentrated dispersions.* AIChE journal, 1990. **36**(3): p. 321-332.
169. Farr, R., Melrose, J.R., and Ball, R., *Kinetic theory of jamming in hard-sphere startup flows.* Physical Review E, 1997. **55**(6): p. 7203.
170. Silbert, L., Melrose, J., and Ball, R., *A structural analysis of concentrated, aggregated colloids under flow.* Molecular Physics, 1999. **96**(11): p. 1667-1675.
171. Phung, T.N., Brady, J.F., and Bossis, G., *Stokesian dynamics simulation of Brownian suspensions.* Journal of Fluid Mechanics, 1996. **313**: p. 181-207.
172. Brady, J.F., *Model hard-sphere dispersions: statistical mechanical theory, simulations, and experiments.* Current Opinion in Colloid & Interface Science, 1996. **1**(4): p. 472-480.

173. Boersma, W.H., Laven, J., and Stein, H.N., *Computer simulations of shear thickening of concentrated dispersions.* Journal of Rheology (1978-present), 1995. **39**(5): p. 841-860.
174. Bröckel, U., Meier, W., and Wagner, G., *Product design and engineering: formulation of gels and pastes*. 2013: John Wiley & Sons.
175. Ball, R. and Melrose, J.R., *A simulation technique for many spheres in quasi-static motion under frame-invariant pair drag and Brownian forces.* Physica A: Statistical Mechanics and its Applications, 1997. **247**(1): p. 444-472.
176. Fredrickson, G.H. and Pincus, P., *Drainage of compressed polymer layers: dynamics of a"squeezed sponge."* Langmuir, 1991. **7**(4): p. 786-795.
177. Ball, R. and Melrose, J.. *Shear thickening in colloidal dispersions*. in *The 8th tohwa university international symposium on slow dynamics in complex systems*. 1999. AIP Publishing.
178. Mewis, J. and Wagner, N.J., *Colloidal suspension rheology*. 2012: Cambridge University Press.
179. Yziquel, F., Carreau, PJ., Moan, M., Tanguy, PA., *Rheological modeling of concentrated colloidal suspensions.* Journal of Non-Newtonian fluid mechanics, 1999. **86**(1): p. 133-155.
180. Wilson, H.J. and Davis, R.H., *The viscosity of a dilute suspension of rough spheres.* Journal of Fluid Mechanics, 2000. **421**: p. 339-367.
181. Chevalier, J., Tillement, O., and Ayela, F., *Structure and rheology of SiO 2 nanoparticle suspensions under very high shear rates.* Physical Review E, 2009. **80**(5): p. 051403.
182. Barnes, H.A., *Shear-Thickening ("Dilatancy") in Suspensions of Nonaggregating Solid Particles Dispersed in Newtonian Liquids.* Journal of Rheology, 1989. **33**: p. 329-366.
183. Laun, H., Bung, R., and Schmidt, F., *Rheology of extremely shear thickening polymer dispersionsa)(passively viscosity switching fluids).* Journal of Rheology (1978-present), 1991. **35**(6): p. 999-1034.
184. Chow, M. and Zukoski, C., *Gap size and shear history dependencies in shear thickening of a suspension ordered at rest.* Journal of Rheology (1978-present), 1995. **39**(1): p. 15-32.
185. Schowalter, W.R., *Mechanics of non-newtonian fluid*. 1978: Pergamon.
186. Van der Werff, J. and Kruif, C. De, *Hard-sphere colloidal dispersions: The scaling of rheological properties with particle size, volume fraction, and shear rate.* Journal of Rheology (1978-present), 1989. **33**(3): p. 421-454.
187. Giesekus, H. and Langer, G., *Determination of real flow curves of non-Newtonian liquids and plastic materials using method of representative viscosity.* Rheologica Acta, 1977. **16**(1): p. 1-22.
188. Szczepanski, J.M., *Modification and integration of shear thickening fluids into high performance fabrics*, 2011, M. Sc. Thesis, Ryerson University.
189. Zhang, X., Li, W., and Gong, X., *The rheology of shear thickening fluid (STF) and the dynamic performance of an STF-filled damper.* Smart Materials and Structures, 2008. **17**(3): p. 035027.

190. Chaffey, C., *Mechanisms and equations for shear thinning and thickening in dispersions.* Colloid and Polymer Science, 1977. **255**(7): p. 691-698.
191. Wetzel, E.D., Lee, YS, Egres, RG, Kirkwood, KM., Kirkwood, JE, Wagner, NJ., *The effect of rheological parameters on the ballistic properties of shear thickening fluid (STF)-Kevlar composites*. in *AIP Conference Proceedings*. 2004. Citeseer.
192. Lee, B.W., Kim, I.J., and Kim, C.G., *The Influence of the Particle Size of Silica on the Ballistic Performance of Fabrics Impregnated with Silica Colloidal Suspension.* Journal Of Composite Materials, 2009. **43**(23): p. 2679-2698.
193. Kalman, D.P., Merrill, RL., Wagner, NJ., Wetzel, ED., *Effect of particle hardness on the penetration behavior of fabrics intercalated with dry particles and concentrated particle− fluid suspensions.* ACS applied materials & interfaces, 2009. **1**(11): p. 2602-2612.
194. Kang, T.J., Kim, C.Y., and Hong, K.H., *Rheological behavior of concentrated silica suspension and its application to soft armor.* Journal of Applied Polymer Science, 2012. **124**(2): p. 1534-1541.
195. Decker, M., Decker, MJ., Halbach, CJ., Nam, CH., Wagner, NJ., Wetzel, ED., *Stab resistance of shear thickening fluid (STF)-treated fabrics.* Composites Science and Technology, 2007. **67**(3): p. 565-578.
196. Fischer, C., Neagu, R., Bourban, PE., Michaud, V., Plummer, C., Lavanchy, S., Manson, JA., *Structures with adaptive stiffness and damping integrating shear thickening fluids*, 2009.
197. Helber, R., Doncker, F., and Bung, R., *Vibration attenuation by passive stiffness switching mounts.* Journal of sound and vibration, 1990. **138**(1): p. 47-57.
198. Williams, T.H., Day, J., and Pickard, S., *Surgical and medical garments and materials incorporating shear thickening fluids*, 2007, Google Patents.
199. Aizenberg, J., Reichmanis, E., Sydorenko, O., Vyas, B., *Multi-layered apparatus for stopping projectiles*, 2006, Google Patents.
200. Petel, O.E., Ouellet, S., Loiseau, J., Frost, DL., Higgins, AJ., *A comparison of the ballistic performance of shear thickening fluids based on particle strength and volume fraction.* International Journal of Impact Engineering, 2015. **85**: p. 83-96.
201. Lim, A.S., Lopatnikov, SL., Wagner, NJ., Gillespie, Jr JW., *Investigating the transient response of a shear thickening fluid using the split Hopkinson pressure bar technique.* Rheologica Acta, 2010. **49**(8): p. 879-890.
202. Grujicic, M., Hariharan, A., Pandurangan, B., Yen, CF., Cheeseman, BA., Wang, Y., Miao, Y., Zheng, JQ., *Fiber-level modeling of dynamic strength of Kevlar® KM2 ballistic fabric.* Journal Of Materials Engineering And Performance, 2012. **21**(7): p. 1107-1119.
203. Hassan, T.A., Rangari, V.K., and Jeelani, S., *Synthesis, processing and characterization of shear thickening fluid (STF) impregnated fabric composites.* Materials Science and Engineering: A, 2010. **527**(12): p. 2892-

2899.
204. Wetzel, E.D., Lee, YS., Egres, RG., Kirkwood, KM., Kirkwood, JE., Wagner, NJ., *The effect of rheological parameters on the ballistic properties of shear thickening fluid (STF)-Kevlar composites*. in *AIP Conference Proceedings*. 2004. Citeseer.
205. Houghton, J., Schiffman, BA., Kalman, DP., Wetzel, ED., Wagner, NJ., *Hypodermic needle puncture of shear thickening fluid (STF)-treated fabrics.* Proceedings of SAMPE, 2007. **3**: p. 1-11.
206. Kalman, D., Schein, JB., Houghton, JM., Laufer, CH., Wetzel, ED., Wagner, NJ., *Polymer dispersion based shear thickening fluid-fabrics for protective applications.* Proceedings of SAMPE, 2007: p. 1-9.
207. Egres Jr, R., Lee, YS., Kirkwood, JE., Kirkwood, KM., Wetzel, ED., Wagner, NJ., *Liquid armor: protective fabrics utilizing shear thickening fluids*. in *Proceedings of the 4th International Conference of Safety and Protective Fabrics, Pittsburg, PA*. 2004.
208. Egres Jr, R., Decker, MJ., Halbach, CJ., Lee, YS., Kirkwood, JE., Kirwood, KM., Wagner, NJ., Wetzel, ED., *Stab resistance of shear thickening fluid (STF)-Kevlar composites for body armor applications*, 2004, DTIC Document.
209. Wagner, N. and Wetzel, E., *Advanced body armor utilizing shear thickening fluids*, 2004, Google Patents.
210. Majumdar, A., Butola, B.S., and Srivastava, A., *Optimal designing of soft body armour materials using shear thickening fluid.* Materials & Design, 2013. **46**: p. 191-198.
211. Srivastava, A., Majumdar, A., and Butola, B.S., *Improving the impact resistance performance of Kevlar fabrics using silica based shear thickening fluid.* Materials Science and Engineering: A, 2011. **529**: p. 224-229.
212. Egres, R., Lee, YS., Kirkwood, JE., Kirkwood, KM., Wetzel, ED., Wagner, NJ., *Novel flexible body armor utilizing shear thickening fluid (STF) composites*. in *Proceedings, 14th Int. Conf. on Composite Materials, San Diego, CA, Soc. Manufacturing Engineers, paper*. 2003.
213. Chin, W.K. and Wetzel, E.D., *Breathability characterization of ballistic fabrics, including shear thickening fluid-treated fabrics*, 2008, DTIC Document.
214. Sun, L.L., Xiong, D.S., and Xu, C.Y., *Application of shear thickening fluid in ultra high molecular weight polyethylene fabric.* Journal of Applied Polymer Science, 2013. **129**(4): p. 1922-1928.
215. Kang, T.J., Hong, K.H., and Yoo, M.R., *Preparation and Properties of Fumed Silica/Kevlar Composite Fabrics for Application of Stab Resistant Material.* Fibers and Polymers, 2010. **11**(5): p. 719-724.
216. Gong, X., Xu, Y., Zhu, W., Xuan, S., Jiang, W., *Study of the knife stab and puncture-resistant performance for shear thickening fluid enhanced fabric.* Journal of composite materials, 2013: p. 0021998313476525.
217. Afshari, M., Sikkema, DJ., Lee, K., Bogle, M., *High performance fibers*

based on rigid and flexible polymers. Polymer Reviews, 2008. **48**(2): p. 230-274.
218. Gadow, R. and Von Niessen, K., *Lightweight ballistic with additional stab protection made of thermally sprayed ceramic and cermet coatings on aramid fabrics.* International Journal of Applied Ceramic Technology, 2006. **3**(4): p. 284-292.
219. *http://www.sigmaaldrich.com/catalog/product/sigma/s5505*.
220. *https://www.alfa.com/en/catalog/B21918/*.
221. Bender, J. and Wagner, N.J., *Reversible shear thickening in monodisperse and bidisperse colloidal dispersions.* Journal of Rheology (1978-present), 1996. **40**(5): p. 899-916.
222. Boersma, W., Baets, PJ., Laven, J., Stein, H., *Time-dependent behavior and wall slip in concentrated shear thickening dispersions.* Journal of Rheology (1978-present), 1991. **35**(6): p. 1093-1120.
223. Hoffman, R.L., *Discontinuous and dilatant viscosity behavior in concentrated suspensions III. Necessary conditions for their occurrence in viscometric flows.* Advances in colloid and interface science, 1982. **17**(1): p. 161-184.
224. Warren, J., Offenberger, S., Toghiani, H., Pittman, Jr CU., Lacy, TE., Kundu, S., *Effect of temperature on the shear-thickening behavior of fumed silica suspensions.* ACS applied materials & interfaces, 2015. **7**(33): p. 18650-18661.
225. Fernandez, N., Mani, R., Rinaldi, D., Kadau, D., Mosquet, M., Lombois-Burger, H., Cayer-Barrioz, J., Herrmann, HJ., Spencer, ND., Isa, L., *Microscopic mechanism for shear thickening of non-Brownian suspensions.* Physical review letters, 2013. **111**(10): p. 108301.
226. Qin, J., Zhang, G., and Shi, X., *Study of a Shear Thickening Fluid: The Suspensions of Monodisperse Polystyrene Microspheres in Polyethylene Glycol.* Journal of Dispersion Science and Technology, 2016(just-accepted).
227. Yang, Y. and Chen, X., *Study of energy absorption and failure modes of constituent layers in body armour panels.* Composites Part B: Engineering, 2016. **98**: p. 250-259.
228. Walker, C., Gray, TG., Nicol, AC., Chadwick, EK., *Evaluation of test regimes for stab-resistant body armour.* Proceedings of the Institution of Mechanical Engineers, Part L: Journal of Materials Design and Applications, 2004. **218**(4): p. 355-361.

Appendix

Engineered Knife Blades

The two engineered knife blades in this standard are designed to represent two types of edged weapons used in assaults. One represents a typical small knife and is referred to as the **P1** knife blade in this standard. The other knife blade represents the performance of larger commando-style blades or larger kitchen knives and is referred to as the **S1** knife blade in this standard. Both knife blades feature a pointed tip and a stiff backbone. The **P1** blade is thinner and has one cutting edge, while the **S1** blade is thicker and has two cutting edges.

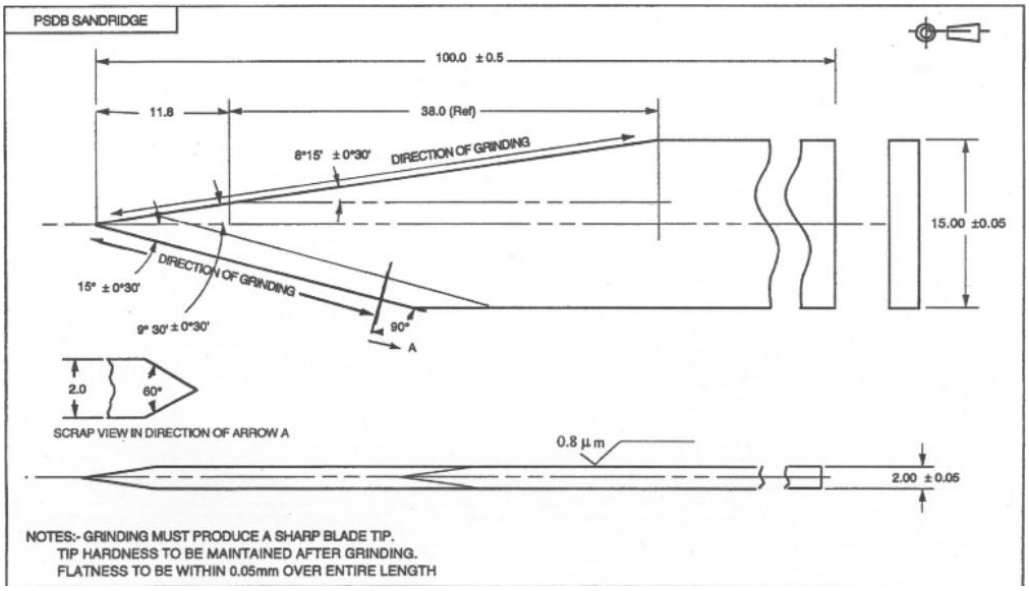

Figure 1. Engineered Knife Blade P1 [62]

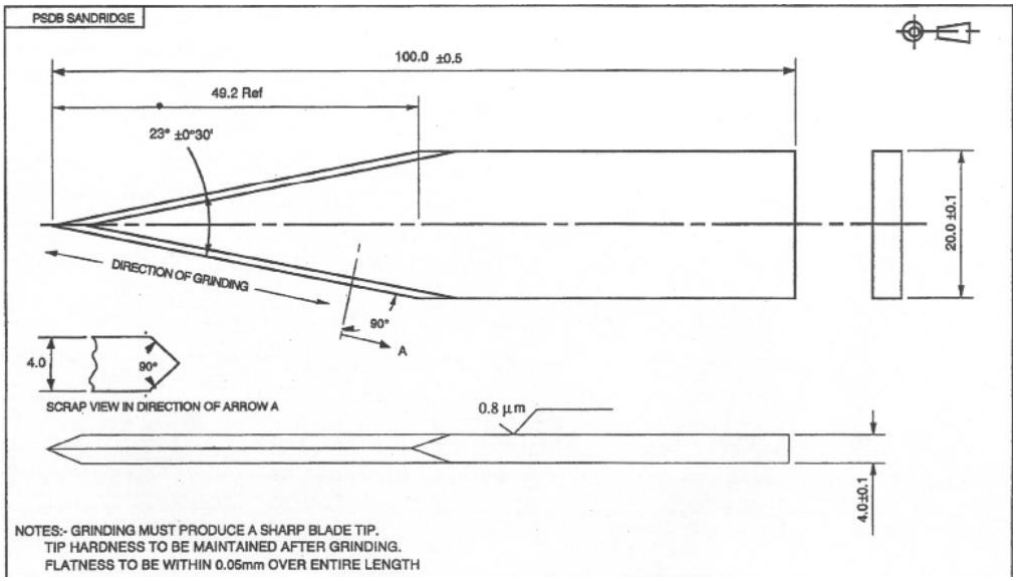

Figure 2. Engineered Knife Blade S1 [62]

Engineered Spike:

A spike-style weapon resembling an ice pick designed to represent a class of pointed weapons used primarily in assaults in corrections environments. There is one spike threat specified in this standard.

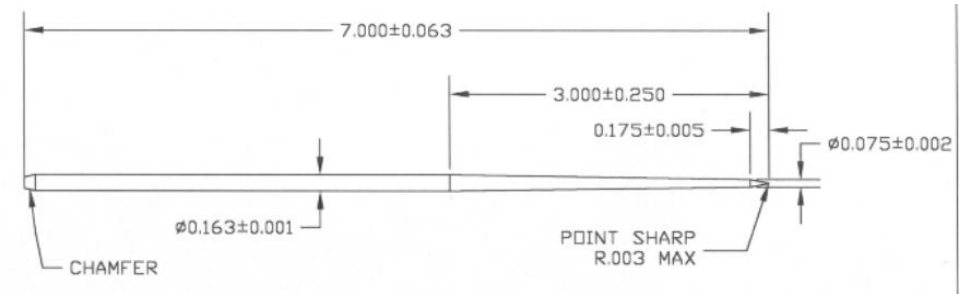

Figure 3. Engineered Spike [62]

Table 1. Ballistic perforation tests results of double layered plain Twaron® woven fabric

Specimen	Impact velocity (m/s)	Residual velocity (m/s)	Energy absorption (J)
1	491.5	475.76	7.61
2	489.14	473.88	7.23
3	494.09	480.19	6.77
4	486.4	468.35	8.61
5	489.9	474.5	7.45
Mean	490.21	474.54	7.53
SD	6.5	14.43	0.37
SE	2.9	6.44	0.165

Table 2. Ballistic perforation tests results of single layered plain 12nm STF-Twaron® woven fabric

Specimen	Impact velocity (m/s)	Residual velocity (m/s)	Energy absorption (J)
1	482.4	458.8	11.1
2	495.1	475.1	9.71
3	487.9	457.1	14.6
4	487.4	464.1	11.1
5	480.9	453.6	12.7
Mean	486.7	461.7	11.8
SD	24.9	56.1	2.8
SE	11.1	25.0	1.25

Table 3. Ballistic perforation tests results of single layered plain 650nm STF-Twaron® woven fabric

Specimen	Impact velocity (m/s)	Residual velocity (m/s)	Energy absorption (J)
1	484.9	462.9	10.4
2	494.6	474.5	9.74
3	475.5	456.5	8.86
4	493.1	463.5	14.1
5	493.2	472.6	9.95
Mean	488.3	466	10.61
SD	52.4	44.4	3.3
SE	23.4	19.8	1.47